Faculdade de Engenharia da Universidade do Porto

Instituto de Ciências Biomédicas Abel Salazar

Immunomodulatory Nanoparticles for Intervertebral Disc Degeneration

Rui Jorge Pereira Almeida

Supervisor: Catarina Leite Pereira, PhD

Co-supervisor: Raquel Madeira Gonçalves, PhD

Dissertação realizada no âmbito do

Mestrado Integrado em Bioengenharia

Ramo de Biotecnologia Molecular

Junho de 2018

RESUMO

Os nanomateriais têm vindo a ser utilizados em diversificadas aplicações biomédicas. As propriedades que possuem podem ser manipuladas para estabelecer novas abordagens que permitam modular o microambiente da inflamação. Como tal, propusemos novas estratégias para melhorar as propriedades imunomodulatórias das nanopartículas de Ch/γ-PGA.

O principal objetivo deste trabalho foi então, desenvolver e otimizar nanoestruturas baseadas em Ch e γ-PGA para controlar e perceber o desenrolar da libertação de um fármaco anti-inflamatório (Diclofenac) de modo a conseguir modular a inflamação associada à degeneração do disco intervertebral.

De forma a alcançar o nosso objetivo, foram desenvolvidas duas estratégias independentes para aperfeiçoar a estabilidade destes nanocomplexos, baseados em Ch e γ-PGA, e aumentar a incorporação, e a posterior libertação controlada de Diclofenac, nomeadamente: i) a reticulação de NPs com Genipina e ii) o desenvolvimento de nanocápsulas baseadas numa metodologia de sucessivas e alternadas deposições de camadas dos dois polímeros (Ch e γ-PGA), sob dois substratos diferentes: nanopartículas de Ch/γ-PGA e nanopartículas de sílica. Estas nanoestruturas foram caracterizadas quanto à sua citotoxicidade e potencial imunomodulatório *in vitro* recorrendo a culturas primárias de macrófagos humanos, derivados do sangue periférico, em condições basais (sem estímulo) e pró-inflamatórias (estimuladas com LPS).

Sendo assim, comprovámos que as nanopartículas de Ch/γ-PGA podem ser reticuladas com Genipina com sucesso, utilizando uma concentração de 20 mM juntamente com 2h de incubação. No entanto, os estudos futuros devem de se concentrar na melhoria deste nanosistema, de forma a estabelecer um claro potencial imunomodulatório e a conseguir uma melhoria no controlo da libertação de Diclofenac. Para além disto, são necessários novos trabalhos para desenvolver nanocápsulas com êxito.

This page was intentionally left in blank

ABSTRACT

Nanomaterials have been used in biomedical field with several applications. Their properties can be engineered to achieve new approaches to modulate inflammation microenvironment. Here, we purposed to design new strategies to improve the immunomodulatory properties of Ch/γ-PGA NPs.

The main goal of this work was to design and optimize novel Ch/γ-PGA-based nanostructures for the control and increment of release of an anti-inflammatory drug (Diclofenac) to modulate IVD degeneration associated inflammation.

In order to achieve our objective, two independent strategies were developed to improve Ch/γ-PGA based nanocomplexes stability and increase Df entrapment, namely: i) cross-linking of NPs using Genipin and ii) Ch/γ-PGA based LbL nanocapsules using a Ch/γ-PGA or Silica nanoparticle core. The nanostructured platforms were characterized regarding their cytotoxicity and immunomodulatory potential *in vitro* in primary cultures of human peripheral blood-derived macrophages, in naïve and pro-inflammatory conditions (LPS-activated).

In this work, we proved that Ch/γ-PGA NPs can be successfully cross-linked with Gn, using a concentration of 20 mM accomplished with an incubation time of 2h. However, future studies should focus on the improvement of this nanosystem in order to establish an undoubted immunomodulatory potential and to potentiate its use as drug delivery system, namely of Df. Furthermore, new studies are required to develop LbL nanocapsules successfully.

This page was intentionally left in blank

AGRADECIMENTOS

No fim desta caminhada, que, embora longa, foi bastante gratificante e enriquecedora, não só pelo saber adquirido, mas também por todos os que me acompanharam, ajudaram e conduziram.

Em primeiro lugar, uma palavra de agradecimento às minhas orientadoras. À Catarina, por sempre me ajudar, pelo apoio e pela paciência com que sempre me ensinou, e por todos os conselhos e incentivos, que me levaram a querer fazer sempre melhor. À Professora Raquel, pelo voto de confiança, pela oportunidade que me proporcionou em fazer parte desta equipa maravilhosa e por toda a ajuda e sabedoria que sempre me transmitiu.

Um agradecimento sentido à equipa do MiNT, por toda a ajuda e companheirismo. Em especial à Daniela Vasconcelos, à Mafalda Gonçalves e à Ana João, que se mostraram sempre disponíveis para me ajudar e ensinar.

Pela amizade, pelos bons momentos partilhados, pelo apoio, e por tudo o que passamos, um muito obrigado à Ana Luísa, ao Avelino, ao Pedro e à Beatriz.

Ao Avô Zé e à Avó Esmeralda, um obrigado pelo encorajamento, pela ajuda nestes anos e por estarem sempre presentes. Ao Avô João e à Avó Zilda, muito obrigado por olharem sempre por mim, e por acreditarem que este trabalho chegaria a bom porto.

Ao Afonso, ao Rui e à Márcia por toda a amizade, apoio e carinho.

À minha grande amiga Raquel, que foi, em parte, responsável por este percurso, pelas conversas, e pelo carinho com que sempre me trata.

À Nini, ao Padrinho e à Inês, por todo o carinho e por toda a preocupação que sempre tiveram para comigo, que mesmo distante se tornou próximo e sentido, um profundo obrigado por toda a ajuda e força que me dão.

À família da Mariana, que sempre me recebeu como se eu fosse parte dela.

À Mariana, por ser a minha melhor amiga. Por ouvir todos os dias o que de bom e mau me aconteceu, e por encontrar sempre uma maneira de os tornar melhores. Muito obrigado por estar sempre comigo e por toda a força que me dá para continuar!

Por último, mas não menos importante, aos meus pais, por terem estado sempre ao meu lado e por me terem proporcionado esta oportunidade. Agradeço-lhes, do fundo do coração, por tudo o que fizeram por mim! Como não podia deixar de ser, à Anita, por compreender as vezes em que estive menos presente, por me deixar crescer com ela e por toda a força que me dá para continuar!

A toda a minha família e a todos os meus amigos, o meu muito obrigado!

Este trabalho teve o apoio financeiro da FCT/MEC através dos fundos nacionais, quando aplicável, co-financiado pelo FEDER via PT2020 Partnership Agreement under the 4293 Unit I&D e através de fundos da União Europeia - Projetos Estruturados de I&D – POCI-01-0145-FEDER-007274, Portugal. Gostaria também de agradecer ao programa Norte Portugal Regional Operational Programme (N2020) no âmbito do projecto “Bioengineered Therapies for infectious diseases and tissue regeneration” (Norte-01-0145-FEDER-000012) e ao projecto Eurospine TRF (Disc degeneration: neuro and immunomodulation 2017_05).

FIGURES LIST

TABLES LIST

This page was intentionally left in blank

ABBREVIATIONS LIST

AF	Annulus fibrosus
ALM	Alveolar like macrophages
APCs	Antigen-presenting cells
ATR-FTIR	Attenuated Total Reflectance-FTIR
APTMS	(3-Aminopropyl)triesthoxysilane
Buffer	0.05 M Tris-HCl Buffer with 0.15 M NaCl (pH 5.0)
BSA	Bovine serum albumin
CEP	Cartilaginous endplate
Ch	Chitosan
Ch/γ-PGA NPs	Chitosan/gamma-poly-glutamic acid nanoparticles
COX-2	Ciclo-oxigenase-2 (COX-2)
DA	Degree of acetylation
DAMPs	Danger-associated molecular patterns
DAPI	4',6-Diamidino-2-Phenylindole
DCs	Dendritic cells
Df	Diclofenac
Df-NPs	Chitosan/Diclofenac/gamma-poly-glutamic acid nanoparticles
DPPC	Dipalmitoylphosphatidylcholine
ECM	Extracellular matrix
EDC	1-ethyl-3-(3-dimethylaminopropyl) carbodiimide hydrochloride
EE	Entrapment efficiency
ELISA	Enzyme-Linked Immunosorbent Assay
EtOH	Ethanol
FBGCs	Forming foreign body giant cells
FBR	Foreign body response
FBS	Fetal Bovine Serum
FTIR	Fourier transform infrared spectroscopy
GM-CSF	Granulocyte macrophage colony-stimulating factor
Gn	Genipin
Gn-Df-NPs	Genipin(Chitosan/Diclofenac/gamma-poly-glutamic acid NPs)
Gn-NPs	Genipin(Chitosan/gamma-poly-glutamic acid NPs)
IFN-γ	Interferon-γ

IL-6	Interleukin-6
IL-12	Interleukin-12
iNOS	Nitric oxide synthase
IVD	Intervertebral disc
LbL	Layer-by-Layer
LBP	Low back pain
LPS	Lipopolysaccharide
M-CSF	Macrophage colony-stimulating factor
Mw	Molecular weight
MWCNT	Multi-walled carbon nanotubes
NCs	Nanocapsules
NK	Natural killer
NO	Nitric oxide
NPs	Nanoparticles
O.N.	Overnight
OVA	Ovalbumin
PAMPs	Pathogen-associated molecular patterns
PBMCs	Peripheral blood mononuclear cells
PBS	Phosphate-buffered saline
PdI	Polydispersity index
PEG	Polyethylene glycol
PEOS	Polyethoxysiloxane
PGE_2	Prostaglandin E_2
PLGA	Poly(lactic-co-glycolic acid)
PMNs	Polymorphonuclear neutrophils
PPRs	Pattern recognition receptors
PS	Polystyrene
RNS	Reactive nitrogen species
ROS	Reactive oxygen species
RPM	Rotation per minute
RT	Room temperature
SDS-PAGE	Sodium dodecyl sulfate polyacrylamide gel electrophoresis
Si	Silica
Si-NPs	Silica nanoparticles

Si-A NPs	Commercial Aminated-Silica nanoparticles
Si-A NPs*	Aminated-Silica nanoparticles
SLNs	Solid lipid NPs
TEM	Transmission electron microscopy
TNF-α	Tumor necrosis factor-α
ZP	Zeta potential
γ-PGA	Gamma-poly-glutamic acid

This page was intentionally left in blank

INDEX

INTRODUCTION

1. Intervertebral disc in homeostasis and degeneration

1.1. Intervertebral disc physiology

The healthy adult intervertebral disc (IVD) is composed by different and interrelated tissues: the central nucleus pulposus, the surrounding annulus fibrosus (AF), and the cartilaginous endplates (CEP), which provides the connection to vertebral bodies. The IVD is a critical organ in the spine, by providing the flexibility and the capacity to absorb biomechanical forces and corresponds to one-third of the total human spine length (Pattappa *et al.*, 2012). The nucleus pulposus is composed by a gelatinous extracellular matrix (ECM) rich in proteoglycans, namely aggrecan and collagen type II, that regulate the hydration levels of the IVD while the AF consists primarily of collagen type I fibers that cross obliquely in alternate directions, between the vertebral bodies (Vadala *et al.*, 2016). The IVD plays a key role in spinal articulation, force coordination, axial cushioning and as a mechanical support to the spine, by providing flexibility, bending, flexion and torsion (Raj, 2008). The IVD degeneration is mainly triggered by the individual genetic background (Battie *et al.*, 2004), but can also occur due to high mechanical solicitation together with the natural ageing process or unnatural pathological events; this is considered the major cause of low back pain (LBP) (Raj, 2008), accounting for more than 40% of the cases (Cheung *et al.*, 2009). LBP affects up to 85% of people in industrialized countries at some time in their life, having high societal costs (Smith *et al.*, 2011) and is the number one disorder in terms of years lived with disability in western countries.

1.2. Intervertebral disc degeneration and associated inflammation

Embryonic development of IVD lies on the notochord that will give rise to nucleus pulposus. During the early postnatal years, blood vessels starts to recede, turning the IVD, the largest avascular organ of the whole body and therefore, limiting its self-repair capacity. Moreover, due to the lack of vascularization in the IVD of healthy individuals the nucleus pulposus remains invisible to the immune system throughout life (Smith *et al.*, 2011).

IVD degeneration process involves a cascade of structurally disrupting events, normally starting with declining nutrition of cells within the central IVD, followed by accumulation of cell waste products and degraded matrix molecules (Molinos *et al.*, 2015). This creates an increasingly acidic environment which further compromises cell viability (Urban *et al.*, 2004). An increase in the production of inflammatory cytokines and metalloproteinases by IVD cells occurs, along with an unbalanced anabolic/catabolic activity, resulting in a progressive loss of

proteoglycans and consequently, water content (Vadala *et al.*, 2007). Together with the IVD degeneration process and the pro-inflammatory environment associated, there is an increase of vascularization throughout the clefts and tears in the AF allows immune cell invasion.

Inflammation has been correlated with disease progression, but it is still uncertain if it is a cause or a consequence of IVD degeneration, and the exact mechanisms that triggers the inflammatory response. Degeneration is characterized by a great alteration of the IVD homeostasis and ECM composition: decrease of native cell numbers, malnutrition, matrix breakdown, loss of proteoglycan content, dehydration and tissue calcification. During the IVD degenerative process, disc herniation might occur when the AF is not capable to sustain the nucleus pulposus. In these particular situations, ECM fragments and microcrystals may stimulate endogenous IVD cells to produce pro-inflammatory mediators that activate the cascade of tissue degeneration by the production of catabolic cytokines such as – IL-1β, IL-8 and IL-6 (Figure 1 (1)), triggering a pro-inflammatory environment. Another hypothesis suggest that herniation may stimulate an immunological response, elicited by the exposure of the non-self nucleus pulposus, that is characterized by the recruiting macrophages, lymphocytes and other inflammatory cells to eliminate foreign body. Pro-inflammatory mediators, such as tumor necrosis factor-α (TNF-α), prostaglandin E_2 (PGE_2), nitric oxide (NO) and interferon-γ (IFN-γ) can be secreted by macrophages and are believed to be the main related to discogenic pain (Figure 1 (2)). Activated B and T lymphocytes are also recruited to the site, contributing to the positive pro-inflammatory feedback loop established (Molinos *et al.*, 2015). Overall, the pro-inflammatory milieu can trigger ingrowth of the nerve root fibers from dorsal root ganglia, thus causing pain.

Current treatments for IVD degeneration are focused in conservative approaches such as physiotherapy and anti-inflammatory drugs that only target the IVD degeneration associated symptoms. As last resource, the patients may undergo surgery for discectomy and spinal fusion. However, these procedures do not preserve the function of the IVD. Moreover, they reduce the mobility of the associated spinal motion segment and increase the mechanical load and stresses on adjacent discs (Sakai, 2008). Recent advances in regenerative medicine resulted in new approaches for the biological treatment of disc degeneration. These include cell-based strategies (Acosta *et al.*, 2011), treatment with bioactive factors (Henry *et al.*, 2017), gene therapy (Moon *et al.*, 2008) and tissue engineering (Xu *et al.*, 2015), but their clinical application is still very limited and only few studies have focused in the development of new therapies to target IVD associated inflammation (Teixeira *et al.*, 2016; Yang *et al.*, 2014).

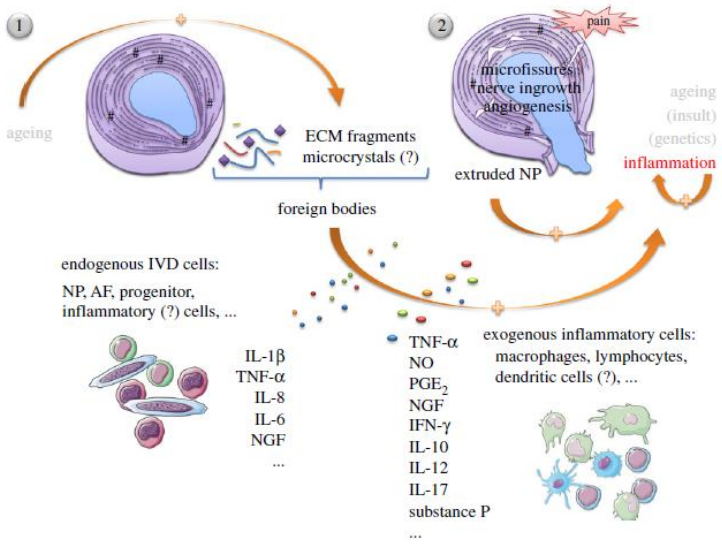

Figure 1. Inflammation on IVD. (1) Disc herniation may happen when the AF is not able to sustain the nucleus pulposus. ECM fragments induce an inflammatory response, leading to tissue degeneration. (2) Nucleus pulposus is recognizes as non-self by the immune system, and its microfissures and herniation could propagate an immune reaction, with recruitment of macrophages and other inflammatory cells, in order to eliminate the foreign body (Molinos *et al.*, 2015).

Inflammatory-like cells have been previously described in degenerated IVD. These cells shown to have phagocytic activity (Jones *et al.*, 2008) and to express CD68, a common marker of macrophages (Nerlich *et al.*, 2002). Macrophages are involved in many cartilage inflammatory diseases such as osteoarthritis (Fahy *et al.*, 2014) or in IVD degeneration (Nakazawa *et al.*, 2017; Yang *et al.*, 2016a). Recently, Nakazawa *et al.* (Nakazawa *et al.*, 2017) characterize the accumulation and the localization of macrophages in IVD degeneration. The authors described three different macrophages markers (CCR7, CD163 and CD206) in degenerative IVDs, but not in healthiest ones, suggesting that IVD degeneration involves macrophages and the expression of multiple markers increased with degeneration, especially around unhealthy nucleus pulposus, AF and CEP. Furthermore, Yang and colleagues have investigated macrophages as the unique type of inflammatory cells present in the degenerated disc. Their work further suggested that macrophages infiltrated in nucleus pulposus tissues presented an M1 phenotype and that there is a correlation between the frequency of M1 macrophages and the degeneration degree (Yang *et al.*, 2016a).

2. Engineering Immunomodulatory biomaterials

2.1. Immune response to biomaterials implantation

The biological response upon biomaterials implantation is triggered by the host immune system and involves an innate and an adaptive immune response, that play an important role in protect the body from harmful agents (Andorko *et al.*, 2017; Vishwakarma *et al.*, 2016).

Innate immunity is the first line of defense that is performed by phagocytic cells which normally phagocyte pathogens of foreign bodies as biomaterials, and release cytokines to clear pathogens, or in this case foreign bodies as biomaterials. Innate immune response cascade initiates by action of complement proteins in conjugation with danger-associated molecular patterns (DAMPs) and pathogen-associated molecular patterns (PAMPs), that are recognized by pattern recognition receptors (PPRs) primarily expressed on macrophages and dendritic cells (DCs) (Vishwakarma *et al.*, 2016). As well as pathogens, also biomaterials can exhibit features that can stimulate DAMPs and PAMPs and therefore intensify inflammation by introducing antigens to the injury site.

Initially, neutrophils and other innate immune cells (macrophages, DCs, mast cells) infiltrate the injury/implantation site (Anderson, 2001). This cascade triggers the release of pro-inflammatory chemokines, inducing the chemotaxis of other innate inflammatory cells, leading to the activation of adaptive immunity via T lymphocytes (Esche *et al.*, 2005). If the pathogen/biomaterial cannot be effectively cleared by innate immunity, some of the phagocytic cells act as antigen-presenting cells (APCs) recognizing antigens in the foreign bodies and trigger a second line of defense in the human body, an antigen-specific adaptive immune response (involving T cells and B cells) (Janeway *et al.*, 1996). Chemotaxis of polymorphonuclear neutrophils (PMNs) and recruitment of systemic monocytes differentiating into macrophages is essential for clearing debris and eradicating pathogens (Kruger *et al.*, 2015). Migrating monocytes/macrophages attach to the provisional matrix on biomaterial surface through integrins that are crucial to macrophage activation (Simms *et al.*, 1997). Cells and proteins involved in mediating these tightly organized responses are illustrated in Table 1.

Host reactions to the biomaterial following implantation determine the success of integration and biological performance of implants as biomedical implants and tissue engineering scaffolds. The outcome of biomaterial implantation varies depending on the extent of the foreign body response (FBR) that corresponds to a series of inflammatory and wound healing responses following implantation of a medical device or biomaterials, leading to fibrosis (Anderson *et al.*, 2008). Macrophages and T lymphocytes activated by mature antigen-

presenting DCs appear to dominate the progression from chronic inflammation towards regeneration.

Table 1. Overview of the Cells and Proteins involved in Mediating Effective Immune Responses (adapted from (Vishwakarma *et al.*, 2016)).

Biomaterial Implantation	
Immediate innate immune response: 0-4 h	• Blood proteins precipitation (provisional matrix) • Coagulation, platelets • Complement • DAMPs, PAMPs
Induced innate immune response: 4h to 4 days	• Tissue macrophages, PMNs • Monocytes, DCs, mast cells • ROS, IL-1β, TNF-α, IFN-γ, IL-12, IL-16, IL-8
Adaptive immune response: 4 days until resolution or healing	• B and T lymphocytes • Antibodies • TNF-α, IFN-γ, IL-2 • IL-4, IL-10, IL-13, TGF-β

2.2. The role of macrophage polarization on immunomodulation

Macrophages are one of the most important immune cells after biomaterials implantation. Macrophages can fuse forming foreign body giant cells (FBGCs) to phagocyte larger implants, a process normally associated to “frustrated phagocytosis”. These cells create a fibrotic capsule around implanted material, isolating the material from the surrounding environment (Anderson *et al.*, 2008). The first macrophages to arrive at the injury site exhibit an inflammatory phenotype known as M1 (Figure 2). M1 macrophages phagocyte pathogens and damaged cells, and produce various enzymes, including collagenases and pro-inflammatory factors, such as inducible nitric oxide synthase (iNOS), TNF-α, IL-1, IL-6, IL-8, IL-10 and IL-12 that further stimulate the inflammatory response. These factors promote inflammation and removal of pathogens, and recruit lymphocytes involved in generating adaptive immune responses (Mosser *et al.*, 2008). M1 macrophages stand at the wound or implant site for 2–3 days after injury, after which their function shifts toward a M2 phenotype (Figure 2). This shift occurs through the stimuli with factors such as glucocorticoids, IL-4 or IL-13 (Martinez *et al.*, 2014). M2 macrophages exhibits increased expression of key genes involved in wound repair (e.g., Fizz1 and arginase) (Anderson, 2001), and releases anti-inflammatory cytokines to resolve

inflammation as well as growth factors to stimulate cell proliferation and the deposition of ECM to support tissue regeneration (Murray *et al.*, 2014). This phenotype is crucial for tissue repair and formation of new blood vessels. Failure of the host immune system in switching towards a regenerative state by increasing M2 macrophages, can impair functional tissue formation and promote wound healing (Brown *et al.*, 2012).

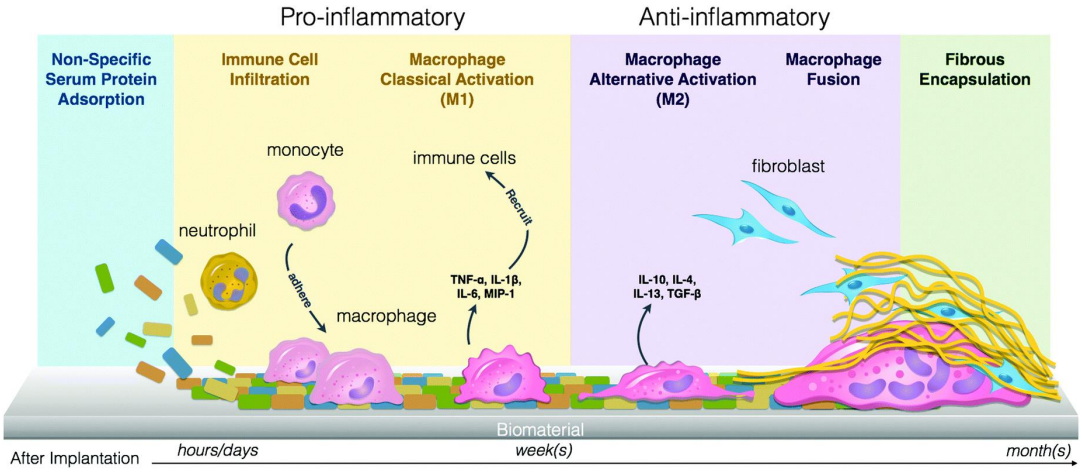

Figure 2. The role of macrophages on FBR. Macrophages are initially classically activated (M1), secrete pro-inflammatory cytokines leading to the recruitment of other immune cells. After several days, macrophages polarize towards a pro-healing, alternatively activated (M2) phenotype (Kim *et al.*, 2016).

Several *in vitro* models have tried to reproduce the spectra of macrophages phenotypes using different stimuli (Mosser *et al.*, 2008). Upon stimulation of IFN-γ+lipopolysaccharide (LPS) or TNF-α, macrophages were shown to acquire M1 (classical) phenotype, associated with secretion of pro-inflammatory cytokines. Macrophages can be alternatively activated into various M2 (Alternative) phenotypes: M2a (alternative), M2b (type II) and M2c (deactivated). M2a (induced by IL-4 and IL-13) and M2b (induced by immune complex + TLR or IL-1R ligands) produce higher amounts of IL-10 and low levels of IL-12. M2c (induced by IL-10) produce elevated amounts of IL-10 and transforming growth factor-β (TGF-β). In addition, M2c is associated with immunosuppression and tissue remodeling (Murray *et al.*, 2014). Macrophages are able to retain their plasticity and respond to environmental signals (Stout *et al.*, 2005). Classically activated macrophage produce high levels of IL-12 and low levels of IL-10 while regulatory macrophages present an opposite trend (Edwards *et al.*, 2006). Macrophages that were treated with IL-4 adopt a wound-healing phenotype, express Fizz1 and, low levels of IL-

10 and IL-12 (Raes *et al.*, 2002). Furthermore, IL-4-primed macrophages treated with LPS and immune complexes results in an hybrid macrophage, in which continue to express Fizz1 (similarly to wound-healing macrophages) and also produce high and low levels of IL-10 and IL-12, respectively (like regulatory macrophages) (Edwards *et al.*, 2006). Presently, it is known that the phenotype and activation of macrophages is not a binary process but instead a mechanism where cells suffer up-regulation or down-regulation of specific markers as they transition from a pro-inflammatory to wound healing phenotype. Furthermore, a correlation of M1/M2 phenotype in macrophages with T cell response by Th1/Th2 has been found, suggesting T lymphocytes as strong targets to promote resolution of inflammation and regeneration (Anderson *et al.*, 2011).

The host cell reaction to biomaterials implantation triggers complex host-defense mechanisms. How the properties of materials alter immune interactions in the context of tissue engineering has been widely explored in several biomaterials (Andorko *et al.*, 2017; Santos *et al.*, 2013; Vasconcelos *et al.*, 2016). Taking into consideration that different materials can trigger specific immune responses, specifically towards a M1/M2 macrophage phenotype, biomaterials can be designed to improve tissue regeneration upon biomaterials implantation. Therefore, the next section will focus on immunomodulatory biomaterials developed to date, in particular, those designed at the nano-scale.

3. Immunomodulatory materials at the Nano-scale

Immunomodulatory biomaterials arise as novel approach to modulate the immune system and thus achieve better tissue response (Vishwakarma *et al.*, 2016). Adverse immune reactions to biomaterials are frequently seen to interfere with healing, resulting in pain, excessive inflammation, tissue destruction and often leads to the rejection of the implant. Avoid undesired side effects and escape immune recognition represents an huge challenge in the biomedical field, that immunomodulatory biomaterials aim to respond (Andorko *et al.*, 2017; Vishwakarma *et al.*, 2016).

Nanomaterials in particular have a major impact in advanced therapeutic approaches, namely in improving substances delivery to the human body. Nanoparticles (NPs) are defined as particulate dispersions or solid particles with a size ranging from 1 to 1000 nm, that can be prepared from a wide variety of materials such as polymers (Yang *et al.*, 2016b) or metals (Luo *et al.*, 2015), and by several different methods like nanoprecipitation (Fessi *et al.*, 1988), co-acervation (Pereira *et al.*, 2012), double emulsification (Garti, 1997), polymer-coating (Calvo *et al.*, 1997) and layer-by-layer (LbL) (Sukhorukov *et al.*, 1998). NPs are classified according to

their size, polydispersity index (PdI), chemical composition and charge (Mohanraj *et al.*, 2006). The use of NPs as drug delivery systems display several advantages compared with drugs itself, such as site specific delivery of substances, improved drug stability and reduction of side effects. Nevertheless, NPs are recognized as foreign materials by the immune system, namely macrophages, inducing undesirable interactions such as immunostimulation, ultimately resulting in a multilevel response to the NPs by eliciting toxicity and the loss of therapeutic effect (Jiao *et al.*, 2014).

The immunomodulatory ability of nanomaterials can be tailored by tuning different features such as size, shape, composition and surface (charge and chemistry), that ultimately, modulate NPs communication with biological systems and the subsequent immune response. Additionally, NPs can be further designed to function as platforms for the delivery of substances that will themself also act in the immune system, namely in inflammation resolution. In table 2 and table 3, examples of nano-scaled immunomodulatory materials and their effects in the immune system were reviewed.

These studies, demonstrate numerous examples of tailored materials for immunomodulation that resulted in different roles depending on their chemical functionalization and on their size. Gold (Au) NPs for instance, were covered with polyethylene glycol (PEG), this surface chemical alteration was shown to stimulate the immune system (Cho *et al.*, 2009b) while similar NPs, when functionalized with citrate demonstrated a shift towards immunosuppression reaction (Sumbayev *et al.*, 2013). Furthermore, amorphous silica (Si) NPs causes inflammation whereas amorphous Si NPs modified with carboxyl groups suppressed inflammation (Morishige *et al.*, 2012). These examples clearly shows how surface modification strongly affects how the immune system recognizes the material and how it can be tuned towards a desirable effect. Examples of how size can tune NPs properties, is the case of silver (Ag) NPs that depending on their diameter have been shown to trigger different immune reactions: NPs with higher diameter shows to enhance immune function (Liu *et al.*, 2013a), whilst Ag NPs with lower diameter present immunosuppression properties (Lee *et al.*, 2010). These parameters will be discussed with more detail in the following sections.

Table 2. Nanomaterials shown to stimulate the immune system.

Materials		Size	Biological Response	Reference
Graphene		Area: 4 ± 1 μm^2 Thickness: 2 ± 1 nm	↑ IL-33, IL-5 and IL-13	(Wang *et al.*, 2013)
Au NPs	PEG-Au NPs	13 nm	↑ IL-6, IL-10 and TNF-α	(Cho *et al.*, 2009b)
Ag NPs		52.25 ± 23.64 nm	↑ IL-1, IL-6, TNF-α	(Liu *et al.*, 2013a)
Si NPs	Nonporous Si NPs	15 nm	↑ TNF-α	(Chen *et al.*, 2013)
	Amorphous Si NPs	30 – 70 nm	↑ IL-5, IL-6, keratinocyte chemoattractant	(Morishige *et al.*, 2012)
Nanoceria		8 nm	↑ TNF-α and IL-6	(Hardy *et al.*, 2012)

3.1. Composition

NPs composition play a critical role in their interactions with the host immune system. In the past years, several studies have been able to demonstrate how the biomaterial composition can affect and modulate the immune system recognition. Graphene and multi-walled carbon nanotubes (MWCNTs) are good examples of how the composition can influence immune response. Although both are composed of carbon atoms, they have different architectures and, by consequence, different physicochemical properties, presenting, respectively immunostimulatory (Wang *et al.*, 2013) and immunosuppression effects (Mitchell *et al.*, 2009).

NPs composed of polymeric materials are commonly used to biomedical applications. Poly(lactic-co-glycolic acid) (PLGA) NPs are an attractive nanomaterial due to their biodegradability and biocompatibility (Mundargi *et al.*, 2008). In the work of Chong *et al.* (Chong *et al.*, 2005), PLGA NPs with monophospholipid A, a Th1-favoring immunomodulator, loaded with hepatitis B core antigen, induced stronger Th1 cellular immune response when compared to the antigen alone, suggesting that appropriate design of nanomaterials formulation is important in the successful development of therapeutic vaccines. Furthermore, PLGA NPs loaded with oligonucleotides induced higher T cell proliferation and cytokine production than the oligonucleotide alone (Diwan *et al.*, 2004). Moreover, polystyrene (PS) NPs were shown to

inhibit the generation of allergic lung inflammation and allergen-specific Th2-based immunity, by inducing an immunosuppression effect (Hardy *et al.*, 2012).

Table 3. Nanomaterials shown to suppress the immune system.

Materials		Size	Biological Response	Reference
MWCNT		Diameter: 10 – 20 nm Length: 5 –15 μm	↑ TGF-β and IL-10	(Mitchell *et al.*, 2009)
Au NPs	Citrate-stabilized Au NPs	5 nm	↓ IL-1β	(Sumbayev *et al.*, 2013)
Ag NPs		22.18 ± 1.72 nm	↓ Expression of genes associated with immune cell function	(Lee *et al.*, 2010)
Si NPs	Amorphous Si NPs modificated with carboxyl groups	70 nm	Not referred	(Morishige *et al.*, 2012)
Fullerol NPs		Not referred	↓ IL-1β, ROS and inflammatory cytokines	(Liu *et al.*, 2013b)
		Not referred	↓ ROS, TNF-α and inflammatory cytokines ↑ Anti-oxidative enzyme gene expression	(Liu *et al.*, 2013c)
Polystyrene NPs		50 nm	↓ IL-4, IL-5 and IL-13	(Hardy *et al.*, 2012)
Iron Oxide NPs		35 – 147 nm	↓ IL-4	(Ban *et al.*, 2013)

Immunomodulatory properties of nanoliposomes have been studied. Nanoliposomes consists on liposomes at nanoscale, composed of bilayers of amphipathic lipid molecules enclosing one or more aqueous compartments. From immunomodulatory prospective, two types of nanoliposomes were developed: one that present an immunostimulatory effect, by eliciting immune response to an antigen encapsulated in the liposome, and other that

corresponds to liposomes with a polymer coat to prevent immune recognition, performing an immunosuppressor effect (Zolnik *et al.*, 2009).

As well as nanoliposomes, also solid lipid NPs (SLNs) effect on immune response was studied. SLNs are colloidal particles of a lipid matrix solid at physiological temperature (Joshi *et al.*, 2009). SLNs are able to encapsulate either hydrophobic or hydrophilic substances. A study where a comparison between free antisense oligodeoxyribonucleotide G3139 and SLN-encapsulated G3139, the second present higher immunostimulatory effect and antitumor activity (Pan *et al.*, 2009). *In vivo* studies with nanoemulsions (emulsions with droplet size at nanoscale) showed a strong antigen-specific immune response (Makidon *et al.*, 2008). Another study, analyzed the influence of composition of different NPs on their interactions with bovine serum albumin (BSA) and they found that citrate-coated Au and Ag NPs interact more with BSA than polymeric or polymer-coated NPs (Treuel *et al.*, 2010).

These studies have proven the importance of NPs composition in their interaction with the immune system, and that NPs organization constitutes a key parameter in immunomodulation capacity (Figure 3).

3.2. Size

Size is probably the most important parameter when defining a nano-scaled material, but it is also a very important parameter in what concerns to immune reaction. Therefore, the great majority of the studies have focus their attention on the influence of NPs size on the host biological response. Tan *et al.* (Tan *et al.*, 2013) analyzed the influence of size on NPs distribution. They found that smaller NPs bind faster than bigger ones, as the diffusion coefficient is proportional to the inverse of particle size. On the other hand, larger NPs are subjected to large magnitude of drag force from fluid flow, which result in lower binding probability. This is in accordance with the statement that the critical shear stress required to remove adhered particles decreases as particle size increases (Cozens-Roberts *et al.*, 1990). NPs binding is dependent of particle, shear rate and vessel geometry. NPs with smaller size and rod shape have higher binding capacity due to the larger contact area (Tan *et al.*, 2013). Therefore, particles size plays a significant role in the uptake, trafficking and retention of these materials.

A study by Inoue *et al.* (Inoue *et al.*, 2008), examined the effects of pulmonary exposure to TiO_2 nanomaterials on lung inflammation induced by LPS and consequent systemic inflammation, regarding size-dependency. Several formulations were tested (15, 50 and 100 nm TiO_2 NPs, LPS alone and NPs + LPS). The authors described that NPs + LPS with a size

< 50 nm, presented both lung and circulatory elevated levels of pro-inflammatory cytokines and chemokines compared with LPS alone. Exposure to NPs alone did not induce significant production of these cytokines. Furthermore, this enhancement was greater with the smaller NPs than with the larger ones, suggesting that NPs + LPS have a synergistic effect on systemic inflammation. Alessandrini *et al.* (Alessandrini *et al.*, 2017) further reported using an ovalbumin (OVA)-mouse allergy model that increased size of Ag NPs reduced pro-inflammatory effects. Smaller Ag NPs were shown to be more toxic than bigger particles, because smaller NPs release greater amounts of toxic silver ions compared to bigger ones, proportionally to the greater surface area/μg of deposited Ag NPs. Further, smaller NPs create higher silver burden, enhancing their persistence in macrophages. The pulmonary effects of Ag NPs indicates that size plays a critical role. Chithrani and colleagues investigated the uptake of 14, 50 and 74 nm Au NPs in Hela cells. They discovered that kinetics of uptake and saturation concentration varied with the different sized NPs, being 50 nm NPs the most efficient (Chithrani *et al.*, 2007; Chithrani *et al.*, 2006). Si NPs also exhibit different immunomodulatory effects accordingly to their size. Si NPs of 30 nm induce the secretion of IL-8 and ROS as well as an inflammatory reaction, demonstrating that Si NPs induce innate immune responses (Yang *et al.*, 2013). Other study, verified that 30 and 70 nm Si NPs increased the production of TNF-α and stronger inflammatory reaction than 300 and 1000 nm NPs, through intraperitoneally injection *in vivo* (Morishige *et al.*, 2012).

In addition, it has been suggested that the enhanced immune reaction observed with nanoliposomes formulations could be due to the inherent ability of APCs to sequester nanoliposomes more efficiently than large-sized liposomes (Nakanishi *et al.*, 1999). Additionally, it was found that smaller SLNs present an increased activity, resulting in more efficient uptake of SLNs by tumor-resident macrophages and DCs. The pharmacokinetic profile of the encapsulated drug may also contribute to the enhanced immunostimulatory effect (Pan *et al.*, 2009).

Together, these examples further confirm the importance of particle size in host reaction to NPs presence. From an immunological perspective, size must be taken into consideration when planning different applications and the design of nano-scaled biomaterials (Figure 3).

3.3. Shape

As well as the size, also the shape of a nano-scaled biomaterial has a role in determining its immunogenicity. Several studies have been interested in the role of shape, namely in NPs

adhesion (Caruso *et al.*, 2012), cell penetration (Huang *et al.*, 2013), drug delivery (Liu *et al.*, 2012) and preferential targeting (Adriani *et al.*, 2012).

Zhang and colleagues have produced and studied extensively the effect of spherical and needle-shaped PLGA-PEG NPs on the physiological response of the HepG2 cells (Zhang *et al.*, 2017). They verified that both types of NPs entered cells via endocytosis and upon internalization, NPs stayed in membrane bound vesicles. Only the needle-shaped NPs presented sharp ends and the authors suggests that local sharpness significantly affected the interaction of NPs with the lipid bilayer membrane. Needle-shaped NPs induced much more cytotoxicity than the spherical ones. Cytotoxicity of needle-shaped NPs was induced through the lysosome membrane disruption. This work demonstrated the importance of NPs shape in the physiological response of the cells (Zhang *et al.*, 2017).

Shape can also have a role in the penetration capacity of NPs. A study conducted by Lin *et al.* (Lin *et al.*, 2015), the length-to-diameter aspect ratio of cylindrical NPs was shown to affect their penetration ability and structural disturbance on dipalmitoylphosphatidylcholine (DPPC) monolayers. Compared with barrel and disk-like NPs, rod-like NPs presented an higher penetration ability and the lowest side effects to the DPPC monolayer, suggesting that the toxicity of nanomaterials might also depends on their shape (Lin *et al.*, 2015). In another study, the authors analyzed the influence of shape on cellular uptake by Hela cells. They found that spherical NPs of similar size were taken up 500% more than rod ones, which is explained by greater membrane wrapping time required for the elongated NPs (Chithrani *et al.*, 2007).

Together, these studies have demonstrated the importance of NPs shape in their ability to be internalized and uptake by the host cells, suggesting that spherical-like NPs are more internalized by the cells than other shapes. Regarding cytotoxicity, shape becomes also very important with needle and barrel-like NPs inducing more toxicity than spherical and rod ones. Moreover, these studies suggest that does not exist a relationship between cellular uptake and cytotoxicity, because both internalized NPs and not, exhibit cytotoxicity. However, further studies on this issue must consider more shapes, different materials and the physiological response of other cells types (Figure 3).

3.4. Surface Modification

Several studies show that surface modification, such as alterations of charge or surface chemistry, can change the crosstalk between NPs and biological fluid, namely blood and, by consequence, influence the adsorption of proteins to biomaterials and different immune responses (Lin *et al.*, 2015; Liu *et al.*, 2012; Lundqvist *et al.*, 2008; Zhang *et al.*, 2017).

Moreover, also the material hydrophobicity has been shown to have a key role in the extent of interactions with the immune system (Andorko *et al.*, 2017).

Nano-scaled biomaterials are more prone to macrophages phagocytosis in the absence of surface modification to prevent opsonins adsorption, that leads to their removal from bloodstream within seconds. Opsonization is the process where a particle or a foreign organism is covered by opsonin proteins, to facilitate the recognition by phagocytic cells (Owens *et al.*, 2006). Several strategies have been developed to camouflage NPs from phagocytosis. The most commonly used method is PEGylation that consists on grafting or adsorbing PEG chains to a particle surface aiming at create a barrier layer to block the adhesion of opsonins, so NPs can remain invisible to phagocytic cells (Owens *et al.*, 2006; ten Hagen *et al.*, 2002).

Different properties can influence protein binding to the NPs surface, such the NPs preparation method, its surface chemistry and physicochemical composition. When NPs, such as polymeric NPs, iron oxide particles, liposomes and carbon nanotubes were analyzed for bound proteins, it has been found that the most abundant ones were albumin, apolipoprotein, immunoglobulins, fibrinogen, granulocyte macrophage colony-stimulating factor (GM-CSF), transferrin and proteins of the complement system (Dobrovolskaia *et al.*, 2007; Jiao *et al.*, 2014). Although structural and functional status of these proteins adsorbed to the surface of NPs are still unknown, they may act as signals for immune responses contributing to the biological effects of NPs (Hussain *et al.*, 2012).

Surface modification can improve NPs-blood compatibility. Adsorption of plasma proteins depends primarily on NPs surface charge or hydrophobicity. Illustrating an example, when polyhexadecylcyanoacrylate NPs were more densely coated with PEG, less proteins were bound (Peracchia *et al.*, 1999). It has been reported that protein adsorption decreases with increasing of surface charge for several polymer-based NPs (Luck *et al.*, 1998). However, it has also been shown that increasing surface charge density, more proteins are adsorbed (Gessner *et al.*, 2002), suggesting that alterations in one physicochemical parameter, such as changing the charge of the surface, can have implications also in the material hydrophobicity by the addition of different functional groups (Dobrovolskaia *et al.*, 2007).

Comparison between PEGylated and non-PEGylated cetyl alcohol/polysorbate NPs, showed that haemolysis – disruption of red blood cells -, coagulation and platelet aggregation were dose and time-dependent and that were major for non-PEGylated NPs (Koziara *et al.*, 2005). Interaction of polyvinyl chloride resin particles increased blood coagulation time, aggregation and adhesion of platelets to these NPs. Although, when coated with PEG did not affect platelet counts or coagulation (Balakrishnan *et al.*, 2005). In addition, folate-coated and

PEG-coated gadolinium NPs present the same outcomes. Both did not activate neutrophils or aggregate platelet (Oyewumi *et al.*, 2004).

Another study shows that citrate-coated Au and Ag NPs exhibit much stronger interactions with serum albumin than polymeric or polymer-coated metallic NPs. The authors also conclude that these interactions are more influenced by surface composition than the core of the NPs (Treuel *et al.*, 2010). Through surface modification with carboxyl groups, Si NPs of 70 nm that induced strong inflammatory reaction (as described at 3.2 section - Introduction), dramatically suppressed the inflammatory response due to surface modification (Morishige *et al.*, 2012). Different authors verified that MWCNTs-PEG induced minor cytotoxicity and production of ROS in macrophages than MWCNTs-COOH, which was in correspondence with the lower cellular uptake of MWCNTs-PEG (Jiang *et al.*, 2013).

Verma and colleagues suggests that neutral charged ligands can provide a very useful route to minimize nonspecific interaction of NPs with their biological environment if positioned favorably on the NPs surface (Verma *et al.*, 2010). While neutral functional groups are excellent in preventing unwanted nanomaterial-biological interactions, most charged functional groups are responsible for activate NPs interaction with cells. Neutral and negatively charged NPs adsorbed much less on the negatively charged cell membrane surface and consequently show lower levels of internalization as compared to the positively charged NPs (Verma *et al.*, 2010). Moreover, the authors examining the interaction of positively charged NPs have shown that regardless of the type of particle, cationic particles penetrate cell membranes, which may contribute to the observed cytotoxicity with such NPs (Verma *et al.*, 2010). NPs with neutral surface coatings, such as PEG, resist interaction with cells and consequently display minimal internalization, if none at all. In PEGylated NPs, the molecular architecture of PEG on the NPs surface is a key determinant of NPs–cell interactions. The uptake of negatively charged NPs into cells, despite their interaction with the negatively charged membrane, have also been reported (He *et al.*, 2010). However, positively charged nanoparticles are most effective in crossing cell-membrane barriers and localizing in the cytosol or nucleus (He *et al.*, 2010). Studies examining the interaction of positively charged NPs have shown that regardless of the type of particle, cationic particles penetrate cell membranes, which may contribute to the observed cytotoxicity with such particles.

He *et al.* (He *et al.*, 2010) studied the effects of surface charge of Ch derivate NPs and found that small physicochemical differences such as 10 mV alteration of Zeta Potential (ZP) played a vital role in non-phagocytic cell uptake. Moreover, NPs with high surface charge and large particle size were phagocytized more efficiently by macrophages. NPs with slight negative

charges and particle size of 150 nm were tended to accumulate in tumor more efficiently. The authors demonstrate that particle size and surface charge of NPs were more important parameters than NPs composition.

Nanomaterials surface may be engineered to modulate effects on biochemical and cellular components of the blood. Further studies, should vary only one parameter at a time, in order to understand the crucial structural factors for protein binding. Comprising the relationship structure-activity of the particle, namely, at the level of interaction with blood cellular and protein components will breakdown many barriers and allow the development of a new generation of immunomodulatory nanomaterials (Figure 3).

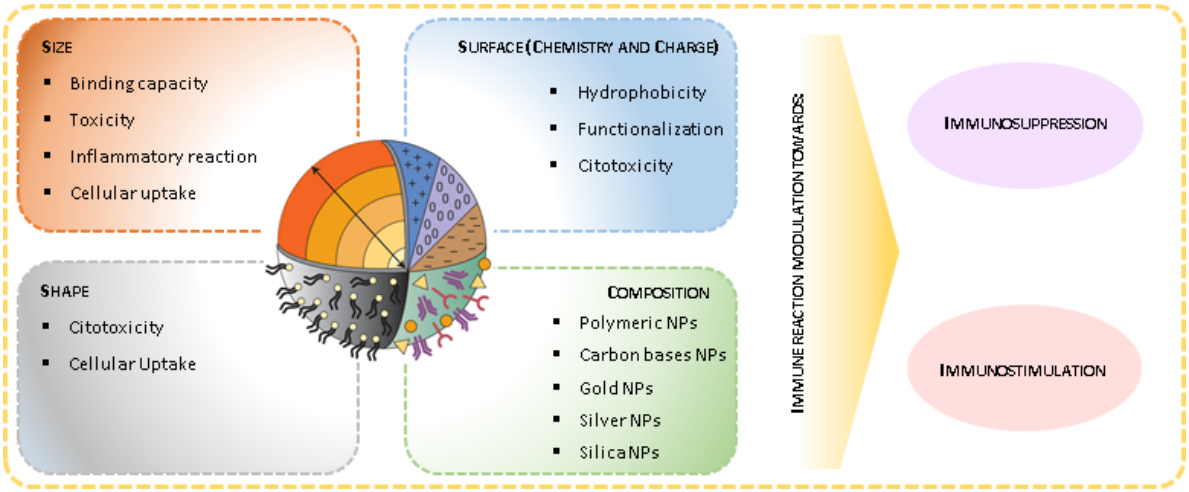

Figure 3. NPs properties such as composition, size, shape, charge and surface influences the interaction with the immune system. Modification of these properties allows the development of immunomodulatory nanobiomaterials towards an immunosuppressive or immunostimulatory response (adapted from (Dobrovolskaia *et al.*, 2007)).

4. Combined therapies

Many applications take advantage of immunomodulatory nanomaterials to create anti-inflammatory molecules combined with drug delivery systems. PLGA core with a chitosan (Ch) shell, functionalized with 1,3-β-glucan NPs were designed to stimulate reactive oxygen species (ROS)/reactive nitrogen species (RNS), induce pro-inflammatory cytokines secretion and delivery of rifampicin inside human alveolar like macrophages (ALM) to treat tuberculosis. This new NPs significantly enhanced ALM secretion of IFN-γ, TNF-α and IL-12 and double ROS/RNS generation compared to controls. Additionally, could delivery higher amounts of

rifampicin into ALM. This study provides a proof-of-concept of multimodal NPs, supporting their future progress (Dube *et al.*, 2014).

These combined therapies are also very interesting to improve cancer immunotherapy. Wang and colleagues were able to modulate adaptive immune responses, through cellular immunity by treating metastatic cancer by photothermal ablation of tumors with injection of single-wall carbon nanotubes functionalized with PEG (PEG-SWCNTs) intratumorally (Wang *et al.*, 2014). Another study, described the development of nanolipogels (nLGs) composed of drugs complexed to cyclodextrins and cytokine-encapsulating biodegradable polymers to deliver hydrophilic IL-2 and a hydrophobic small molecular inhibitor of TGF-β to tumor microenvironment (Park *et al.*, 2012). The nLGs treatment delayed tumor growth, improved survival and increased the activity of natural killer (NK) cells (Qiu *et al.*, 2017). In the cancer treatment context, nanomaterials have also been used for gene delivery. Lipid-assisted PEG-PLGA-based NPs were used to deliver CTLA-4 siRNA (NP-siCTLA-4). These particles were shown to enter T cells and enhance their proliferation. Moreover, NP-siCTLA-4 inhibited tumor growth and increased survival time in mice with melanoma (Fang *et al.*, 2011). In the same line, Xu *et al.* (Xu *et al.*, 2014) used liposome-protamine-hyaluronic acid NPs to delivery TGF-β siRNA, aiming to augment the efficacy of lipid calcium phosphate vaccines. The resulting TGF-β down-regulation improved vaccine efficacy and inhibited tumor growth by 52% compared with vaccine treatment alone. Other strategies have been taking benefit from the ability of cytokines to direct the immune response and immunotherapy became an attractive alternative to modulate inflammation. With this purpose, Hagen and colleagues demonstrate that PEGylated liposomes containing TNF-α reduced toxicity and synergistic antitumor activity when combined with liposomal chemotherapy in soft tissue sarcoma-bearing rats (ten Hagen *et al.*, 2002). Furthermore, it was showed that liposomes could deliver, IL-1α, IL-2 and IL-6, suggesting expansion of array of cytokines in future liposome formulations (Anderson *et al.*, 1994). In addition, it was demonstrated that nanoliposomes with bacterial DNA stimulated higher DCs maturation than the DNA alone (Cui *et al.*, 2005), and that immunostimulatory properties of nanoliposomes may benefit cancer treatment because of anti-tumor effects they presented in animal cancer models (Dileo *et al.*, 2003).

Nano-scaled platforms composed of Ch and poly-gamma glutamic acid (γ-PGA) are an example of a promisor immunomodulatory nanomaterial due to the immunomodulatory properties of these two polymers. Ch by itself enhances the inflammatory cells function, such as macrophages, inducing the production of cytokines and the expression of activation markers (Porporatto *et al.*, 2003). A very important property that influence the biological response to Ch

is the polymer degree of acetylation (DA). Ch with higher DA induce a more intense inflammatory response when compared with Ch with lower DA (Barbosa *et al.*, 2010). Moreover, it was proved that Ch with higher DA caused an intense inflammatory reaction mediated by M1 pro-inflammatory macrophages, characterized by high levels of pro-inflammatory cytokines. On the other hand, Ch with lower DA induce an inflammatory response characteristics of a M2 macrophage reparative response, defined by lower and higher levels of pro-inflammatory and anti-inflammatory cytokines, respectively (Vasconcelos *et al.*, 2013). Relatively to γ-PGA, a lack of immune response after repeated polymer injections demonstrate the non-immunogenicity of this polymer (Sutherland *et al.*, 2008). These properties opened new perspectives on the use of these polymers in the immunotherapy field. More properties of Ch and γ-PGA are summarized on table 4 (Antunes *et al.*, 2011). In the past years, these two polymers have been conjugated in different structures for both tissue engineering and immunomodulation strategies (Antunes *et al.*, 2016). Ch/γ-PGA NPs were developed in the work of Pereira *et al.* (Pereira *et al.*, 2012) to target different inflammatory contexts, by combination with various biologically active substances, such as anti-inflammatory drugs and proteins, for their delivery in the human body. Gonçalves *et al.* (Goncalves *et al.*, 2015) produced Ch/γ-PGA NPs as platforms for the delivery of diclofenac (Df), an anti-inflammatory drug. These nanocarriers were able to decrease PGE_2 concentration in LPS-activated macrophages *in vitro*, making these particles an attractive strategy to control macrophage response locally and promote inflammation resolution. On the other hand, Castro and colleagues used Ch/γ-PGA NPs to tune macrophages to a pro-inflammatory phenotype, by promoting the secretion of TNF-α. Furthermore, Ch/γ-PGA NPs induced an immunostimulatory phenotype in DCs, by increasing the expression of co-stimulatory molecules and the production of pro-inflammatory cytokines, such as TNF-α and IL-6. These immune cells modifications suppress the APCs capacity on induce colorectal cancer cell invasion (Castro *et al.*, 2017). Moreover, a recent study by Yang *et al.* (Yang *et al.*, 2017) proves the efficacy of Ch/γ-PGA nanogel as an adjuvant for the influenza vaccine. Ch/γ-PGA nanogel significantly increased cytotoxic T lymphocyte (CTL) activity and the long-lasting protection to the pandemic H1N1 influenza vaccine. Thus, this nanogel can largely prevent influenza virus infection. Therefore, Ch/γ-PGA NPs represent an attractive promising strategy for immunomodulatory therapies.

Table 4. Properties and chemical structure of Chitosan and γ-PGA.

Chitosan	γ-PGA
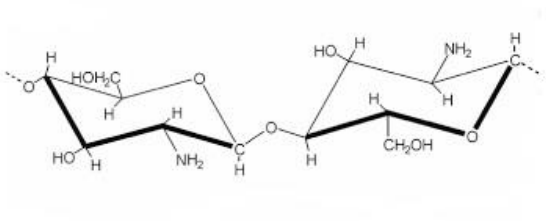	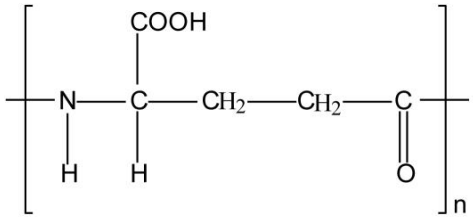
▪ Polycation; ▪ Nontoxic polysaccharide; ▪ Biochemical activity; ▪ Biocompatibility; ▪ Several uses in the biomedical field; ▪ pK_a = 6.5.	▪ Polyanion; ▪ Microbially produced by *B. subtillis*; ▪ Low immunogenicity and cytotoxicity; ▪ Biodegradable biomaterial; ▪ Improve Ch properties as biomaterial; ▪ pK_a = 2.19.
Interact electrostatically at pH 5.0	

5. Immunomodulation strategies in the context of IVD degeneration

The development of immunomodulatory strategies to treat the IVD degeneration-associated inflammation/pain represents a recent and poorly explored approach in IVD degeneration therapies. Different anti-inflammatory strategies have been used for years to target patients pain and alleviate the symptoms, such as the use of nonsteroidal anti-inflammatory drugs (NSAIDs), like Df (Roelofs *et al.*, 2008). Currently, new strategies are being designed to locally target the inflammation. The work of Teixeira *et al.* (Teixeira *et al.*, 2016) proposed the local delivery of an immunomodulatory carrier (Df-Ch/γ-PGA NPs) to revert the pro-inflammatory/degenerative environment - in an *ex vivo* organ culture of IVDs from bovine origin, under pro-inflammatory stimulation with needle-puncture and IL-1β. Using this model, the authors were able to show that IVD cells internalized Df-Ch/γ-PGA NPs, decreased PGE_2 production and down-regulated IL-6, IL-8, MMP1 and MMP3 gene expression. Besides that, Df-Ch/γ-PGA NPs treatment, up-regulated the expression of ECM proteins, namely collagen type II and aggrecan. Thus, Df-Ch/γ-PGA NPs not only reduced the inflammation, but also delayed and decreased ECM degradation, becoming a promisor therapy for degenerated IVD regeneration, based on the inflammation modulation (Teixeira *et al.*, 2016).

In an *in vivo* study, Shimamura and colleagues implanted directly in sheep artificially generated wear particles of a material known as Sinux, an elastomer. Their results showed no significant evidence of inflammation neither macrophage accumulation, suggesting that Sinux

particles did not induced any significant biologic response in the sheep (Shimamura *et al.*, 2008).

Gorth *et al.* (Gorth *et al.*, 2012) encapsulate interleukin-1 receptor antagonist (IL-1ra) in PLGA microspheres and verified, *in vitro* using nucleus pulposus cells, that IL-1ra release attenuated the degradation caused by IL-1β as defined by mechanical properties, loss of glycosaminoglycans (GAG) content, NO production and mRNA expression of inflammatory mediators for up to 20 days. The authors gone further and extrapolated this system to an *in vivo* study, using a rat model. They found that IL-1ra release from PLGA microspheres can effectively prevent GAG loss *in vivo*, induced IL-1β in nucleus pulposus (Gorth *et al.*, 2014). These results prove the efficacy of this therapy, which may be appropriate for treating cytokine-mediated disc degeneration.

Concerning evidences that ROS play a key role in IVD degeneration, a study using fullerol NPs, which have the ability to scavenge ROS, verified the efficacy of these NPs in preventing disc degeneration using *in vitro* and *in vivo* models (Yang *et al.*, 2014). For *in vitro* tests, an inflammatory cytokine, IL-1β, or a pro-oxidant H_2O_2 was used to induce degeneration in human nucleus pulposus cells and fullerol NPs were added to the culture medium. The authors verified that fullerol NPs suppressed NO production induced by IL-1β and diminish cytotoxicity and cellular ROS level induced by H_2O_2. *In vivo*, an annulus-puncture model with rabbit was created and NPs were injected into discs. Fullerol NPs injection were shown to prevented disc degeneration, by increasing water and proteoglycan content, and inhibited ectopic bone formation (Yang *et al.*, 2014). Another study evaluated the anti-inflammatory effects and the potential as free radical scavenger of fullerol NPs to prevent dorsal root ganglia (DRG) tissue and neuron inflammatory response under TNF-α induction *in vitro* (Liu *et al.*, 2013b). Results indicate that fullerol treatment reduced cellular apoptosis along with concomitant suppression of ROS, induced by TNF-α. Besides suppressing ROS and inflammatory cytokine production, fullerol NPs also inhibits adipogenic differentiation of vertebral bone marrow stromal cells *in vitro* and could prevent vertebral fatty marrow deposition and inflammatory responses during disc degeneration (Liu *et al.*, 2013c). Allover, these studies demonstrate the therapeutic potential of nanofullerol for IVD degeneration treatment.

These examples demonstrate the growing potential of immunomodulation strategies IVD degeneration treatment. However, more studies are needed to deepen the knowledge and develop novel and better immunomodulatory strategies.

Immunomodulation therapies using nano-scaled biomaterials can produce a long-lasting and effective immune response. NPs for biomedical applications can be engineered to either interact with immune system, specifically inhibiting (immunosuppression) or enhancing (immunostimulation) the immune response, or by avoiding immune system recognition. The different studies herein reviewed, showed that nanobiotechnology offers many advantages in what respects to the soft tuning of nano-scaled materials for specific applications. NPs can be manipulated by changing their physicochemical properties, such as size, shape, composition, surface chemistry and charge. Moreover, nano-scaled materials further offer the ability of work as platforms for drug/gene/growth factors release. All these properties can direct materials to target specific cell populations and to function as anti- or pro-inflammatory mediators in pathologic conditions. However, there is still a need to improve, in what concerns to the design of specific and unique effects, namely by increasing the knowledge on the materials properties and their relationship with the immune system. Unravel this talk is essential in the biomedical field. Future studies should evaluate, in a controlled manner, the influence of each particular property of the material and their interplay with immune cells and the tissue microenvironment.

This page was intentionally left in blank

AIM

Nanomaterials properties can be tuned, as described above, to design new approaches to modulate inflammation at nano scale. In this work, we purpose to outline new strategies to further improve the immunomodulatory properties of Ch/γ-PGA NPs.

The main goal of this work is to design and optimize novel Ch/γ-PGA-based NPs for the control and increment of release of Diclofenac (Df) to modulate IVD degeneration associated inflammation, based on the previous work developed by the group (Goncalves *et al.*, 2015; Pereira *et al.*, 2012).

With this aim, we purpose to develop 2 independent strategies to improve Ch/γ-PGA based NPs stability and increase Df entrapment, namely: a) cross-linking of Ch/γ-PGA NPs and b) Ch/γ-PGA based LbL nanocapsules using a Ch/γ-PGA or Silica core. These nanostructures will be characterized regarding their physico-chemical characteristics, such as size, PdI, morphology and charge, as well as Df entrapment efficiency and release at the IVD physiological and degenerative conditions. The nanostructured platforms will be further characterized regarding their biological behavior, namely their cytotoxicity and immunomodulatory potential will be evaluated *in vitro* in primary cultures of human peripheral blood-derived macrophages, in naïve and pro-inflammatory conditions (LPS-activated). Macrophages will be characterized regarding their metabolic activity, morphology and pro-inflammatory cytokine production.

Overall, this project expects to contribute to develop new immunomodulatory NPs based on Ch/γ-PGA with Df that could be applied in the context of IVD degeneration associated inflammation.

This page was intentionally left in blank

MATERIALS AND METHODS

1. Chitosan Purification and Characterization

Ch was purchased from France-Chitine (Orange, France) and purified as previously described (Crompton *et al.*, 2007; Nguyen *et al.*, 2008). First, Ch was dried in a vacuum oven at 60ºC, for 48h and afterwards, hydrated with Milli-Q water and dissolved in 0.1 M HCl with stirring. When completely dissolved, it was filtered through the 100, 41 and 20 µm filters (Millipore). Subsequently, Ch was precipitated by dropwise addition of 0.1 M KOH to the Ch acidic solution, at high stirring. The precipitate was collected by centrifugation (4000 g for 10 min) and rinsed with distilled deionized water, by repeat the centrifugations, until neutralization of the solution pH (pH 12). The Ch obtained was finally freeze-dried for 48h and then milled (IKA Mill), until a fine powder was obtained.

Ch with an average molecular weight of 324 ± 27 kDa resultant from this batch and this purification methodology was further characterized concerning the degree of acetylation (DA). The DA was determined based on Ch content in N-acetyl glucosamine units by Fourier transform infrared spectroscopy (FTIR) spectrum (FTIR system 2000, PerkinElmer, Massachusetts, USA). Ch samples were prepared in KBr pellets (2 mg of Ch in 200 mg of KBr) and stabilized under controlled relative humidity before acquiring the spectrum (Brugnerotto *et al.*, 2001). A spectrum was recorded using Spectrum software with specific parameters. Initially, baseline correction was performed, and the decay analyzed in the transmittance spectra. The determination of the DA as based on peak height of Amide III band (1320 cm^{-1}) and the analytical band (1420 cm^{-1}) as internal reference according to Brugnerotto *et al.* (Brugnerotto *et al.*, 2001), from the equation below.

v = 1420 cm^{-1} – Internal reference band

Amide III band (v = 1320 cm^{-1}) – Analytical band

$$A_{1320}/A_{1420} = 0.3822 + 0.03133 \times DA$$

2. γ-PGA Production and Purification

γ-PGA was produced microbially by *Bacillus subtilis* IFO3335. For γ-PGA biosynthesis, *B. subtillis* was cultured in modified E medium. Bacteria was initially grown in 400 mL of Luria broth and cells removed by centrifugation (8.000 g, 15 min). 1 g of cells were inoculated in 1 L of a specific medium and distributed in 1 L flasks (200 mL of medium per each). Cells were then cultured in E medium with modifications, based on (Goto *et al.*, 1992). This medium was constituted by: L-glutamic acid (3%), citric acid (2%), $(NH_4)_2SO_4$ (1%), KH_2PO_4 (0.1%),

$Na_2HPO_4.12H_2O$ (0.1%), $MgSO_4.7H_2O$ (0.05%), $MnSO_4.nH_2O$ (0.002%), $FeCl_3.6H_2O$ (0.05%), $CaCl_2$ (0.02%) and Biotin (0.00005%), at pH 7.0. Cultivation was carried out for 72h at 37ºC, 120 RPM. γ-PGA was purified from the bacteria culture broth following previously described methodology (Pereira *et al.*, 2012). Briefly, the bacteria culture medium containing γ-PGA was centrifuged at 12000 g for 1 h at 4ºC in a high capacity centrifuge (Beckman Avanti J-26XP from Beckman Coulter Inc., US). The cells pellet was washed with 0.14 M NaCl to collect the polymer remaining on cells. The wash solution was combined with the supernatant, the pH adjusted to 3.0 with 6 M H_2SO_4 and incubated at 4ºC for 12h, with the aim of removing polysaccharides that may had been produced during fermentation. To the resulting solution, three volumes of ethanol (99%) were added and left for 30 min to allow precipitation. The precipitate was collected by centrifugation at 13000 g for 10 min at RT and dissolved in 0.2 M Tris-HCl buffer (pH 8.0 adjusted with 0.1/0.3 M NaOH). The resultant solution containing γ-PGA was dialysed (7Spectra&por® Dialysis: 10000 Spectrum Laboratories, Inc., Rancho Dominguez, CA, USA) three times against 10 mM Tris-HCl buffer (pH 8.0) and then centrifuged at 12000 g for 1h at RT. The supernatant was incubated with 20 µg mL^{-1} of proteinase K at 37ºC overnight (o.n.) for α-peptides removal. This step was followed by desalting using dialysis. The solution containing γ-PGA was lyophilized and the dry matter weighted for yield assessment (Ashiuchi *et al.*, 1999; Pereira *et al.*, 2012).

The Mw of γ-PGA was estimated by SDS-PAGE (NuPAGE®Novex® Pre-Cast gradient gels of 4-12%, Invitrogen), according to (Pereira *et al.*, 2012). Alcian Blue, a basic dye, was used to stain the anionic γ-PGA polymer. Mw was evaluated by densitometry (Molecular Imager GS800 Calibrated Densitometer, Bio-Rad) and the analysis software ImageJ (Fiji). Mw was estimated based on a standard curve generated by plotting log Mw vs. migration distance of bands of known Mw (Precision Plus Protein ™ Dual color standards 250, 150, 100, 75, 50, 37, 25, 20, 15, 10 kDa), through a Sodium dodecyl sulfate polyacrylamide gel electrophoresis (SDS-PAGE) gel. Linear regression was used to interpolate the Mw of samples. Reagents, unless indicated otherwise were from Sigma-Aldrich®.

3. Ch/γ-PGA based nanoparticles preparation

Co-acervation method was used for the production of Ch/γ-PGA NPs, based on literature (Hajdu *et al.*, 2007; Lin *et al.*, 2005; Pereira *et al.*, 2012). In brief, 1 mL of γ-PGA solution (0.2 mg mL^{-1} in 0.05 M Tris-HCl buffer with 0.15 M NaCl at pH 5.0 (buffer)) was added to 1 mL of Ch solution (0.2 mg mL^{-1} in buffer) with high magnetic stirring at RT (Figure 4). γ-PGA was dropwised with a 1 mL syringe in a syringe pump (KD Scientific Inc., Holliston, MA), at a

constant velocity (3.6 µL s^{-1}). Ch/γ-PGA NPs were prepared at a molar ratio of 1:1.5 (mol Ch:mol γ-PGA), as previously optimized (Goncalves *et al.*, 2015; Teixeira *et al.*, 2016).

Df-NPs were prepared using the described methodology, by adding Df to the γ-PGA solution (Figure 4). Df was incorporated in Ch/γ-PGA NPs at a molar ratio of 2:0.35:1.5 (mol Ch:mol Df:mol γ-PGA), according to Gonçalves *et al.* (Goncalves *et al.*, 2015).

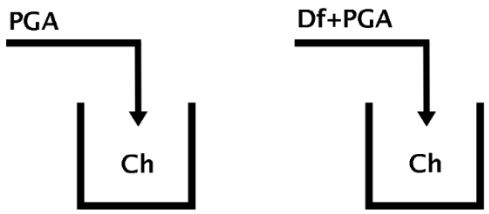

Figure 4. Ch/γ-PGA and Df-NPs preparation.

4. Diclofenac entrapment efficiency in the Ch/γ-PGA NPs

Df incorporation on Ch/γ-PGA NPs was evaluated through the entrapment efficiency (EE). Briefly, Df-NPs were prepared and 1h after centrifuged during 1h at 20.000 g. The concentration of Df in the NPs supernatant was determined by UV/Vis spectroscopy (absorbance (Abs) at 275 nm) (Synergy Mx, BioTek) using different concentrations of Df in buffer as calibration curve. Df incorporation in Ch/γ-PGA NPs was calculated by the formula: % $Df_{incorporated}$ = ($[Df]_{initial}$ – $[Df]_{supernatant}$) × 100/$[Df]_{initial}$, in which $[Df]_{initial}$ was the theoretical [Df] in the solution (0.06 mg mL^{-1}) and $[Df]_{supernatant}$ is the [Df] determined in NPs supernatant obtained after centrifugation.

5. Ch/γ-PGA nanoparticles cross-linking

Ch/γ-PGA NPs, with and without Df, were cross-linked using two different cross-linking agents: 1-ethyl-3-(3-dimethylaminopropyl) carbodiimide hydrochloride (EDC) (Imoto *et al.*, 2010) or Genipin (Gn) (Fernandes *et al.*, 2013; Li *et al.*, 2016). Different concentrations were used as a first assessment, based on the literature: 50 mM of EDC and 0.4 mM of Gn were prepared in buffer and NPs incubated in each solution. Briefly, Ch/γ-PGA NPs were centrifuged at 20.000 g during 30 min (RT), resuspended in the cross-linking agent (EDC or Gn) and incubated for 12h, at RT. Afterwards, NPs were centrifuged again (20.000 g, 30 min, RT) and resuspended in buffer at pH 5.0 to eliminate the remaining cross-linking agents. After cross-linking, Ch/γ-PGA NPs were characterized regarding size, PdI and charge. Through this analysis, it was observed that both Gn and EDC cross-linking performances were similar. Gn was chosen to continue optimizations in the subsequent studies, as it is the most common

cross-linking agent used in Ch based materials (Fernandes *et al.*, 2013; Jin *et al.*, 2004; Li *et al.*, 2016). Best Gn concentration and incubation times to achieve NPs cross-linking and higher NPs stability at the physiological pH were optimized. For that, four different concentrations of Gn were tested: 1, 10, 20 and 40 mM at different time points, 1h, 2h and 24h, under agitation (120 RPM) at RT. Briefly, previously prepared NPs were centrifuged at 20.000 g during 30 min, at RT and then resuspended in the different concentrations of the Gn solutions, prepared in buffer at pH 5.0. To eliminate the remaining Gn, Gn-NPs were afterwards centrifuged (20.000 g for 30 min) and resuspended in buffer at pH 5.0. NPs were analyzed regarding size, PdI and charge by DLS.

To assess Gn-NPs stability at the physiological pH, Gn-NPs resultant from the different Gn cross-linking concentrations and time points were incubated at a concentration of 10% or 25% (v/v) in PBS (pH 7.4). Stability was assessed immediately by analyzing size and PdI by DLS. A concentration of 20 mM and a time of incubation of 2h were the optimal conditions for higher NPs stability. Cross-linking was further confirmed by Attenuated total reflectance (ATR-FTIR). These conditions were used throughout this thesis.

6. Ch/γ-PGA Layer-by-Layer

LbL using Ch/γ-PGA has been previously described in 2D by Antunes *et al.* (Antunes *et al.*, 2011). Here, the 3D assembly of this polymers was assessed both on: 1) Ch/γ-PGA NPs and 2) on a silica NPs core.

6.1. LbL on Ch/γ-PGA NPs

LbL on Ch/γ-PGA NPs was tested up to 6 layers (3 of γ-PGA and 3 of Ch). Briefly, Ch/γ-PGA NPs previously prepared were evaluated in terms of size, PdI and charge to assess the next layer of polymer. Following this analysis, positively charged Ch/γ-PGA NPs were centrifuged at 14000 g for 15 min at RT and resuspended in γ-PGA solution (negatively charged) in buffer at pH 5.0. Then, these NPs were centrifuged and resuspended in Ch solution in buffer at pH 5.0. The process was repeated until 6 layers were deposited, being the last layer of Ch. Between each layer, the samples were analyzed regarding size, PdI and charge and washed in buffer. All depositions steps were performed under a gentle orbital shaking (100 RPM) for 15 min. After deposition of the 6 layers, the NPs were washed in buffer and analyzed regarding size, PdI, and charge by DLS. The same protocol was applied to Df-NPs, producing a LbL structure of 6 layers containing Df in between.

6.2. Silica NPs

Silica (Si) NPs of 200 nm (negatively charged) were purchased from Nanocomposix Europe. Their stability in buffer at pH 5.0, at different concentrations (0.1, 1 and 10 mg mL^{-1}) was evaluated by assessing their size, PdI and charge. In parallel, stability of Si-NPs at 1 mg mL^{-1}, in Milli-Q water (pH 5.0) and in a 0.5 M NaCl solution (pH 5.0), based on the work of Hu *et al.* (Hu *et al.*, 2015) were also evaluated. Due to Si-NPs instability and aggregation in buffer, at pH 5.0, the ideal pH for the electrostatic interaction of Ch and γ-PGA, we have tried in parallel to: a) acquire positively charge Si-NPs: aminated Si-NPs (commercial Si-A NPs) and to b) aminate the purchased Si-NPs in house (Si-A NPs*):

Commercial Si-A NPs:

Si-A NPs of 200 nm (positively charged) were purchased from Nanocomposix Europe. Their stability in buffer at pH 5.0, Milli-Q water (pH 5.0) and 0.5 M NaCl solution (pH 5.0) at the concentration of 1 mg mL^{-1} was evaluated by assessing their size, PdI and charge.

Si-A NPs*:

To obtain positively charged Si-NPs, an amination protocol was applied based on (Roy *et al.*, 2010). Briefly, to a Si-NPs solution at a concentration of 10 mg mL^{-1} was added acetic acid to a final concentration of 0.1 vol% and (3-Aminopropyl)triesthoxysilane (APTMS) to a final concentration of 2 vol% with bath sonication for 1 min. The solution was stirred at 400 RPM for 2h and 12h at RT followed by incubation at 90ºC for 1h. Following this incubation, NPs were centrifuged at 1500 g for 5 min and washed three times with EtOH 99% and water. The new Si-A NPs* were analyzed regarding size and charge by DLS both in buffer (0.1 mg mL^{-1}, pH 5.0) and Milli-Q water (1 mg mL^{-1},pH 5.0). Amination was confirmed by ATR-FTIR.

6.3. LbL on Si-NPs and Si-A NPs

LbL was tested both on Si-NPs and on commercial Si-A NPs. Regarding Si-NPs and Si-A NPs stability in different solutions, a screening study was performed for LbL deposition of the first layer on Si-NPs and Si-A NPs at 2 mg mL^{-1} in 0.5 M NaCl and Milli-Q water. At this point, based on literature (Hu *et al.*, 2015), we noticed that a proportion of 1:10 of polymers concentration to Si-NPs concentration was described and, therefore, we opted to adapt the concentration of Si-NPs (0.2 mg mL^{-1} of each polymer vs. 2 mg mL^{-1} Si-NPs).

A second LbL deposition test, on Si-NPs and commercial Si-A NPs, was performed at different concentrations (0.5, 1 and 2 mg mL^{-1}). Briefly, Si-NPs and Si-A NPs were sonciated

on ultrasound bath for 3 min. After that, 1 mL of Ch (+) solution was added to the same volume of Si-NPs (-) following agitation at 100 RPM for 15 min, according to Antunes *et al.* (Antunes *et al.*, 2011). After, Si-NPs/Ch (+) solution was centrifuged at 1.000 g during 3 min, washed and resuspended in 2 mL of 0.5 M NaCl, pH 5.0 following 3 min of sonication. Next, 1 mL of γ-PGA (-) solution was added following agitation at 100 RPM for 15 min. Then, the solution was centrifuged at 1.000 g during 3 min, washed, resuspended in 2 mL of 0.5 M NaCl, pH 5.0 and sonicated for 3 min. This cycle was repeated until the 2º layer of Ch was obtained. Between each layer deposition, NPs were analyzed regarding and charge and morphology by TEM. The same protocol was applied to the aminated Si NPs (Si-A NPs) (+), by starting LbL deposition with the γ-PGA (-) solution.

Based on the results obtained (more consistent PdI values), Si-A NPs at a concentration of 1 mg mL^{-1} were chosen to continue LbL studies with some modifications to the previously described protocol, by increasing incubation time and number of layers deposited. Briefly, after sonication of Si-A NPs for 3 min, 1 mL of γ-PGA solution was added and placed in the orbital shaker at 120 RPM for 1h, based on (Hu *et al.*, 2015; Yilmaz, 2016). Si-A NPs with the first layer were centrifuged at 1000 g for 5 min at RT, washed and resuspended in 1 mL of 0.5 M NaCl, pH 5.0, twice. Following the same method, Ch solution was added to the solution. This process was repeated until a total of 12 layers as represented in Figure 5. LbL-NPs with 12 layers were analyzed regarding size and morphology by TEM.

Finally, another step was added to the described protocol in order to improve layers' deposition: LbL was performed up to 6 layers and afterwards cross-linking with Gn was performed following the previously methodology used for Ch/γ-PGA NPs (Li *et al.*, 2016). Briefly, LbL-NPs were centrifuged at 2.000 g, for 20 min and resuspend in 20 mM of Gn solution in 0.5 M NaCl, pH 5.0. After 2h agitation (120 RPM, RT), LbL-NPs were centrifuged again and resuspended in 0.5 M NaCl at pH 5.0 and characterized by TEM (Figure 5).

6.4. Si-core removal from the Ch/γ-PGA LbL Nanocomplexes

Si-A NPs core were removed following the previously described protocol of Imoto *et al.* (Imoto *et al.*, 2010). First of all, a removal solution, consisting in an aqueous solution of 0.2 M HF including 0.8 M NH_4F at pH 5.0, was prepared. Si-A-LbL-NPs were centrifuged at 2.000 g for 15 min at RT and resuspended in the removal solution. Different times of reaction were tested: 10 min, 1h and 2h. At the end of each time point, the solution was centrifuged at 2.000 g for 15 min washed with 0.5 M NaCl (pH 5.0) three times, and sonicated for 3 min (Figure 5). Si-A core removal was confirmed by the analysis of particles morphology by TEM.

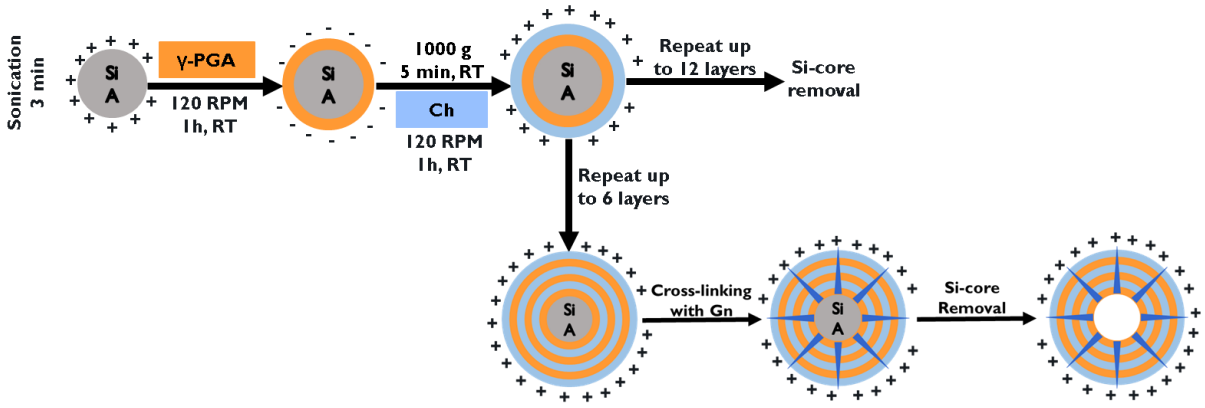

Figure 5. Ch/γ-PGA LbL on Si-A NPs followed by Si-core removal.

7. Physico-chemical characterization of nanostructures

All the nanostructures developed in the course of this work were characterized regarding their size, PdI and charge by DLS (ZetaSizer Nano ZS, Malvern Instruments). This model equipped with a 633 nm red laser, which it uses to irradiate the sample and measure the intensity of the signal that is originated. DLS allows to measure by illuminating the particles with the laser and then analyzing the intensity fluctuations. Particles in dispersion have Brownian movements depending on their size. Size is determined using the relationship between diffusion speeds and size, defined in Stokes-Einstein equation: $D=KT6\pi\eta RH$ (D: the intensity-weighted diffusion coefficient; RH: Hydrodynamic radius; η: Dispersant / Solvent viscosity; K: Boltzman constant; T: Absolute temperature). When a particle travels through the solution, the ions that are strongly attached move with the particle. In diffuse boundary, the ions do not move with the molecule. Viscous forces oppose the movement of the particles until the equilibrium, where a constant velocity is reached. Between the particle surface and the dispersing liquid, which varies with the distance from the particle surface, there is a potential – the Zeta Potential (ZP), that is determined using the Henry's relation: $UE=2\varepsilon zf(ka)/3\eta$ (UE: the electrophoretic mobility; f(ka) the Henry's function; z: Zeta Potential).

Some of the formulations were further characterized by TEM. TEM observations were performed using a Zeiss 902 A TEM and a Orius SC 1000 (Gatan) digital camera. Samples were prepared by placing a drop (5-10 µL) of the particles suspension onto a 400 mesh copper grid coated with carbon during 1 min. In some samples, after 1 min of deposition, the grid was tapped with a filter paper and negatively stained with uranyl. TEM images were obtained at different magnifications.

8. Nanostructures stability studies up to 3 weeks

Nanostructures stability at different pHs was evaluated up to 3 weeks in the Ch/γ-PGA NPs, Df-NPs, Gn-NPs and Gn-Df-NPs platforms. Both LbL structures, on Ch/γ-PGA NPs and Si-A NPs core, were excluded from subsequent studies due to their instability and the need for further future optimization. Long term stability at different pHs was analyzed at 1, 2 and 3 weeks after preparation by assessing size and PdI at:

- pH 5.0 (optimal electrostatic interaction of Ch/γ-PGA), based on (Pereira *et al.*, 2012);
- pH 6.2 (severely degenerated intervertebral disc environment);
- pH 6.8 (mild degenerated intervertebral disc environment);
- pH 7.4 (physiological pH and non-degenerated intervertebral disc environment), based on (Li *et al.*, 2012; Razaq *et al.*, 2003).

For pH 5.0, NPs were maintained in buffer solution while PBS was used for pH 6.2, 6.8 and 7.4.

9. Diclofenac release from the nanostructures

Df release from the nanostructures containing Df, Df-NPs and Gn-Df-NPs, was evaluated as previously described in the work of Gonçalves *et al.* (Goncalves *et al.*, 2015). Df-NPs and Gn-Df-NPs were incubated at a concentration of 25% (v/v) in PBS at three different pH's (6.2, 6.8 and 7.4), to mimic the previously mentioned IVD physiological and non-physiological environment, with agitation (50 RPM) at RT. At distinct time-points (2h, 24h, 48h and 72h) the solutions were centrifuged at 20000 g for 1h and Df concentration in the supernatant determined by absorbance levels at 275 nm (Synergy Mx, BioTek), accordingly with the following equation: $\%\ Df_{released} = [Df]_{supernatant} \times 100/[Df]_{initial}$. Absorbance levels of Ch/γ-PGA NPs and Gn-NPs were used as control and the absorbance levels subtracted to those obtained with Df-NPs and Gn-Df-NPs, respectively, to exclude possible Ch, γ-PGA and Gn interferences. The results obtained were further confirmed by Enzyme-Linked Immunosorbent Assay (ELISA) for Df. ELISA protocol was performed according to manufacturer's instructions (MaxSignal® Eltenac/Diclofenac ELISA Kit, Catalog No. 5108, Bioo Scientific). The plate was read on a plate reader (Synergy Mx, BioTek) at 450 nm.

For long-term evaluation of Df release from Df-NPs and Gn-Df-NPs, the nanostructures were incubated at 25% (v/v) in PBS during 1w, 2w and 3w under agitation (50 RPM), at 37ºC. At distinct time-points (1w, 2w and 3w) the solutions were centrifuged at 20000 g for 1h and Df concentration in the supernatant determined by absorbance levels at 275 nm, as previously described.

10. Evaluation of Nanostructures Cytotoxicity and Immunomodulation potential

10.1. Human primary monocyte isolation

Human monocytes were isolated from buffy coats from healthy blood donors, kindly provided from Hospital São João (Porto, Portugal), as previously optimized in our lab (Oliveira *et al.*, 2012). Briefly, buffy coats were centrifuged at 1.200g, without brake, for 20 min at RT. The whitish layer containing peripheral blood mononuclear cells (PBMCs) was collected and incubated, during 20 min under continuous rotation, with the RosetteSep® Human Monocyte Enrichment Cocktail (StemCell Technologies, Grenoble, France), according to manufacturer's instructions. This mixture was diluted 1:1 with PBS supplemented with 2% FBS (heat inactivated fetal bovine serum, Biowest), carefully added over Lymphoprep (Sigma-Aldrich) and centrifuged as before. The intermediate layer, enriched in human monocytes, was then collected and washed three times in PBS, being centrifuged at 700 RPM for 17 min between washes.

10.2. Macrophage differentiation

For monocyte-macrophage differentiation, 250 000 monocytes/well (24-wells plate) were cultured for 7 days in complete RPMI medium, supplemented with 10% Fetal bovine serum (FBS) and 100 U mL^{-1} penicillin and 100 lg mL^{-1} streptomycin, containing macrophage colony-stimulating factor (M-CSF) (50 µg mL^{-1}), based on (Cardoso *et al.*, 2014). After 7 days, the medium was renewed to RPMI complete medium without M-CSF.

10.3. Nanostructures Cytotoxicity and Immunomodulatory profile

To evaluate the different nanostructures cytotoxicity, Ch/γ-PGA NPs, Df-NPs, Gn-NPs and Gn-Df-NPs were added to macrophages cultures. At 0.07, 0.7 or 1.8 mg mL^{-1}, corresponding to 1, 10 and 25% (v/v) in solution, respectively. The same concentrations of buffer (pH 5.0) were used as control. A control without any addition of NPs was used (no stimulation). After 24h of contact, macrophages culture media was collected, centrifuged (16.200 g, 5 min) and the supernatant kept at -20ºC for posterior analysis. Macrophage metabolic activity was assessed by resazurin assay and compared with control cultures without any stimulation. Briefly, resazurin assay consisted on adding to the culture renew RPMI medium with 10% of resazurin during 3h. Medium was afterwards collected, and 100 µL were placed on a 96-well black plate (in duplicates). Resazurin conversion into resorufin was assessed on a Synergy Mx, BioTek, at 530/590 nm.

Macrophages morphology upon contact with different nanostructures was further evaluated by microscopy. For that, right after resazurin assay, cells were washed twice with PBS and fixed with PFA 4% during 15 min at 4ºC. Immunofluorescence staining of the macrophages was performed using Alexa®594-conjugated phalloidin (Invitrogen) and DAPI. Cell cytoskeleton was stained with Alexa®594-conjugated phalloidin, followed by an incubation for 45 min with agitation (120 RPM) protected from light. After PBS washes (5 min, three times), cell nuclei were stained with VectaSheild® with DAPI. Cells were imaged with a Zeiss Axio Imager Z1 Apotome microscope. Representative images of each selected condition were acquired using the 20x and 40x objectives.

The levels of the pro-inflammatory cytokines: TNF-α, lL-6 and IL-12, were qualified by ELISA (Human TNF-α/lL-6/IL-12(p70) ELISA MAX™, BioLegend®, San Diego, CA) following the manufacturer's instructions. The results were compared with levels of unstimulated macrophages as control.

10.4. Immunomodulation potential of Df-NPs and Gn-Df-NPs

To assess the anti-inflammatory potential of Df-NPs and Gn-Df-NPs, monocytes were seed at 250.000 monocytes/well (24-wells plate) and cultured during 6 days in complete RPMI medium, supplemented with 10% FBS and 100 U mL^{-1} penicillin and 100 lg mL^{-1} streptomycin, containing M-CSF (50 µg mL^{-1}), based on (Cardoso *et al.*, 2014). After 6 days, the medium was renewed to complete RPMI medium without M-CSF. At day 7, macrophages were activated with bacterial (*Escherichia coli*) lipopolysaccharide (LPS, 100 ng mL^{-1}, Sigma) during 3h. The effect of Df-NPs and Gn-Df-NPs on LPS-stimulated macrophages was evaluated by their capacity of revert LPS stimulus. A control using soluble Df at the theoretical loaded concentration of Df (0.06 mg mL^{-1}) was also performed. Df-NPs, Gn-Df-NPs and soluble Df were added to macrophages cultures 3h after LPS stimulation to a final concentration of 10% (v/v). 24h after stimulation the macrophages culture media was collected, centrifuged (16.200 g, 5 min) and the supernatant kept at -20ºC for posterior analysis.

Metabolic activity and morphology of LPS-stimulated macrophages was also analyzed, as described in the sub-section above, as well as the levels of the pro-inflammatory cytokines: TNF-α, lL-6 and IL-12.

11. Statistical Analysis

Statistical analysis was conducted using GraphPad Prism version 6.0 for Mac OS X (GraphPad Software, California, USA). The parametric distribution of the data was evaluated

by D'Agostino and Pearson normality test. For non-parametric data, when two groups were compared Mann-Whitney test was used; when more than two groups were compared, Kruskal-Wallis test with Dunn's multiple comparison test was used. The two-away ANOVA with Tukey multiple comparison test was used to compare two groups of data regarding time and conditions. Statistical significance was considered at least for *$p<0.05$, (**$p<0.01$, ***$p< 0.005$, ****$p<0.001$).

This page was intentionally left in blank

RESULTS AND DISCUSSION

1. Chitosan Characterization

Ch was purified as described in the Materials and Methods section and characterized according to the molar fraction of N-acetylated units, designated as acetylation degree (DA), by FTIR. This characterization is important, since DA is a parameter that can affect solubility, crystallinity, charge density and propensity to enzymatic degradability (Amaral *et al.*, 2007; Tomihata *et al.*, 1997). Additionally, the number of primary available amines provided by glucosamine units is determinant for the surface chemistry and wettability, which are key parameters for the modulation of cell adhesion and proliferation, and consequently the inflammatory response (Anselme, 2000; Barbosa *et al.*, 2010; Baxter *et al.*, 1992). The FTIR spectrum of purified Ch is represented on Figure 6. It is characterized by a large and intense band at 3430 cm^{-1} (-OH stretching overlapped with several –NH stretching bands), a peak at 2909 cm^{-1} (-CH stretching), C=O stretching peak at 1655 cm^{-1} due to GlcNAc units; primary amine at 1596 cm^{-1} (NH_2 deformation); at 1420 cm^{-1}, C-N stretch; C-N stretching at 1320 cm^{-1} coupled with N-H plane deformation (Amide III band); O-H plane deformation at 1259 cm^{-1}; 1155 and 896 cm^{-1} bands are characteristic of β(1→4) glycosidic bridge and at 1032 cm^{-1}, C-O-C stretching vibration in the glucopyranose ring (Brugnerotto *et al.*, 2001). The determination of DA was calculated using Amide band III at 1320 cm^{-1} (C-N stretching coupled with N-H in plane deformation) as the analytical band and the band at 1420 cm^{-1} as the internal reference band. The DA was calculated based on the calibration curve established in Brugnetotto´s work (Brugnerotto *et al.*, 2001).

The purified Ch presented a DA of 14.2% (molar fraction of N-acetylated units = 0.142). Considering the literature describing the preparation of Ch-based nanomaterials, the Ch used in this work is in the range of DAs commonly used (12-15%) (Hajdu *et al.*, 2007; Lee *et al.*, 2008). However, it was shown that the lower DA of Ch (≤13%) is favorable for cell adhesion, spreading and proliferation. Additionally, recent studies shown that the lower DA (4%) results in a less intense inflammatory response, when compared to DA of 15% (Amaral *et al.*, 2007; Barbosa *et al.*, 2010; Chatelet *et al.*, 2001).

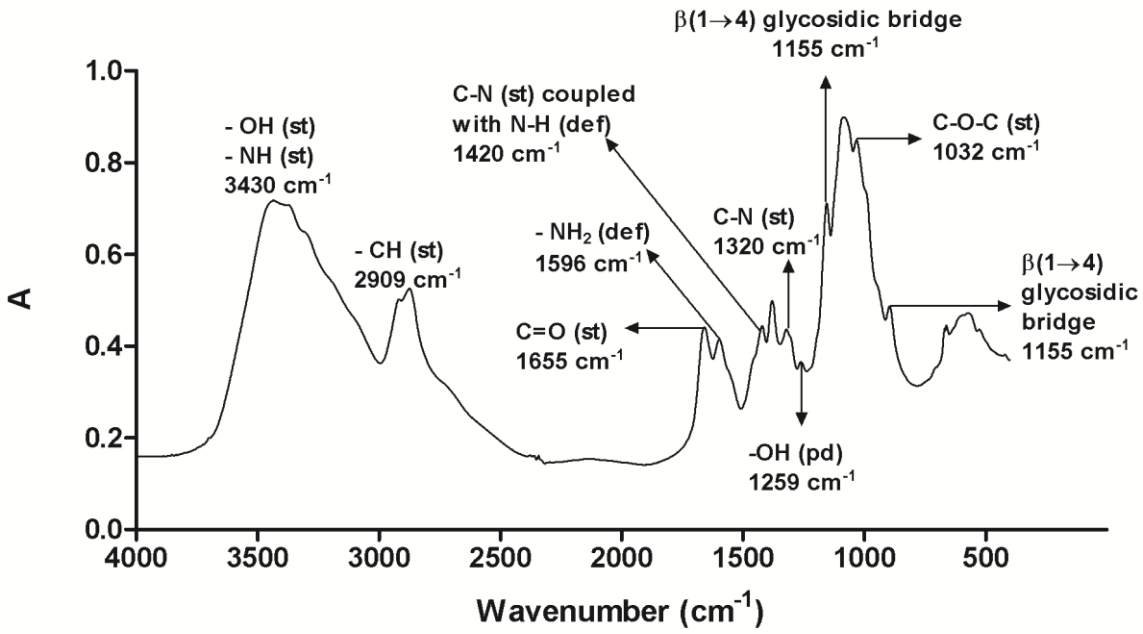

Figure 6. FTIR spectra of Ch in absorbance units. Narrows in the figure are indicative of reference bands for Ch identification. The internal reference band (1420 cm^{-1}) and the analytical band (Amide III 1320 cm^{-1}) for which peak height was estimated, were used for DA calculation (A_{1320}/A_{1420} = 0.3822 + 0.03133).

2. Poly-γ-Glutamic Acid production and characterization

γ-PGA was produced by *Bacillus subtillis*, as previously described (Pereira *et al.*, 2012). By being a product of the biosynthetic activity of this bacteria, this polymer presents an heterogeneous Mw as previously described in the work of Pereira *et al.* (Pereira *et al.*, 2012). Herein, the Mw of the γ-PGA produced, ranged from 50 to 95.5 kDa, with a median value about 65.2 kDa (Figure 7). This Mw was within the range of previously reported Mw of γ-PGA (Ashiuchi *et al.*, 2002), although slightly higher when compared to the one reported in the work of Pereira *et al.*, of 10-50 kDa (Pereira *et al.*, 2012). The smearing bands observed in the SDS-PAGE could correspond to saccharide contaminants and to the presence of salts not completely removed from the sample. The purity of the polymer was not addressed in this work, although previous work from our team has reported a purity grade of 99,5%, using the same purification method (Pereira *et al.*, 2012). The heterogeneity of the polymer Mw is an inherent parameter when using microorganisms for the production of such biopolymers. Furthermore, heterogeneity can be a consequence of the accumulation of γ-PGA depolymerase in the culture medium, which has been reported to be produced by *B. subtillis* during the polymer synthesis,

and produce γ-PGA within a Mw range of 10 to 1000 kDa (Ashiuchi *et al.*, 2002) and by *B. licheniformis* (Birrer *et al.*, 1994). Comparing with the work of Ashiuchi and collaborators (Ashiuchi *et al.*, 1999), where the same purification method was used, the γ-PGA Mw here obtained is within the low end of the Mw range previously reported for *B. subtillis* (10-200 kDa) and is, consequently, less heterogeneous.

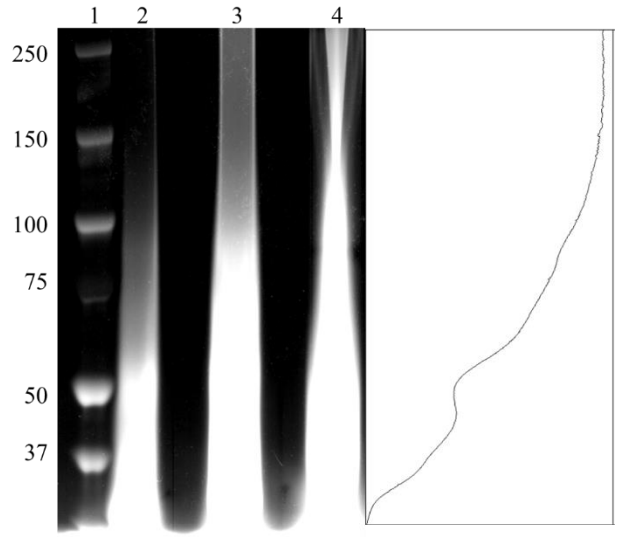

Figure 7. SDS-PAGE for Mw estimation of γ-PGA produced by *B. subtillis*. SDS-PAGE gel stained with Alcian Blue. Different amounts of γ-PGA were loaded in the gel: lane 1) Mw standards (from the top: 250, 150, 100, 75, 50 and 37 kDa); lane 2) 400 µg of γ-PGA; lane 3) 240 µg of γ-PGA and lane 4) 80 µg of γ-PGA. The densitometry profile of lane 1 is shown to illustrate the Mw distribution of the γ-PGA sample.

3. Ch/γ-PGA NPs and Df-NPs characterization with and without cross-linking

Ch/γ-PGA NPs were prepared and characterized based on the previous work of our team (Pereira *et al.*, 2012; Teixeira *et al.*, 2016). NPs were formed spontaneously by electrostatic interaction of Ch amino groups and γ-PGA carboxyl groups. Previously, considering the pK_a of both polymers (γ-PGA = 2.19 and Ch = 6.5), three intermediates pHs (3.0, 4.0 and 5.0) were studied. It was shown that the pH 5.0 was the best pH for the electrostatic interaction of these oppositely charged polymers (Pereira *et al.*, 2012). Besides that, the previous work showed that Ch and γ-PGA were able to form stable NPs using a molar ratio of 1:1.5 (mol Ch : mol γ-PGA).

The same methodology was used in this work and NPs were characterized according to their size, PdI and charge by DLS and by TEM. The results showed Ch/γ-PGA NPs with a

diameter of 171.57 ± 15.09 nm, a low PdI of 0.17 ± 0.05 and a charge of 17.51 ± 2.35 mV (Figure 10).

TEM images provided visual evidence of the NPs morphology and size, in a dry state (Figure 11). Spherical NPs can be observed and the nano size of the complexes was confirmed. The diameter of the NPs was in the range of 100 – 200 nm. As expected, size was slightly different from the obtained from DLS, once these nanosystems can swell in aqueous media. The concentrations of Ch and γ-PGA solutions used, the order of addition and the Ch/γ-PGA ratio were optimized based by Pereira *et al*. (Pereira *et al.*, 2012) based on previous results by Hajdu *et al.* (Hajdu *et al.*, 2007). The Ch/γ-PGA NPs size obtained here and in the work of Pereira *et al.* were more reproducible than those reported in Hadju's study, which were in the range 20 - 285 nm. The NPs prepared presented positive charges, suggesting that a core γ-PGA polymer is surrounded by a positively charged Ch shell ensuring colloidal stabilization, which is in accordance with the literature for these NPs (Lin *et al.*, 2005). The NPs size determined by TEM was in the range of sizes estimated by DLS, although slightly smaller, which can be related with water loss samples preparation for TEM.

The γ-PGA solution was added to the Ch solution with a syringe pump, at controlled speed, ensuring that there was no variability in NPs production in the course of time (Pereira *et al.*, 2012). This methodology allows a more accurate NPs production and to obtain stable and reproducible NPs, with low PdI than the previously reported by Hajdu *et al.* (Hajdu *et al.*, 2007) and present the advantage of using mild conditions without toxic solvents, thus avoiding molecules degradation or potential cytotoxic compounds. Since Ch and γ-PGA interact electrostatically, incorporation of biologically active substances by the same design principle is feasible, without the need to chemically modify them, thus maintaining biological activity, as described in the work of Gonçalves *et al*. (Goncalves *et al.*, 2015).

Herein, following the Ch/γ-PGA NPs preparation, we have also move forward for the preparation of NPs with the incorporation of a well-known anti-inflammatory compound, Df (Roelofs *et al.*, 2008). Ch/Df/γ-PGA (Df-NPs) were prepared at the molar ratio of 21:0.35:1.5 (mol Ch : mol Df : mol γ-PGA) with a mixed solution of Df and γ-PGA being dropped into a Ch solution as previously optimized by our team (Goncalves *et al.*, 2015). Df-NPs were analyzed regarding size, PdI and charge by DLS. The results showed that Df-NPs presents a size of 185.36 ± 8.39 nm, a PdI of 0.25 ± 0.03 and a charge of 22.41 ± 1.28 mV (Figure 10). These values were in accordance to those previously reported by our team (Goncalves *et al.*, 2015).

3.1. Diclofenac entrapment in the Ch/γ-PGA NPs

To assess Df entrapment in the NPs an EE test was performed. Df entrapment was analyzed 1h after Df-NPs preparation, obtaining an entrapment efficiency of Df of 47.5 ± 7.9 %. The values herein described are relatively lower than those obtained in the previous work of the team, which reported an EE of 74.1 ± 2.5 % after 1h (Goncalves *et al.*, 2015). Although lower, the EE demonstrated that Df was being incorporated on Ch/γ-PGA NPs. This difference might be correlated with differences in the Ch and γ-PGA batches, namely relatively to the DA of the Ch. The Ch purified in this work presented an higher DA, of 14.2% when compared to other batches produced previously in our team, of 10.4% (Goncalves *et al.*, 2015) and 11% (Pereira *et al.*, 2012). As a consequence, our Ch presented more acetyl groups and less amine groups, thus resulting in a less positive charges to interact in with the negatively charged Df, that can explain the lower percentage of Df incorporation. Here, the previously described co-acervation method was applied to incorporate Df in Ch/γ-PGA NPs. At pH 5.0 both sodium Df (pK_a of 4.0 (Pourjavadi *et al.*, 2010)) and γ-PGA (pK_a of 2.19) are negatively charged, but when added to Ch, which is positively charged, the electrostatic interaction between Df, Ch and γ-PGA will be promoted. Besides the molar ratio of the components, also their order of addition revealed to be critical to obtain a nano-size particle, as described by other studies (Jintapattanakit *et al.*, 2007). For example, Peng *et al.* described how critic is this parameter to obtain Ch/γ-PGA NPs for DNA delivery (Peng *et al.*, 2009). In the previous study of Gonçalves *et al.* (Goncalves *et al.*, 2015) the incorporation of Df within γ-PGA solution before addition to Ch was the method established to obtain stable NPs and the same methodology was used in this work. Although less amount of Df was incorporated in our Df-NPs, the results obtained suggested that the preparation of the Ch/γ-PGA NPs delivery system containing Df was successful and that this delivery system complexity can be further improved.

3.2. Ch/γ-PGA nanoparticles cross-linking

Ch/γ-PGA NPs and Df-NPs were cross-linked using two different cross-linking agents: EDC (Imoto *et al.*, 2010) and Gn (Fernandes *et al.*, 2013; Li *et al.*, 2016), two cross-linking agents previously used to cross-linking Ch-based materials. In order to address which of the cross-linking agents could be more effective in maintaining NPs properties and increased stability at the physiological pH, both NPs were cross-linked with EDC or Gn and compared in terms of size and PdI (Figure 8). Results showed that both cross-linking agents did not alter significantly the size and PdI at pH 5.0, but at the physiological pH, a significant increase in size was observed (*$p<0.05$*). Interestingly, the PdI values remained low and similar to those

observed at pH 5.0, suggesting that despite a size increase was observed, the sample monodispersity was maintained.

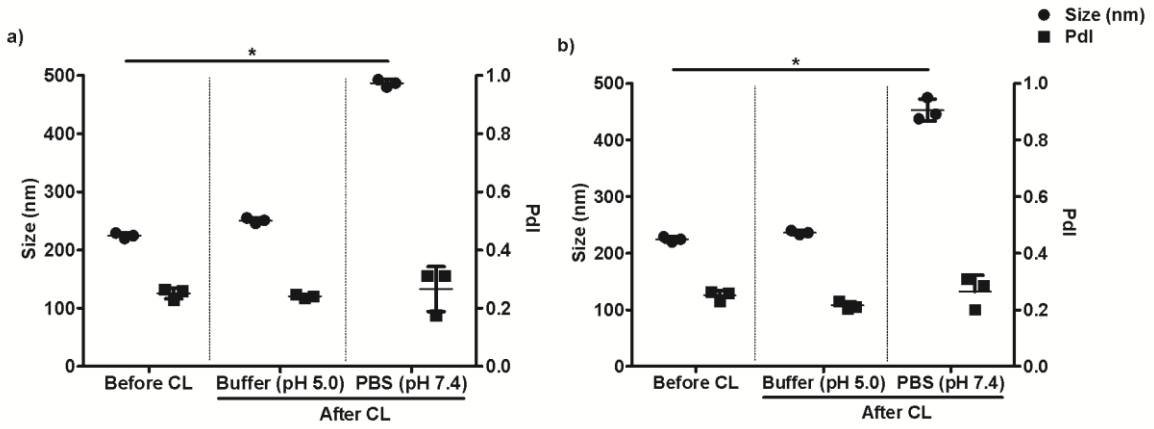

Figure 8. Size and PdI of Ch/γ-PGA NPs cross-linked with a) EDC and b) Gn, before and after CL (pH 5.0 and pH 7.4). Values are presented as a mean ± S.D. (n=3).

Although both cross-linking agent's performance was very similar, both size and PdI of NPs cross-linked with Gn were slightly smaller (452.7 ± 19.7 nm) than those obtained with NPs cross-linked with EDC (486.7 ± 6.4 nm) at pH 7.4, and by consequence, presented a size more similar to the original Ch/γ-PGA NPs and Df-NPs. Additionally, as for size, also PdI was slightly smaller in NPs cross-linked with Gn (0.26 ± 0.06) than for EDC (0.27 ± 0.08), suggesting the presence of monodisperse NPs solutions. Although these differences were very slight, we have chosen to continue this work using Gn over EDC, once Gn is a not only a non-toxic compound (Sung *et al.*, 1999) but also because it is the most commonly used cross-linking agent in for Ch biomaterials (Fernandes *et al.*, 2013; Jin *et al.*, 2004; Li *et al.*, 2016).

3.3. Optimization of Ch/γ-PGA NPs cross-linking with Gn

Aiming to improve not only the Ch/γ-PGA NPs cross-linking with Gn but also their stability at the physiological pH, different concentrations of Gn (1, 10, 20 and 40 mM) and different time-points of incubation (1, 2 and 24h) were tested and compared in what regards to size and PdI (Figure 9). Independently of the concentration and incubation time used, cross-linking with Gn did not altered significantly the size and PdI of the particles when incubated at pH 5.0, in buffer solution (Figure 9 a) and b)). On the other hand, when 10% Gn-NPs (v/v) were incubated in PBS (pH 7.4), a great increase in size was observed, regardless of incubation time, in Gn concentrations of 1, 10 and 40 mM. In these cases, Gn-NPs presented high values of size,

reaching and exceed the double of the size of the initial NPs, in some conditions (Figure 9 c) and d)). At a concentration of 20 mM and 2h of incubation, the best compromise between concentration and time was achieved, the lowest size (298.7 nm ± 27.3) and PdI (0.29 ± 0.04) was observed (Figure 9 c) and d), respectively). To verify this, 25% Gn-NPs (v/v) that resulted from the 1h, 2h and 24h incubation with Gn at 20 and 40 mM (Figure 9 c) and d)) were incubated in PBS (pH 7.4) and analyzed. It was verified that the results were very similar to those obtained using 10% Gn-NPs (v/v) (Figure 9 c) and d)), confirming that a concentration of 20 mM with 2h of incubation, seems to be the optimal concentration and incubation time to achieve stable NPs at the physiological pH (with lower size). Besides that, despite the increasing of size in all PBS conditions, PdI was maintained for 20 mM concentration and 2h of incubation, suggesting that the NPs solution remains monodisperse, suggesting that Gn crosslinking was able to improve NPs stability at the physiological pH.

Using the previously optimized conditions, Gn-NPs were prepared. These particles exhibited, at pH 5.0, a size of 184.45 ± 17.31 nm (Gn-NPs) and of 179.26 ± 5.94 nm (Gn-Df NPs). Gn-NPs presented a PdI value of 0.32 ± 0.09 and a charge of 11.61 ± 2.48 mV (Figure 10). Without presenting any substantial differences, Gn-Df-NPs had a PdI of 0.24 ± 0.04 and a charge of 15.27 ± 1.19 mV (Figure 10).

These results herein presented showed that Df incorporation and the introduction of a cross-linking agent did not alter significantly the size of the NPs. In addition, also PdI did not suffer great variations. However, a significant increase in PdI was observed between NPs and Gn-NPs (***$p < 0.005$) (Figure 10 b)). Moreover, a result near the statistical significance is presented between NPs and Df-NPs ($p=0.06$) suggesting that introduction of Df slightly altered the solution dispersity (Figure 10 c)). The charge of the different nanocomplexes was the parameter that suffer the higher alterations. Although all the nanostructures presented a positive charge, statistical differences were found between Ch/γ-PGA NPs and Df-NPs (*$p<0.05$), and between Gn-NPs and Df-NPs (**$p<0.01$) (Figure 10 c)). Furthermore, the differences between Df-NPs and Gn-Df-NPs were close of the statistical significance ($p=0.05$). Although the variations observed in the charge of the different NPs, all of them were shown to have a positive charge, suggesting an higher capacity of internalization (Cho *et al.*, 2009a).

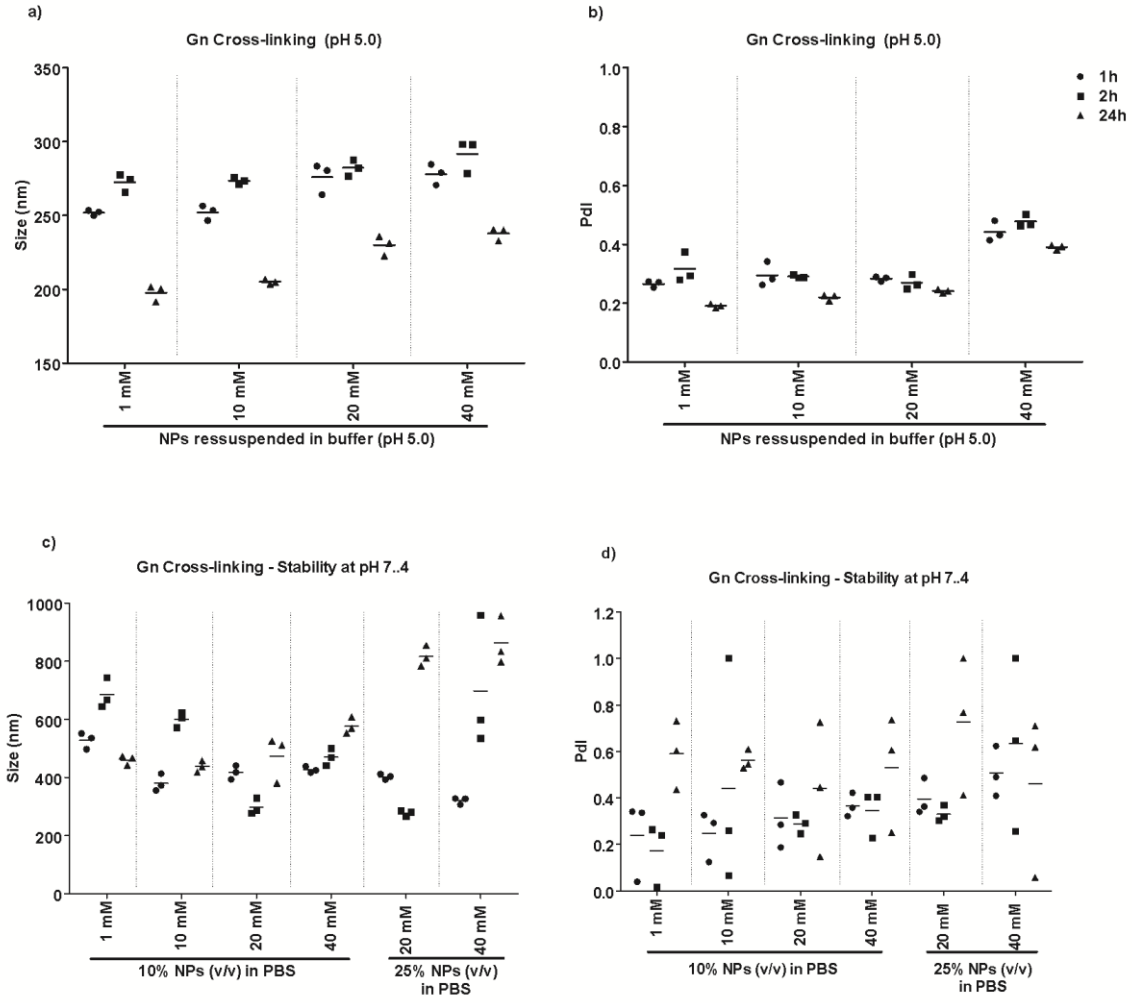

Figure 9. Size and PdI of Gn-NPs at different concentrations and time-points. a) Size and b) PdI of Gn-NPs in buffer; c) Size and d) PdI of 10% and 25% (20 and 40 Mm) Gn-NPs (v/v) in PBS (pH 7.4). Values are mean ± S.D. (n = 3).

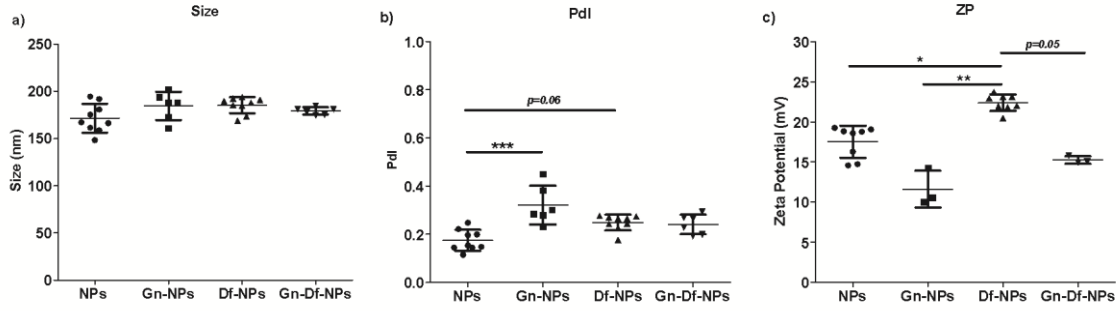

Figure 10. Nanoparticles characterization in terms of size, PdI and charge (Zeta Potential). The a) size, b) PdI and c) charge of Ch/γ-PGA NPs, Df-NPs, Gn-NPs and Gn-Df-NPs were compared. Values are presented as a mean ± S.D. (n = 3 - 9).

The introduction of a cross-linking agent such as Gn was further characterized by Transmission electron microscopy (TEM). For that Gn-NPs morphology was compared to non-cross-linked NPs (Ch/γ-PGA NPs). TEM images (Figure 11) demonstrate that Gn-NPs presented a similar morphology to the Ch/γ-PGA NPs, indicating that Gn cross-linking did not affect significantly NPs morphology. Gn-NPs seemed to have a more spherical morphology than Ch/γ-PGA NPs. This might be explained by the presence of Gn. Furthermore, TEM images showed that Gn-NPs presented a similar size to Ch/γ-PGA NPs, both NPs presented values varying from 166 to 333 nm, measured by TEM.

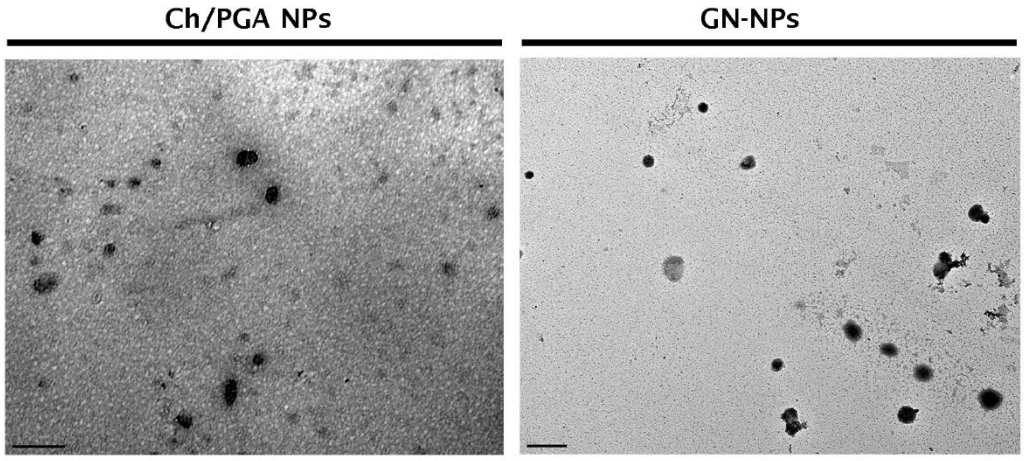

Figure 11. TEM image of Ch/γ-PGA NPs and Gn-NPs. From left to right: Magnification: 80.000x and 25.000x. Scale bar: 200 nm and 0.5 µm. These samples were stained with uranyl.

Cross-linking with Gn was further confirmed by ATR-FTIR analysis. The two spectra of cross-linked and non-cross-linked NPs were compared. A notable alteration in the chemical spectrum of NPs and Gn-NPs in the range from 1000 to 1700 cm^{-1} can be observed (Figure 12). The commons peaks both on Ch/γ-PGA NPs and Gn-NPs are at 3371 cm^{-1} (-OH stretching overlapped with several –NH stretching bands); at 1630 cm^{-1} (hydroxyl groups and attributed to OH-bending) and at 1066 cm^{-1} (C-O-C stretching). Gn-NPs spectrum presents peaks at 2901 cm^{-1} (-C-H aldehydic); a strong peak at 1517 cm^{-1} (NO_2 stretching); a weak peak at 1420 cm^{-1} (C=C aromatic); at 1293 cm^{-1} (C-O-C stretching); at 1150 cm^{-1} and at 1108 cm^{-1} (C-OH stretching). The appearance of a peak at 1420 cm^{-1} is attributable to the ring stretching of the Gn molecule (1500-1300 cm^{-1}) (Fernandes *et al.*, 2013). The peaks at 1597 cm^{-1} and 1574 cm^{-1} do not appear suggesting that cross-linking with Gn on Ch/γ-PGA NPs was successful.

Overall, it was proven that a new chemical modification could be applied to Ch/γ-PGA based NPs without altering the main parameters of these NPs, such as size, PdI, charge and shape.

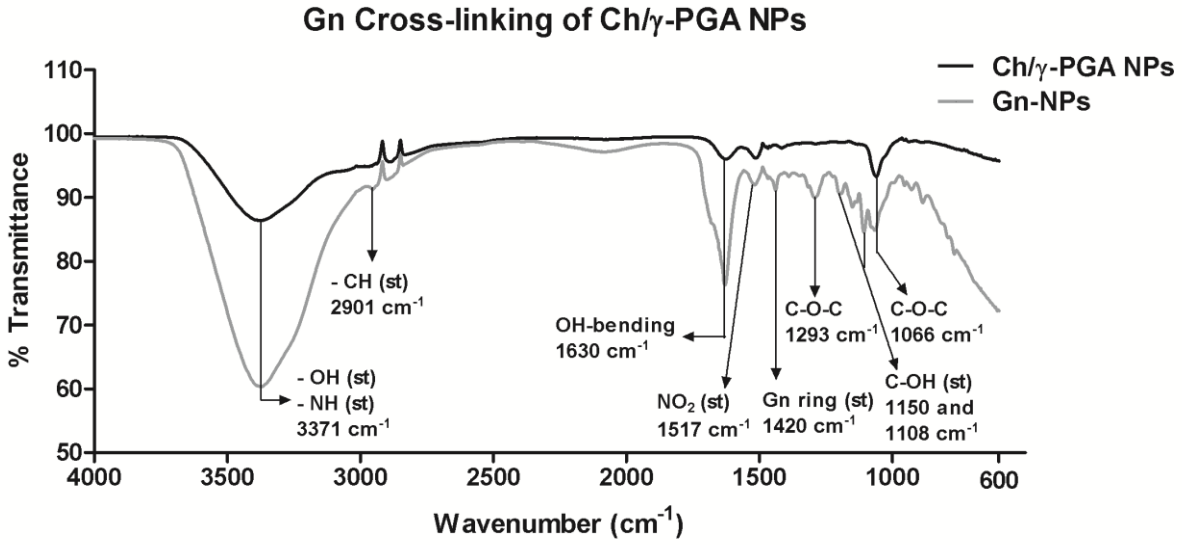

Figure 12. ATR-FTIR spectra of Ch/γ-PGA NPs and Gn-NPs in transmittance.

4. LbL on Ch/γ-PGA NPs, Df-NPs and Si-core NPs

LbL of Ch and γ-PGA has been previously demonstrated by Antunes *et al.* (Antunes *et al.*, 2011) using a 2D system. Here, LbL deposition was attempted in the previously described Ch/γ-PGA NPs and using a Si-core as the base for the LbL build up, aiming at increase/improved Df EE and drug loading in the complexes.

4.1. LbL on Ch/γ-PGA NPs and Df-NPs

Both particles (Ch/γ-PGA NPs and Df-NPs) were previously demonstrated to have a positive charge, therefore, LbL deposition started by the addition of a negative γ-PGA layer, followed by a Ch layer, until 6 layers were achieved. LbL formation was confirmed by alterations in the charge, as demonstrated by the charge alterations (Figure 13). After first layer deposition, charge becomes negative in both cases, indicating that the γ-PGA layer was successfully adsorbed. With the deposition of the second layer (Ch) the ZP becomes positive again. The same trend was followed until 6 layers of polyelectrolyte (3 of γ-PGA and 3 of Ch) were deposited. As defended by Schlenoff *et al.* (Schlenoff *et al.*, 1998), the surface electrical charge reversal allows steady-state increments of oppositely charged polyelectrolyte to the substrates surface, by sequential adsorption steps, which is a requirement for polyion multilayer assembly

driven by electrostatic interactions. Changes in the charge of the NPs were sufficiently large to conclude that electrostatic interaction was responsible for the LbL buildup. Besides charge, also the size and PdI of LbL structures were analyzed during the process (Figure 14 a) and b)). The final structures were analyzed regarding size, PdI and charge after being washed with buffer. LbL of 6 layers on Ch/γ-PGA NPs presented a size of 210.27 ± 38.81 nm, a PdI of 0.88 ± 0.20 and a charge of 24 ± 0.6 mV, while LbL on Df-NPs, a size of 191.93 ± 22.77 nm, a PdI of 0.86 ± 0.11 and a charge of 22.07 ± 1.27 mV was obtained (Figure 14 a)). The size of these new nanostructures was shown to be similar to the both initial Ch/γ-PGA NPs and Df-NPs, but huge variations were noticed in the PdI, suggesting a heterodisperse particles solution. A significant difference in size is patent at the first layer between Ch/γ-PGA NPs and Df-NPs. In Df-NPs case, PdI was significant different among each subsequent layer. In addition, significant differences on PdI between the two last layers of Ch/γ-PGA NPs were observed. This phenomenon can be explained by the fact that Ch/γ-PGA NPs and Df-NPs do not present a perfectly spherical shape, suggesting that layers adsorption do not occur in a regular and homogeneous manner, and consequently, NPs surface becomes more heterogeneous with the increment of the number of layers. Ultimately, this can lead to an incorrect polyelectrolyte deposition. Interestingly, it can be noted that when a layer of γ-PGA is deposited, NPs present a smaller size and a lower PdI value when comparing with Ch layer deposition (Figure 14 a) and b)), suggesting the idea that negative surface charge, promoted by γ-PGA layer outer shell turns LbL on Ch/γ-PGA NPs more stable and lead to a more homogeneous distribution size. These results suggested that LbL could work on both Ch/γ-PGA NPs and Df-NPs, still, further optimizations will be needed to reduce PdI values (solutions heterodispersion/aggregation) and to improve drug delivery, i.e. by increasing the amount of entrapped biological agents. LbL cross-linking with Gn might constitute a good strategy to improve the system dispersity.

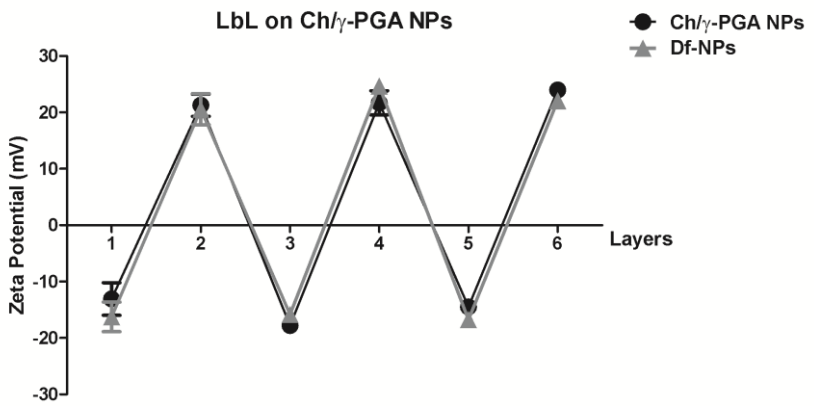

Figure 13. Charge alterations during LbL deposition on Ch/γ-PGA NPs and on Df-NPs. Evolution of the Zeta Potential with the alternate deposition of Ch and γ-PGA as a function of the layer number. Alternatives charges in subsequent layers showed that LbL was achieved successfully. Values are mean ± S.D. (n=3).

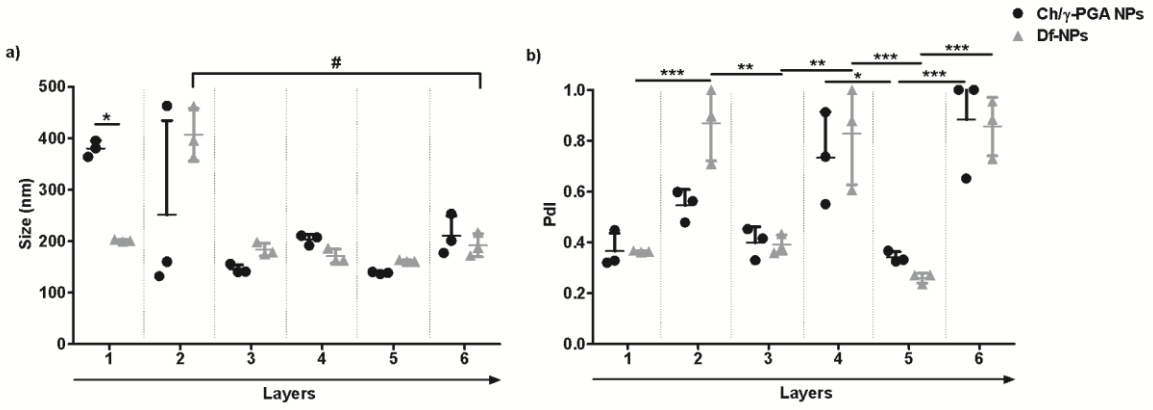

Figure 14. Size and PdI evolution during LbL deposition on Ch/γ-PGA NPs and on Df-NPs. Evolution of the a) Size and b) PdI with the alternate deposition of Ch and γ-PGA as a function of the layer number. Values are mean ± S.D. (n=3).

4.2. Ch/γ-PGA LbL on Si-NPs and Si-A NPs

Before attempt LbL deposition on Si-NPs, stability studies in the commercial Si-NPs (Nanocomposix, Europe) were carried out at pH 5.0 using the commonly used buffer to promote Ch and γ-PGA interaction. Size, PdI and charge were evaluated. Results revealed higher instability at pH 5.0 in the buffer (Figure 15 a)), at different concentrations, suggesting Si-NPs aggregation. This issue boosted us to test other solvent in an attempt to disaggregate Si-NPs, increase stability, and maintain the interaction of the polymers at pH 5.0, for LbL formation. Reviewing the literature, a new solvent that is commonly used to re-disperse Si-NPs appeared.

Several studies suggested the use of 0.5 M NaCl as solvent to work with Si-NPs solutions (Feng *et al.*, 2014; Hu *et al.*, 2015; Yilmaz, 2016). Using the 1 mg mL^{-1}, the concentration with lower values of size and PdI in buffer, the dispersion in the new solvent was attempted. Surprisingly, Si-NPs in 0.5 M NaCl at pH 5.0 presented values similar to those described for normal Si-NPs dispersion in what concerns to size and PdI (Figure 15 a)). This solvent became a potential solvent for Si-NPs (Figure 15 a)). Using the same concentration, different solvents were used to test stability of Si-A NPs. Interestingly, a different trend was observed, although a slight decrease in size was observed in buffer, size was still very high and PdI suggests a heterodisperse solution (Figure 15 b)), indicating NPs aggregation. Similarly to Si NPs, Si-A NPs aggregation seems to occur both in Milli-Q water and NaCl solution. In what concerns to the charge of Si NPs and Si-A NPs, we have noticed that regardless of the solvent, particles were negatively and positively charged, respectively (Figure 15 c)).

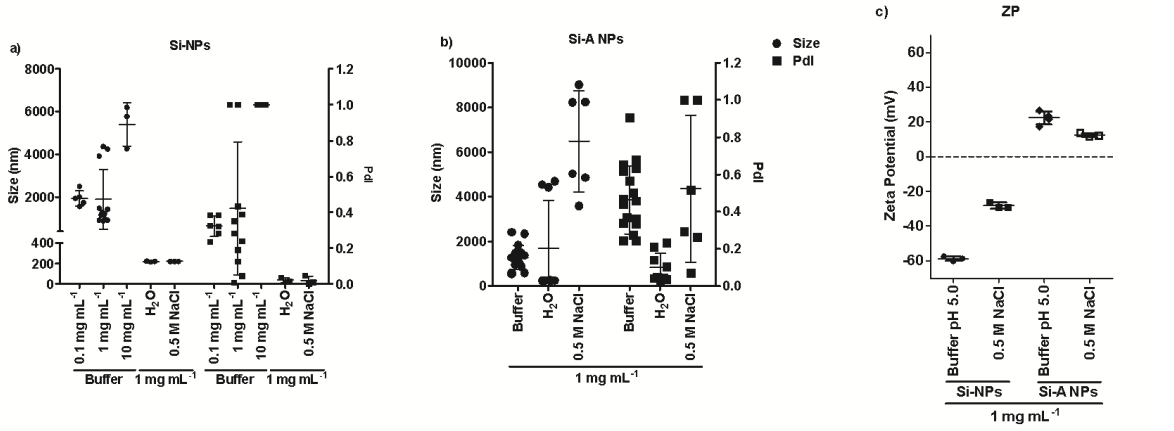

Figure 15. Si-NPs and Si-A NPs characterization in terms of a) size, b) PdI and c) charge. This characterization was performed at various concentrations and various solvents at pH 5.0: buffer, H_20 Milli-Q and 0.5 M NaCl.

Following this first assessment regarding NPs stability, we aimed to address whether this solvent (0.5 M NaCl) allowed LbL deposition in the different NPs. For that purpose, we have performed the deposition of one layer of polymer, depending on the charge of each type of NPs: Si-NPs were dispersed in 0.5 M NaCl and Si-A NPs in both Milli-Q water and 0.5 M NaCl. All the solutions were prepared at concentration of 2 mg mL^{-1}. Although in the first screening, Si NPs performed better in this solvent when compared to the Si-A NPs, in what concerns to stability, in the case of LbL deposition, we observe that after the first layer deposition, Si-A NPs in 0.5 M NaCl, showed lower size values when compared to the Si NPs (Figure 16 a)),

suggesting that the adsorption of one layer of polymer, in this case γ-PGA, reduced size and solution heterogeneity (Figure 16 b)) as observed in the LbL deposition on Ch/γ-PGA NPs (Figure 14).

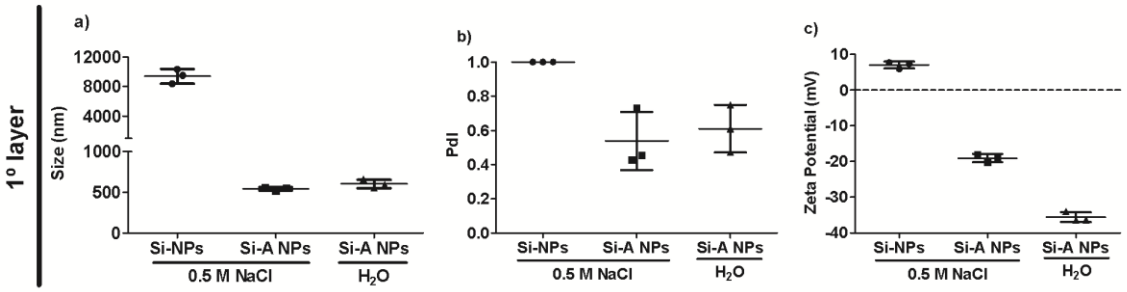

Figure 16. Characterization of Si-NPs and Si-A NPs with the 1ª layer of Ch and γ-PGA, respectively, in terms of a) size, b) PdI and c) charge. This characterization was performed at 2 mg mL^{-1} in 0.5 M NaCl and H_2O Milli-Q, both at pH 5.0.

To consolidate the previous result, LbL on Si-NPs and Si-A NPs was performed until reach the 2ª layer of Ch. Three concentrations were tested to Si-NPs (0.5, 1 and 2 mg mL^{-1}) and two to the Si-A NPs (0.5 and 1 mg mL^{-1}) in 0.5 M NaCl. LbL on Si-NPs and Si-A NPs was verified by analysis of charge alteration after each layer adsorption. The results obtained from this analysis indicated that LbL ran successfully in both NPs and concentrations tested, with an oscillating effect on the charge as the adsorption of polymer layers with alternate charge (Figure 17).

Although the charge alterations lead us to assume LbL occurred successfully, when observing these structures on TEM, we observed that polymer deposition did not occur homogenously around the Si/Si-A core (Figure 19). To confirm this, Si-NPs and Si-A NPs with three and four layers of polymer, respectively were subjected to Si-core removal to address the formation of the LbL structure on the Si/Si-A template.

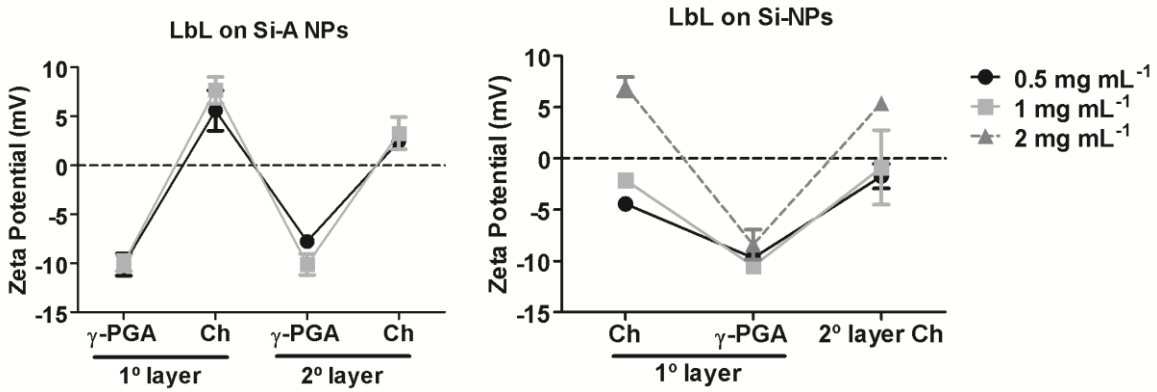

Figure 17. LbL on a) Si-A NPs and on b) Si-NPs. Evolution of the ZP with the alternate deposition of Ch and γ-PGA as a function of the layer number. To Si-NPs three different concentrations were tested (0.5, 1 and 2 mg mL^{-1}), starting with a Ch layer, reaching three layers. In the case of Si-A NPs, two concentrations were tested (1 and 2 mg mL^{-1}) until four layers were obtained.

4.2.1 Si-core removal from LbL nanocomplexes

Si-NPs and Si-A NPs with three and four layers of polymer, respectively (Figure 18), were subjected to Si-core removal following a previously described protocol (Imoto *et al.*, 2010). Size and PdI after Si-core removal was evaluated by DLS and by TEM. High values of size (>500 nm) were observed in Si-NPs and Si-A NPs after Si-core removal. These values were higher than the size of any of the nanostructures developed in this work (Ch/γ-PGA NPs, Gn-NPs and Df-NPs). Si-NPs present a smaller size than Si-A NPs (664.2 ± 104.2 nm and 792.3 ± 85.6 nm, respectively), after Si-core removal. The same trend was observed regarding the PdI values, where in the case of Si-NPs a PdI value of 0.30 ± 0.20 was obtained, compared to the 0.44 ± 0.06 obtained from Si-A NPs. These results suggest that LbL on Si-A NPs exhibit an higher stability than LbL on Si-NPs. Moreover, LbL Si-A NPs was performed until reach a total of 4 layers, having one more polymer layer, could explain the higher size, although a less variable PdI reported.

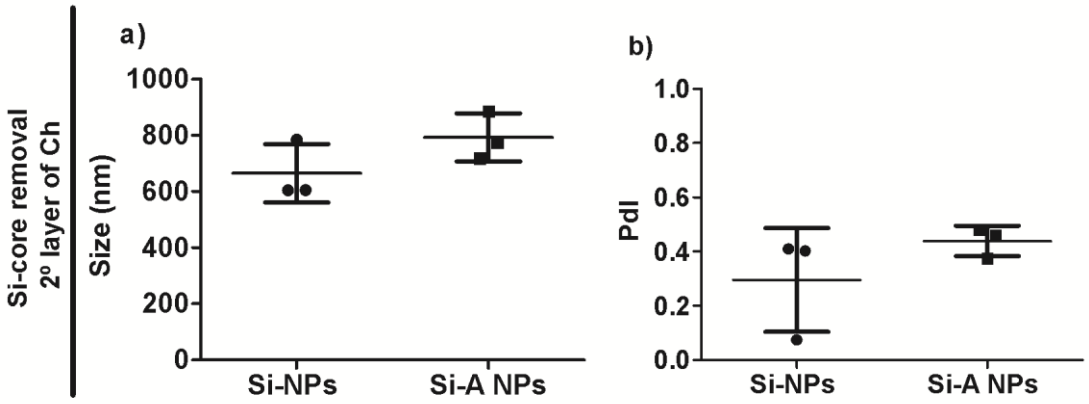

Figure 18. LbL deposition on Si-NPs and Si-NPs (3 layers and 4 layers, respectively). Characterization in terms of a) size, b) PdI after Si core removal.

TEM images of Si-core removal on Si-NPs and Si-A NPs, with a reaction time of 10 min, reveals that Si-core was effectively removed (Figure 19), as no Si or Si-A NPs can be observed in the samples. Unfortunately, TEM images did not reveal the appearance of the layers. This result gives evidence that layers deposition did not occur homogenously around the Si-core, or might have disappeared during Si-core removal protocol. On the other hand, we have also to have in consideration that the number of layers could not be enough to: 1) be observed by TEM or 2) stand cohesive and maintain the spherical shape of the polymers layers that covered the Si-NPs and Si-A NPs surface after Si-core removal, due to their thin wall and Ch swelling in aqueous solution as suggested by Li *et al.* (Li *et al.*, 2016).

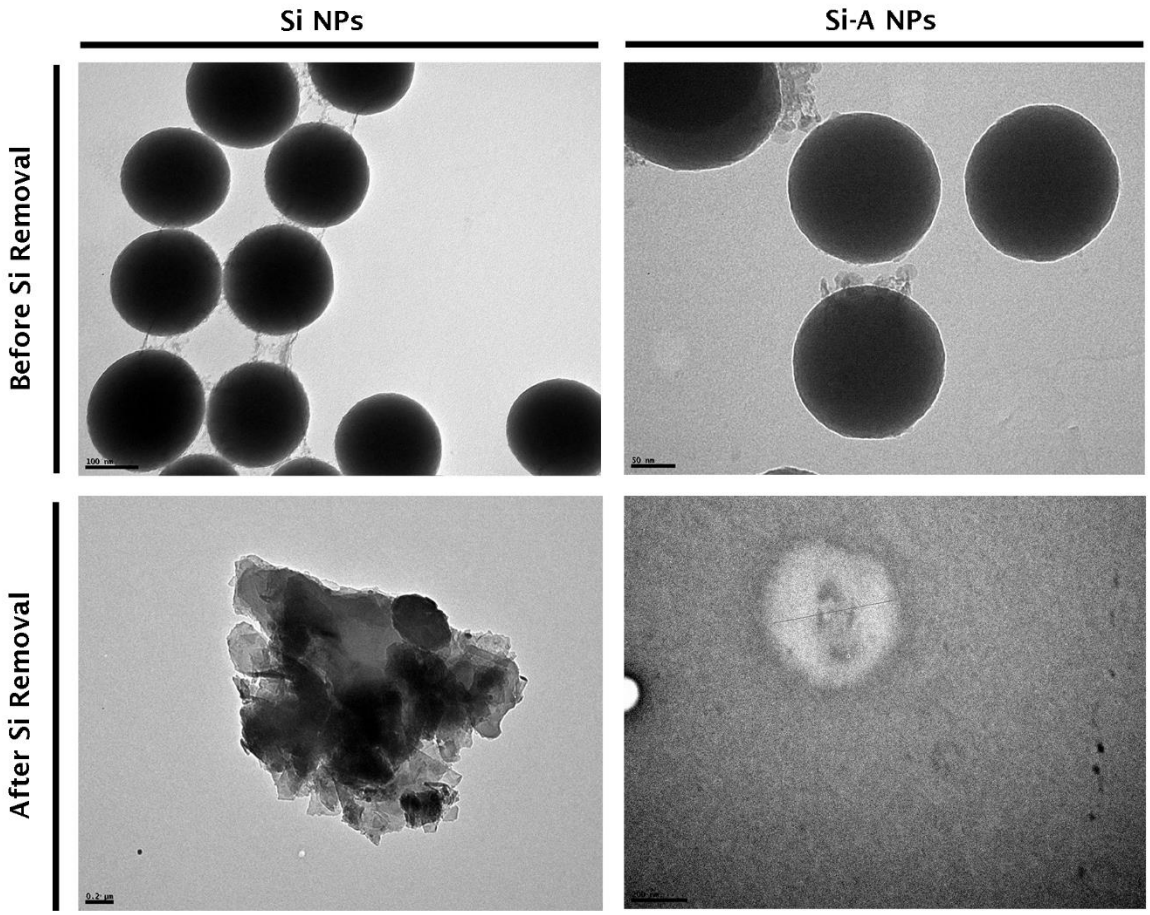

Figure 19. TEM images from Si-NPs with 3 layers and Si-A NPs with 4 layers, before and after Si-core removal (10 min). From left to right: Magnification: 150.000x, 250.000x, 40.000x and 80.000x. Scale bar: 100 nm, 50 nm, 0.2 µm and 200 nm.

To discard the hypothesis of the low number of layers, we performed a new study where LbL was performed up to 12 layers. This approach was tested exclusively on Si-A NPs. It was expected that by increasing the number of layers, they would become more cohesive and stable, preventing the structure from collapse. Si-A NPs were dissolved in 0.5 M NaCl at a concentration of 1 mg mL^{-1} and the LbL deposition was performed as described in Materials and Methods section. LbL on Si-A NPs with 12 layers of polymer were analyzed by TEM. TEM images suggested NPs aggregation and again, polymer deposition in-between the Si-A NPs and not around the Si-A template. To address this hypothesis, Si-A core removal was performed. TEM images (Figure 20) revealed that Si-core removal reaction during 10 min was, in this case, insufficient to remove all the Si-A NPs. Although Si-A NPs presented a lighter color, they could still be observed in the samples, suggesting the need to perform the removal

with additional time as the 10 min could not be enough, and the greater number of layers could have hampered the complete removal of the Si-A core.

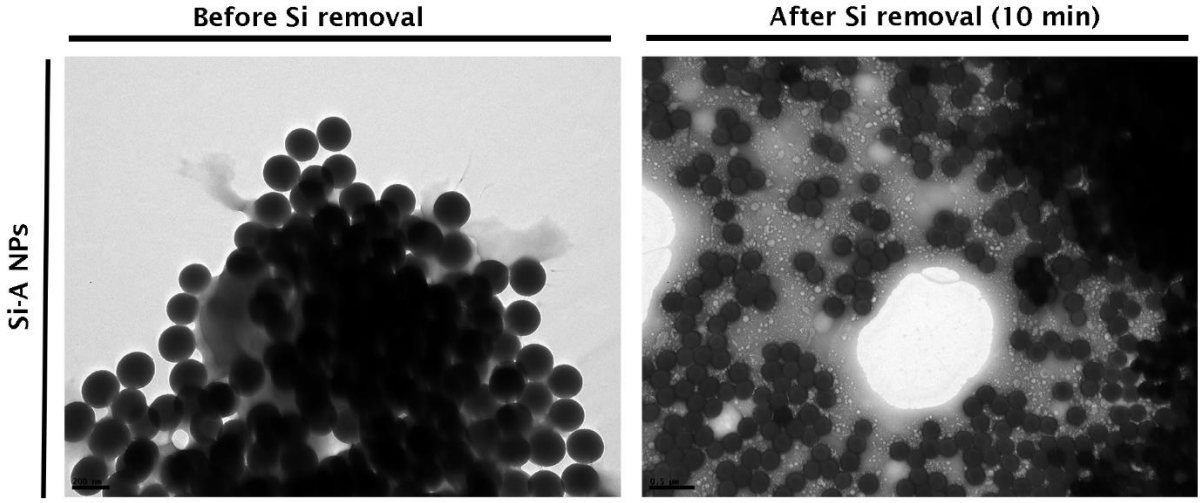

Figure 20. TEM images from Si-A NPs with 12 layers before and after Si-core removal (10 min). From left to right: Magnification: 50.000x and 25.000x. Scale bar: 200 nm and 0.5 µm.

A removal time of 1h and 2h was tested on Si-A NPs with 6 layers of polymers (less layers were used due to materials constrains (amount of γ-PGA)). Additionally, cross-linking with Gn was performed, as described in the work of Li *et al.* (Li *et al.*, 2016), following the same method described to Ch/γ-PGA NPs and Df-NPs. Cross-linking with Gn was employed to certify that after removal of the sacrificial core, the layers deposited were still present and with the same spherical conformation, therefore preventing collapse as observed in the work of Li *et al.* (Li *et al.*, 2016). Gn is expected to cross-linking the Ch chains and tighten the wall by reducing the swelling ratio and slow down the degradation rate (Li *et al.*, 2016). TEM images revealed that after cross-linking with Gn, LbL on Si-A NPs with 6 layers, presented a morphology and a conformation similar to the LbL nanocomplexes obtained before indicating that cross-linking did not change the shape of these nanocomplexes (Figure 21). After removal of the sacrificial template for 1h, we observed a structure with an irregular shape and a translucent aspect, which we assume to correspond to the layers of polymers that were adsorbed to the Si-A NPs surface. Here, the preservation of the layers of polymers seemed to be promoted by the cross-linking with Gn that kept the initial conformation and prevented the collapse (Figure 21).

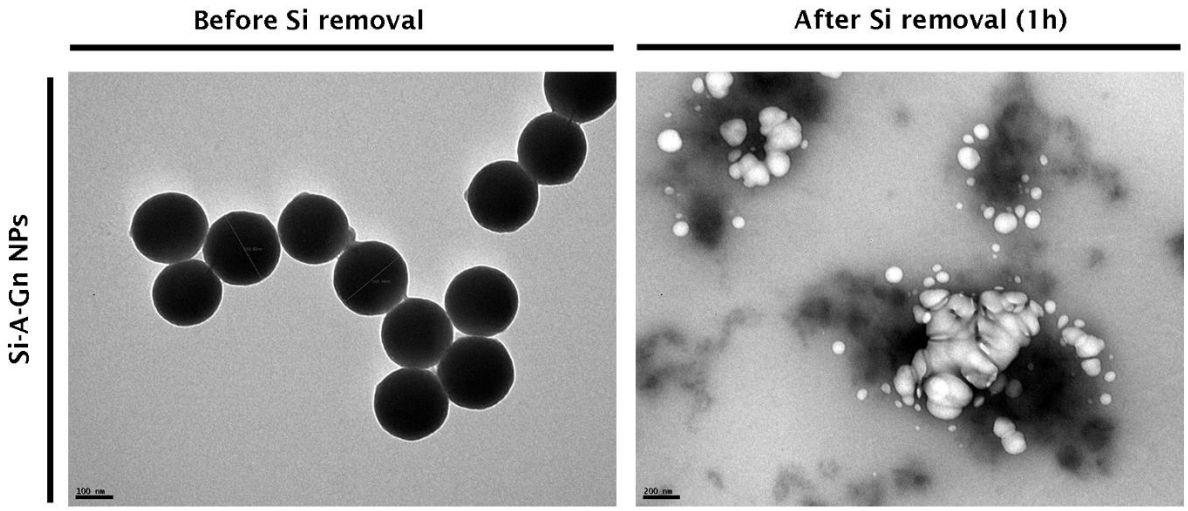

Figure 21. TEM images from Si-A NPs cross-linked with Gn, before and after Si-core removal (1h). From left to right: Magnification: 100.000x and 50.000x. Scale bar: 100 nm and 200 nm.

However, some debris of Si-A NPs remains on the suspension even after the washes performed, which could mean that 1h is not sufficient time to remove both all the Si-A particles and Si-A NPs debris. Despite the increase of reaction time (2h), the removal was not as successful as with 1h (data not shown). A possible explanation for this could be based on the aggregation of Si-A NPs that was observed. Indeed, aggregation was a constant problem in all experiments involving Si-NPs and Si-A NPs, that throughout this study we were unable to solve. Moreover, we could not fully confirm LbL homogenous deposition on these structures, which can also be a consequence of the particles aggregation, but also due to the unstable behavior of these particles at low pH, an important requirement of Ch and γ-PGA interaction. Future studies should be focused on testing methods capable of maintain both Si-NPs and Si-A NPs stable and that prevents the aggregation of these NPs. The agglomeration could be avoid by changing the dispersion media (Tadano *et al.*, 2014) and/or by incorporating Si-NPs and Si-A NPs into PS shells via emulsion polymerization (Hubner *et al.*, 2018). Furthermore, a study performed by Zhao and colleagues (Zhao *et al.*, 2015), describes the use of a new emulsification technique utilizing a hydrophobic silica precursor polymer, hyperbranched polyethoxysiloxane (PEOS), for efficient stabilization of oil-in-water emulsions without any additional classical surfactants due to its hydrolysis-induced interfacial activity, achieving a monodispersed solution Si NCs with almost 100% encapsulating efficiency. Other alternatives should be attempted to the increment of Si-NPs stability, such as the surface modification with

hydrocarbon groups, such as methyl, vinyl, propyl, phenyl and octyl. These groups play several important roles in the biomedical field applications of Si nanocapsules and their functionalization allows to increase of hydrophobicity and to improve the particle dispersion by effectively preventing interparticle agglomeration (Zhang *et al.*, 2015). Unfortunately, LbL on Ch/γ-PGA NPs and on Si-A NPs did not gone to further studies, such as stability at different pHs, Df release and *in vitro* tests, since we were unable to obtain, in the time course of this thesis, a reliable and replicable 3D LbL system on NPs.

4.2.2. Si-NPs Amination

Due to the initial issues of Si-NPs aggregation and poor stability at low pH, a parallel study was conducted to aminate, in our lab, the Si-NPs. A previously described protocol was applied based on the work of Roy *et al.* (Roy *et al.*, 2010). Aminated Si-NPs (Si-A NPs*) size, and PdI was evaluated both in buffer and Milli-Q water and at concentrations of 0.1 and 1 mg mL^{-1}, respectively (Figure 22 a)). Results from Si-A NPs* showed that a decrease on charge relatively to the original Si-NPs occurred. The charge from Si-A NPs becomes negative (Figure 22 b)). However, size and PdI analysis revealed that NPs aggregation continued to occur. Comparing the results obtained for size and PdI of Si-A NPs* with the commercial Si-A NPs, it was verified that Si-A NPs* present a smaller size (1393 ± 354 nm) than commercial Si-A NPs (1679.9 ± 2153.4 nm). However, the opposite tendency was observed to the PdI, where Si-A NPs* present a higher PdI (0.36 ± 0.20) than Si-A NPs (0.10 ± 0.08). A statistical difference was found on the charge, between Si-A NPs* at 0.1 mg mL^{-1} in buffer and 1 mg mL^{-1} in Milli-Q water ($p < 0.05$). Besides the higher charge value was obtained to the lower concentration (0.1 mg mL^{-1}), this significant difference can be attributed to the solvent, since that the salts present in the buffer could interact with Si-A NPs*, and consequently, increase the charge. These results suggest that Si-A NPs* forms smaller (still enormous comparing to the nanoscale used in this work), but more heterogeneous aggregates than commercial Si-A NPs.

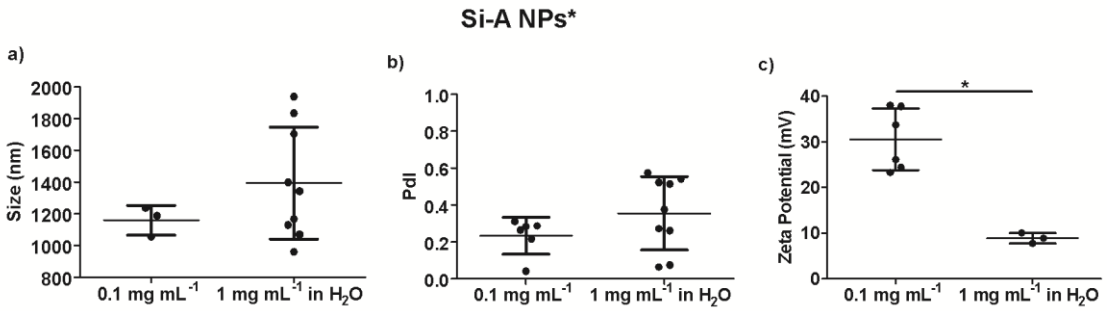

Figure 22. Si-A NPs* characterization in terms of a) size and PdI and b) charge. This characterization was performed at 0.1 mg mL^{-1} in buffer and 1 mg mL^{-1} in Milli-Q water, at pH 5.0.

Amination was confirmed by ATR-FTIR (Figure 23). The obtained results proved that amination of Si-NPs occurred. Contrarily to 2h spectrum, 12h of amination spectrum presented differences comparing to the Si-NPs spectrum, indicating the alteration on the chemical structure of the sample, namely on the nanoparticles surface. The common peaks to the three structures are at 3305 cm^{-1} (C-H stretching) and at 1635 cm^{-1} (C=C alkene). Si-A NPs for 12h spectrum presents a peak at 2883 cm^{-1} (-C-H stretching). A peak at 1105 cm^{-1} (C-O stretching) is observed for Si-NPs and Si-A NPs* for 2h. The absence of this peak in the Si-A NPs for 12h spectrum suggests that Si-NPs surface was attached with NH_2, confirming amination. According to Roy *et al.* (Roy *et al.*, 2010), it was expected to observe peaks between 1300 and 1700 cm^{-1}, both at 2h and 12h, in order to prove amination. Further studies should test new times and ratios of APTMS in order to aminate Si-NPs successfully. Although amination has occurred successfully, when analyzing size and PdI from Si-A NPs it was found that these modified Si-NPs still to aggregate and was unstable both in buffer as in Milli-Q water (Figure 22).

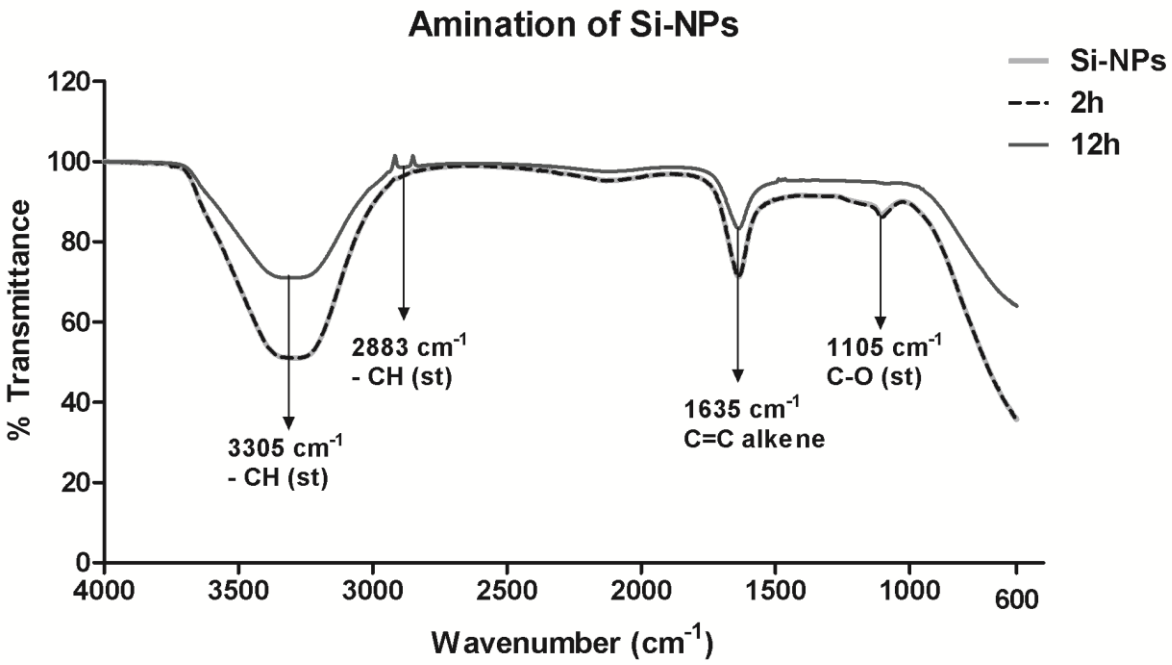

Figure 23. ATR-FTIR spectrum of Si-NPs Amination.

5. Nanostructures Stability up to 3 weeks

Stability of Ch/γ-PGA NPs, Df-NPs, Gn-NPs and Gn-Df-NPs were analyzed at 1, 2 and 3 weeks after preparation by DLS, regarding size and PdI. The different NPs stability was evaluated at different pHs: pH 5.0 (optimal electrostatic interaction of Ch/γ-PGA), pH 6.2 (severely degenerated intervertebral disc environment), pH 6.8 (mild degenerated intervertebral disc environment) and pH 7.4 (physiological pH and non-degenerated intervertebral disc environment), based on (Li *et al.*, 2012; Razaq *et al.*, 2003). For pH 5.0, nanostructures were maintained in buffer solution, and for pH 6.2, 6.8 and 7.4 were placed in PBS at the correspondent pH. The results are expressed on the graphics of Figure 24.

All the nanostructures analyzed here demonstrated to be stable at pH 5.0 during the 3 weeks, presenting the same size after preparation and until the end of the study, and a PdI that did not exceed 0.3, suggesting the existence of a monodisperse solution of NPs. Furthermore, it was observed that when pH increases, Ch/γ-PGA NPs appeared to aggregate. Contrarily, Df-NPs were very stable in all pHs studied among the 3 weeks, with the exception of pH 7.4. This high stability could be explained based on the chemical structure and charge of these NPs. Df-NPs presented the higher charge value, of 22.4 ± 1.3 mV (Figure 10) when compared to all the other nanocomplexes studied, this value is the closest to the one described for stable NPs, of |30 mV| (Clogston *et al.*, 2010). Regarding Gn-NPs and Gn-Df-NPs, it seemed that stability was

improved when compared to Ch/γ-PGA NPs, but not Df-NPs. Although, the peak observed for PdI at 1w (Figure 24 g) and h)) for Gn-NPs and Gn-Df-NPs.

At pH 6.2 the results suggested that Ch/γ-PGA NPs and Df-NPs also presented a stable conformation, with size and PdI similar to those obtained for pH 5.0, with the exception of the Ch/γ-PGA NPs' PdI at 2w and 3w, where an increase on this value was observed. In the case of Gn-NPs, increased size and PdI was observed in most of the time-points for pH 7.4, 6.8 and 6.2, when comparing with pH 5.0. For Gn-Df-NPs, a decrease in size was observed at 1w and 2w, comparing with 0w, in contrast to the increment at 3w. However, the high PdI values observed suggested the presence of a heterogeneous population in pHs higher than pH 5.0. Regarding size, these data suggests that Gn-Df-NPs are more stable at pHs lower than pH 7.4. Overall, as time goes by, nanostructures seemed to become more unstable, with the exception of Df-NPs that were very stable over the 3w. Finally, at pH 7.4, all the nanostructures were unstable along the 3w. Summarily, all the nanostructures were more stable as closer was the solution pH's to the pH 5.0, that corresponds to the optimal electrostatic interaction between Ch and γ-PGA. From all nanostructures, Df-NPs were the ones that were more stable for all the time-points at pH 5.0, 6.2 and 6.8. On the other hand, at pH 7.4, Gn-NPs and Gn-Df-NPs were stable immediately after contact with pH 7.4 (0w), but the size increases progressively with time, accompanied by several alterations of the PdI values.

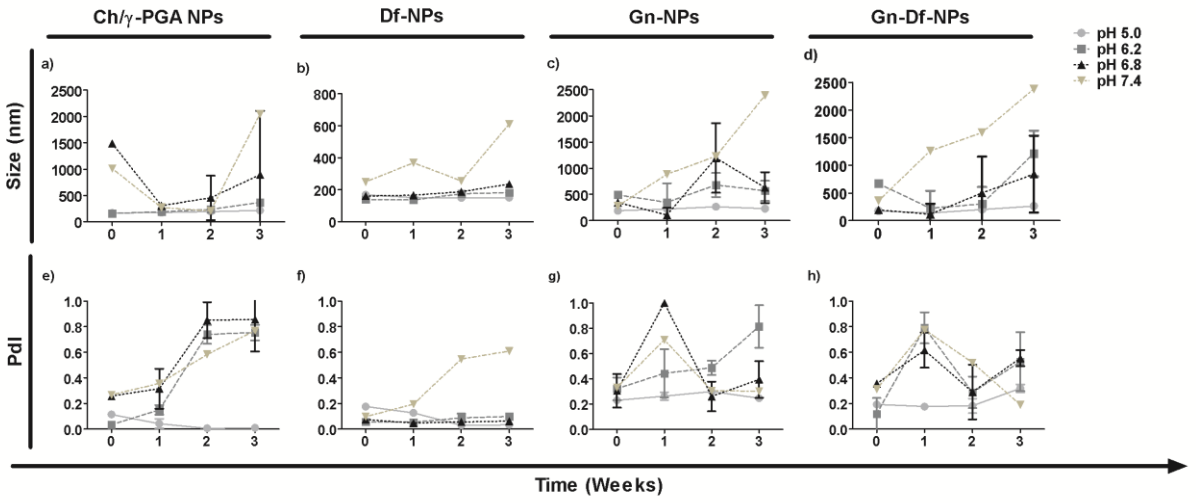

Figure 24. Stability of Ch/γ-PGA NPs (a) and e)), Df-NPs (b) and f)), Gn-NPs (c) and g)) and Gn-Df-NPs (d and h)) up to 3 weeks. Stability was analyzed regarding size (upper graphics) and PdI (downer graphics) of the nanostructures (n = 3).

6. Diclofenac release from Df-NPs and Gn-Df-NPs

Df release from the nanostructures is an important assay to verify which nanostructure is capable of deliver more amount of drug and in a controlled manner. In first screening, the release profile of Df in both Df-NPs and Gn-Df-NPs was performed during 72h at RT, and was measured through the absorbance of Df, as described for Df EE, and using an ELISA kit. Following this first screening, Df release behavior was afterwards evaluated up to 3 weeks, at 37ºC.

These results showed that at pH 6.2, release of Df from Gn-Df-NPs is practically null. From Df-NPs, a decrease on release rate of Df can be observed (Figure 25 a) and d)). For pH 6.8, the percentage of Df released from Df-NPs is identical to those obtained at pH 6.2, although a slightly lower % is revealed by ELISA when compared to the quantification by absorbance. The lower values of Df released from Df-NPs are registered at pH 7.4, where a constant rate was observed. Regarding the release from Gn-Df-NPs, the percentage of released Df was in general lower than those observed for the Df-NPs, in both methodologies, namely at lower pHs. In contrast, at the physiological pH (pH 7.4), some samples presented higher values of Df release were obtained in Gn-Df-NPs when compared to lower pHs (Figure 25 c) and f)).

These results suggest that in degenerative conditions (lower pHs), the electrostatical interaction of the polymers is not disrupted, because NPs present a similar size, especially among the two first weeks at pH 6.2 (Figure 24), namely in the case of Df-NPs (Figure 24 b)) and as consequence, Df is not released. Moreover, is suggests that Gn cross-linking favors the NPs stability. A different trend is observed at the physiological pH, where the % of Df release slightly increases being higher than the release registered at pH 6.2 and pH 6.8.

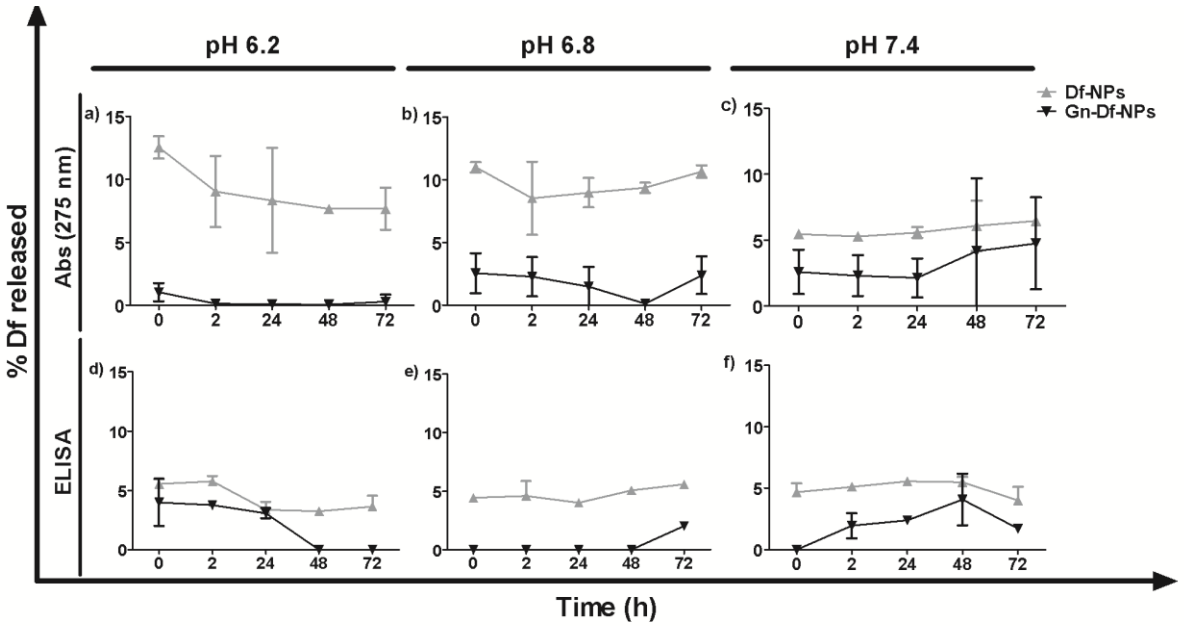

Figure 25. Diclofenac release profile from Df-NPs and Gn-Df-NPs analyzed by Abs (275 nm) at a) pH 6.2, b) pH 6.8 and c) pH 7.4; and by ELISA at d) pH 6.2, e) pH 6.8 and f) pH 7.4, during 72h, at RT.

The long-term analysis during 3w at 37ºC showed that both Df-NPs and Gn-Df-NPs, at pH 6.2, presented an increased Df release during time, being the release rate more pronounced in Df-NPs (Figure 26 a)). The same trend was observed for pH 6.8 and pH 7.4. This long-term study of Df release demonstrates that without Gn (Df-NPs), Df release occurs slowly in the first hours (up to 72h, as demonstrated in Figure 25), but increases after 1w of incubation, with a progressive increase of Df amount released. In the case of Gn-Df-NPs, since the long-term analysis of the stability demonstrated higher variations in size and PdI, a higher Df release was expected here. Contrarily to this, these results showed that in these nanostructures it is likely that more time is need for Df release, or polymers degradation (in an *in vivo* situation). Previous work of our team analyzed the Df release of Df-NPs at pH 7.4 and showed that a high amount of Df was immediately released, and a steady state was achieved after 2h, with a maximum Df release of 81% (Goncalves *et al.*, 2015). Here, a similar maximum value was obtained for Df-NPs (73%), but only after 3w (Figure 26 c)). These Df release studies can be complemented by the stability study mentioned above. It is our believe that NPs release the Df when the electrostatically interaction is dismantled, which supposed to happen at pHs higher than pH 5.0. Following this idea, it can be considered that NPs are disintegrated more extensively at pH 7.4 and less at pH 6.2, and subsequently, release more Df at pH at 7.4 than at pH 6.8 and 6.2,

respectively. This hypothesis was validated at 3w, where a higher % of Df release was achieved, at pH 7.4 than at pH 6.2, both from Df-NPs and Gn-Df-NPs (Figure 26). Moreover, a higher amount of Df was released from Gn-Df-NPs at pH 7.4 than at pH 6.2 on the short-term analysis (Figure 25).

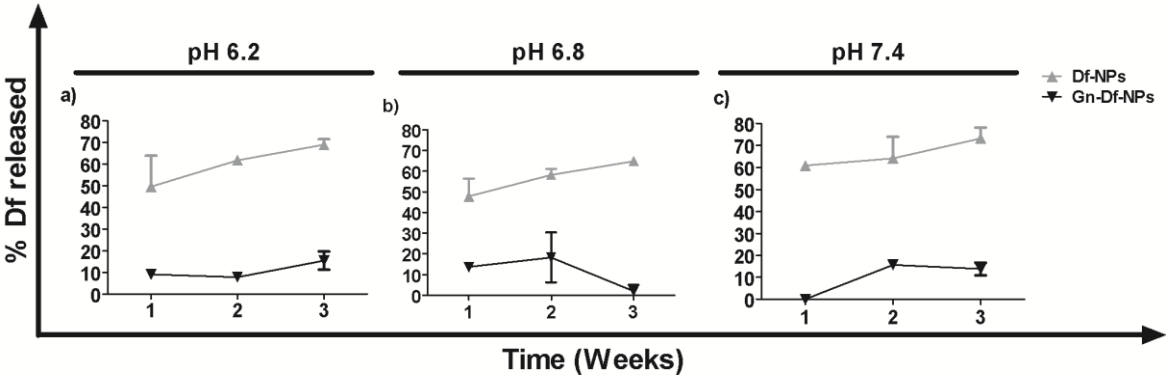

Figure 26. Diclofenac release profile from Df-NPs and Gn-Df-NPs over 3 weeks, at a) pH 6.2, b) pH 6.8 and c) pH 7.4, at 37ºC.

Overall, these results prove that Gn-Df-NPs can control the Df release, producing a slower effect when compared to Df-NPs, in all the conditions tested. The Gn cross-linking is the most reasonable explanation to the slower release of Gn-Df-NPs, once that change chemically the NPs structure, making them less susceptible to release Df. This result is in agreement with a work of Khan *et al.* (Khan *et al.*, 2016). The authors demonstrated that Gn cross-linking of gelatin NPs allowed it to act as a swelling controlled drug release system, maintain the capacity of loading an anticancer drug (cytarabine) and released it in a desirably controlled manner. Moreover, they also found that an optimum drug release was obtained near physiological pH while lower release was observed in basic pH range (Khan *et al.*, 2016). This observation corroborates the result obtained in this study. Therefore, results suggest that Gn-NPs could be a good delivery system in cases where a slower and sustained release is needed, such as cancer (Bikiaris *et al.*, 2007; Khan *et al.*, 2016; Nakagawa *et al.*, 1998; Tufail *et al.*, 2018). In addition, *in vivo* applications of Gn-based nanomaterials exhibited excellent biocompatibility, biodistribution and degradation characteristics (De Clercq *et al.*, 2016).

Furthermore, the results reported above showed a high stability of Df-NPs at pH 5.0, 6.2 and 6.8 (Figure 24). This high stability can be correlated with the high percentage of drug release observed at pH 7.4 when compared to pHs 6.2 and 6.8 during 3 weeks (Figure 26). This correlation implicates that Df-NPs only releases Df *in vivo* at pH 7.4, which means that this

nanosystem might not work in mild to severe degenerated IVDs, due to the low pH of the microenvironment. This can justify the results obtained by our team in an ongoing *in vivo* study, where the anti-inflammatory effect of Df-NPs was not observed, upon delivery of these NPs in degenerated rat IVDs, and in turn, an exacerbated inflammatory response was described (data not published).

7. Evaluation of Nanostructures Cytotoxicity and Immunomodulation potential

7.1. Nanostructures Cytotoxicity and Metabolic activity

The different nanostructures developed in this work (Ch/γ-PGA NPs, Df-NPs, Gn-NPs and Gn-Df-NPs) were evaluated regarding their cytotoxicity, through the assessment of cells metabolic activity using the resazurin assay. Nanostructures were added to macrophages cultures at different concentrations: 0.07, 0.7 or 1.8 mg mL^{-1}, corresponding to 1, 10 and 25% (v/v) in solution, respectively, using previously described culture settings (Goncalves *et al.*, 2015). Although no statistical significant differences were observed, the results showed that Ch/γ-PGA NPs increased macrophage metabolic activity and that this increment was higher as lower was the concentration administered (Figure 27). This tendency was contrary to the one observed in the previous work of the team, where Ch/γ-PGA NPs decreased the metabolic activity at all the concentrations tested (Goncalves *et al.*, 2015). For Gn-NPs, metabolic activity was maintained regardless of the concentration and in levels slightly higher than the control (Figure 27). Relatively to Df-NPs, an increase in metabolic activity was also observed over all the conditions evaluated (Figure 27), relatively to the control (without NPs stimulation). As well as in the case of Ch/γ-PGA NPs, also an opposite trend was noted relatively to the previously work, where in the presence of Df-NPs, the metabolic activity of macrophage slightly increased at the lower concentration (1% (v/v)) and reduce about 33% for the highest concentration (25% (v/v)) (Goncalves *et al.*, 2015). The differences perceived in both works for these nanostructures could be explained due to differences on the polymers properties referred above, such as DA of Ch and Mw of γ-PGA, and/or by donor variability. Regarding, Gn-Df-NPs, it was possible to observe that this formulation trigged a higher metabolic activity when compared to Df-NPs in all the concentrations tested (Figure 27). Overall, by examining the metabolic activity results, we could hypothesize that none of the nanostructures was cytotoxic, and that chemically modification of the NPs with Gn did not induce toxic effects to cells. These results corroborates the study of Sung *et al.* (Sung *et al.*, 1999) where it was described that Gn was not cytotoxic and it potential use as cross-linking agent. On the other hand, this increase in the metabolic activity suggested macrophages activation in the presence of these NPs.

Reviewing the literature, there are several works that demonstrates the activation of macrophages and the expression of several pro-inflammatory cytokines by different NPs, such as ceramic and metallic NPs, by an increased production of TNF-α (Lucarelli *et al.*, 2004), and Au and Ag NPs that also expressed TNF-α and IL-6 (Yen *et al.*, 2009). These referenced studies constitute a reliable source to proves the NPs capabilities in activate macrophages, as demonstrated to Ch/γ-PGA NPs here prepared. Buffer solutions slightly decreased the metabolic activity of macrophages in all conditions tested when compared to the control, although this decrease was not statistically significant.

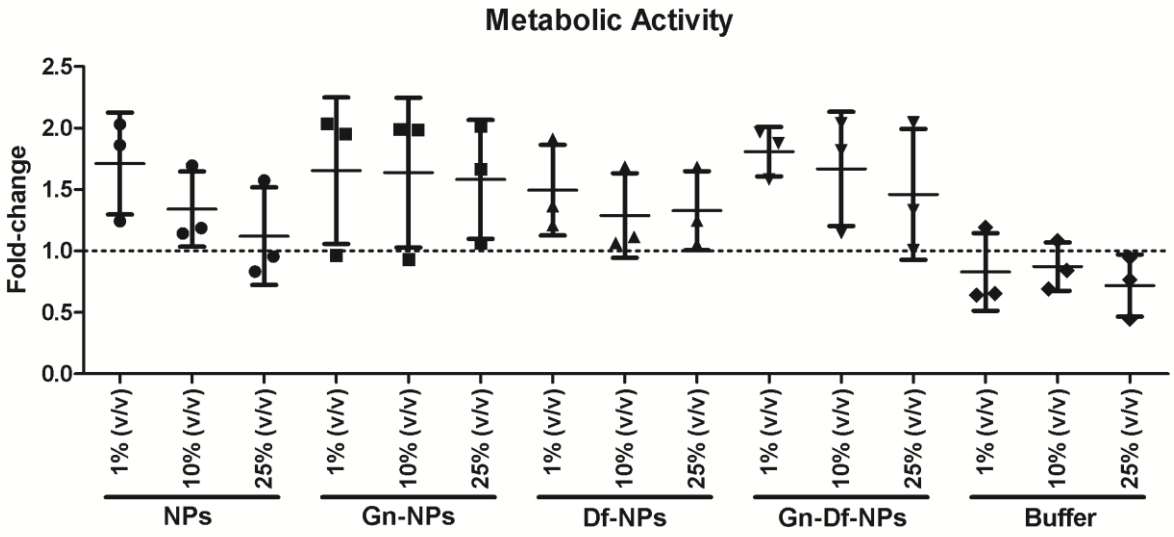

Figure 27. Metabolic activity of human macrophage cultured with Ch/γ-PGA NPs, Df-NPs, Gn-NPs, Gn-Df-NPs, buffer and PBS solutions at different ratios (1%, 10% and 25% (v/v)).

The pro-inflammatory cytokines profile produced by macrophages in contact with Gn was ascertained by analyzing the levels of TNF-α, IL-6 and IL-12 secreted by human macrophages by ELISA (Figure 28). These pro-inflammatory cytokines are known to be produced by macrophages upon activation and their high levels are mainly correlated to the activation of M1 macrophages (pro-inflammatory profile) (Mosser *et al.*, 2008). We observed, by the metabolic activity that NPs contact with the macrophages stimulated an increase in the metabolic activity suggesting cells activation. Still, nothing was known regarding the cytokines profile of macrophages in the presence of Gn. For that purpose, Gn-NPs were compared to Ch/γ-PGA NPs, regarding the levels of TNF-α, IL-6 and IL-12.

The analysis of the pro-inflammatory profile of these cells, showed that Ch/γ-PGA NPs stimulated the production of both IL-6 and TNF-α with statistical significance (*$p<0.05$) by macrophages. Previous work from our team, was already able to demonstrate that Ch/γ-PGA NPs stimulated a pro-inflammatory profile similar to the one promoted by an LPS-stimuli (Castro *et al.*, 2017). Interestingly, the presence of Gn-NPs slightly reduced the levels of TNF-α and IL-6 when compared to the Ch/γ-PGA NPs. This reduction might be related to the anti-inflammatory properties of Gn (Jeon *et al.*, 2011). Thus, Gn cross-linking could have tuned immunomodulatory properties of Ch/γ-PGA NPs to stimulate a less pro-inflammatory profile. Although promising, these results should be further confirmed using a higher number of donors, as well as a vast set of cytokines. If confirmed, this effect by Gn-NPs on macrophages could be also beneficial to IVD degeneration applications, to modulate the macrophages population present in IVD degeneration associated inflammation (Nakazawa *et al.*, 2017). Furthermore, the incorporation of Df in Gn-NPs could play a synergic effect. Relatively to IL-12, both Ch/γ-PGA NPs and Gn-NPs presented values similar to the control. Cytokine production acquired in this work for Ch/γ-PGA NPs followed a similar trend to the previously obtained by Gonçalves *et al.* (Goncalves *et al.*, 2015).

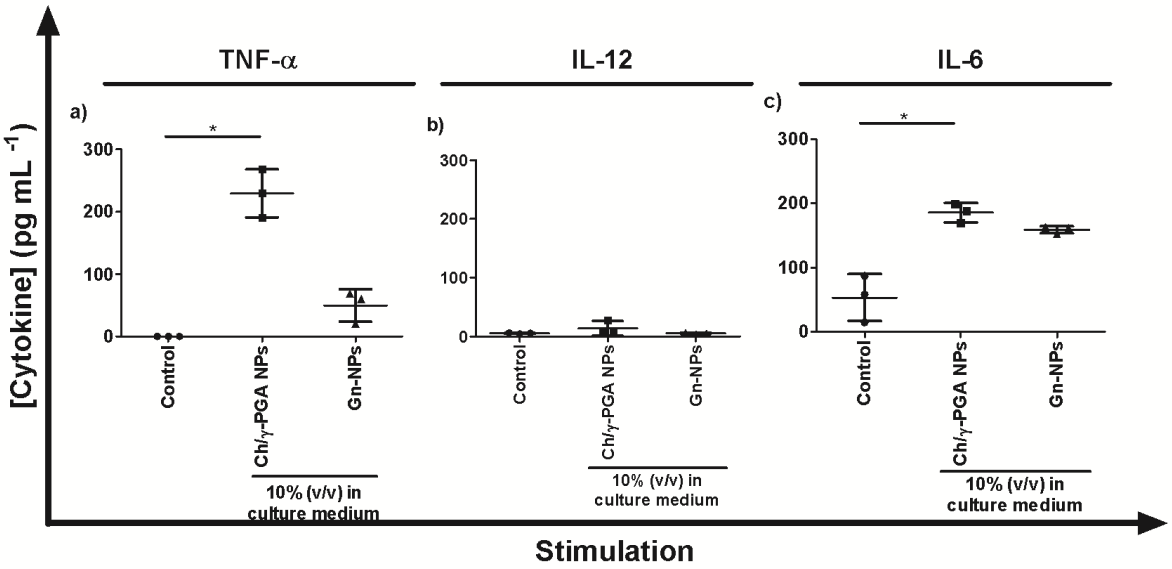

Figure 28. Concentration of pro-inflammatory cytokines of macrophages cultures. Macrophages were cultured with 10% (v/v) Ch/γ-PGA NPs and Gn-NPs in culture medium. a) TNF-α, b) IL-6 and c) IL-12 concentrations were quantified in the medium after 24h by ELISA.

Macrophages can present several morphologies that are related with the microenvironment where they are (McWhorter *et al.*, 2013) and with the biocompatibility of

biomaterials surfaces (Lee *et al.*, 2013). M1 macrophages (pro-inflammatory) present a round morphology with same extensions. On the other hand, M2 macrophages (anti-inflammatory) tend to be more elongated (McWhorter *et al.*, 2013). However, this designation is dubious because its referred to a transition state and macrophages are highly plastics (Rostam *et al.*, 2017).

In Figure 29, representative images of macrophages in the presence of both Ch/γ-PGA NPs and Gn-NPs were compared in terms of morphology, with the unstimulated control. On the control images, the presence of a mixed population can be observed, with is in agreement with a previous study (Cardoso *et al.*, 2015b), while in the presence of Ch/γ-PGA NPs and Gn-NPs, macrophages resemble more on a M1 morphology. Moreover, when Gn is present, some cells appear to be smaller and more elongated, with a few cells presenting extensions, resembling a morphology closer to the one described for M2 (anti-inflammatory) macrophages, still, not all the cells presented this phenotype and seemed to be larger and round, suggesting the presence of a mixed population. These mixed populations could be result of an immunostimulatory effect induced, in part, by pro-inflammatory Ch/γ-PGA NPs and a putative immunosuppression effect, induced by Gn. Moreover, we cannot exclude that cells could be polarized to a more pro-inflammatory phenotype, after NPs degradation in culture. Further studies should also focus the degradation rate of Gn-NPs both *in vitro* and *in vivo*.

7.2. Immunomodulation potential of Df-NPs and Gn-Df-NPs

In this section, we aimed at evaluate the immunomodulatory potential of our nanostructures, namely those containing Df. For that purpose, Df-NPs and Gn-Df-NPs were evaluated by their capacity to revert a LPS stimulus given to macrophages. Df-NPs and Gn-Df-NPs at a concentration of 10% (v/v) were added to previously LPS-stimulated macrophages, using as a control, a Df solution in PBS (10% (v/v)).

Metabolic activity of LPS-stimulated macrophages treated with these nanostructures is represented on Figure 30. It was possible to observe that metabolic activity was slightly increased compared to the control, upon stimulation with LPS, but also in the presence of soluble Df and Gn-Df-NPs (Figure 30), while a slight decrease occurred in Df-NPs. Still, no statistically significant differences were found between the groups. Overall, these results suggest that Df-NPs might reduce cell metabolic activity of LPS-stimulated macrophages and therefore, their state of activation. Still, this would need to be confirmed using a higher number of donors.

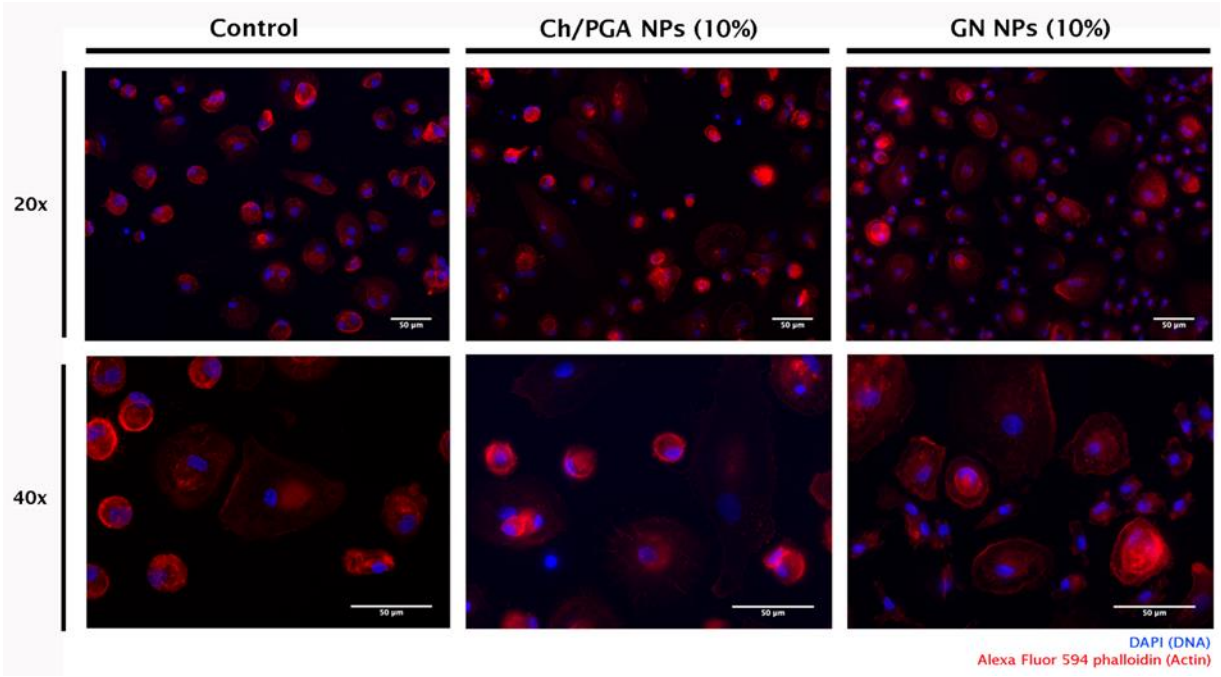

Figure 29. Macrophage morphology without stimulus (control) and in the presence of Ch/γ-PGA NPs and Gn-NPs at a concentration of 10% (v/v). Two representative images are presented for each condition at different magnifications: 20x and 40x.

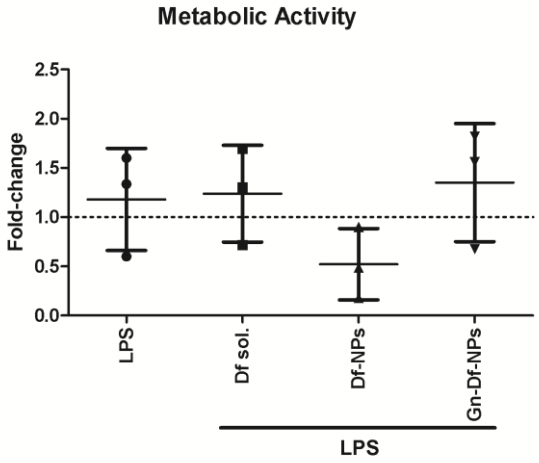

Figure 30. Metabolic activity of human macrophage LPS-stimulated cultured with Df-NPs, Gn-Df-NPs and Df soluble in PBS at concentration of 10% (v/v).

Concerning the cytokine profile of LPS-stimulated macrophages (Figure 31), the immunomodulatory potential of these nanostructures was evaluated through their capacity of reducing/revert the increased pro-inflammatory cytokine levels. For that, the levels of TNF-α and IL-6, but not IL-12 were evaluated. The results showed that the concentration of 100 ng

mL^{-1} of LPS was sufficient to activate macrophages and stimulate the production of pro-inflammatory cytokines such as TNF-α and IL-6, but not IL-12. Previous studies from our team have used different concentrations of LPS to stimulate macrophages activation towards a pro-inflammatory profile. In the work of Gonçalves *et al.* (Goncalves *et al.*, 2015) a concentration of 10000 ng mL^{-1} was given, while in the work of Castro *et al.* (Castro *et al.*, 2017), a concentration of 10 ng mL^{-1} was used. In both, although the disparity in the LPS concentrations used, an activation of macrophages was demonstrated through the increased secretion of TNF-α, IL-6 and IL-12 (Castro *et al.*, 2017; Goncalves *et al.*, 2015). Here, levels of IL-12 were very similar to those observed in the controls, that might be related with the LPS concentration or due to differences regarding cell's donors', their health, sample condition and variability. To confirm this a higher number of donors should be analyzed.

Concerning the immunomodulatory potential of these nanostructures, from the results obtained, we could conclude that none of the treatments was able to revert the LPS stimuli. Contrarily to what was observed in previous work from our group (Goncalves *et al.*, 2015), where Df-NPs were capable of slightly decrease IL-6, here, no reduction in the levels of pro-inflammatory cytokines was observed in the presence of Df-NPs and neither with Gn-Df-NPs or soluble Df. Df is known to selective inhibit Ciclo-oxigenase-2 (COX-2) expression, and consequently reduce the levels of prostaglandins such as PGE_2 (Kato *et al.*, 2001). The work of Gonçalves *et al.* reported an inhibitory effect of Df-NPs followed by an LPS stimulation, by inducing a reduction in PGE_2 and IL-6 levels. This effect was not so strong when Df-NPs were added after the LPS stimulation, suggesting that these nanoparticles may be more efficient in inhibiting the macrophages pro-inflammatory profile. Still, when added after the LPS stimulation, Df-NPs could reduce the levels of PGE_2 and slightly reduced IL-6, but not TNF-α and IL-12 (Goncalves *et al.*, 2015). Herein, no reversion of the LPS stimuli was achieved. This can be related to lower entrapment efficiency of Df in our NPs (47.5 ± 7.9 %), when compared to the one reported in previous work (74.1± 2.5 %) (Goncalves *et al.*, 2015). Future work might consider the use of a higher NPs concentration (25% (v/v)), to increase the concentration of released Df, as this percentage was shown to be non-toxic to the cells. Other explanation can be related to the LPS stimulus given, and future studies might consider the use of a less strong LPS-stimulus, as used in previous studies (Cardoso *et al.*, 2015a; Cardoso *et al.*, 2014; Cardoso *et al.*, 2015b; Castro *et al.*, 2017), but it should be taken in consideration that a compromise between macrophages stimulation and the real immunomodulatory potential of these nanoparticles, as to be ensured.

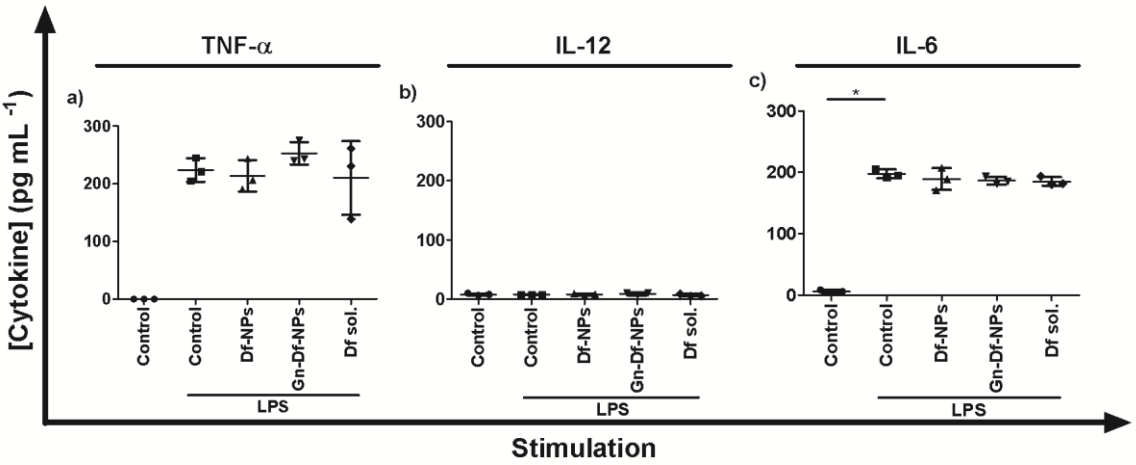

Figure 31. Concentration of pro-inflammatory cytokines of LPS-stimulated macrophages cultures. 10% (v/v) Df-NPs and Gn-Df-NPs in culture medium were added to macrophages 3h after LPS-stimulus. a) TNF-α, b) IL-6 and c) IL-12 concentrations were quantified in the medium after 24h by ELISA.

Regarding macrophages morphology, also in this experiment cells morphology upon LPS stimulation and treatment with Df-NPs, Gn-Df-NPs and soluble Df was studied. A mixed population was observed in the control condition (LPS stimuli) and macrophages presented a round morphology with some extensions (Figure 32). On the other hand, in the LPS + Df-NPs condition, fewer extensions were presented. As referred above for Gn-Df-NPs (Figure 29), also here (Figure 32) less cells were visible in the condition containing LPS + Gn-Df-NPs. In the condition where soluble Df was added, we can observe the presence of larger cells. In general, these results suggest the presence of a morphology closer to the one described for M1 macrophages in all the conditions, with the exception of both controls. Unfortunately, these images corroborate the idea present on metabolic activity of treated LPS-stimulated macrophages that Df-NPs and Gn-Df-NPs were not able to revert LPS stimulus.

Future studies should include macrophage images analysis, such as cell aspect ratio (Cardoso *et al.*, 2015b), image based machine learning for identification of macrophage subsets (Rostam *et al.*, 2017) and real time imaging (Kapellos *et al.*, 2016) in order to accurately identify macrophage polarization and, by consequence, figure out the immunomodulatory outcomes of the developed nanobiomaterials.

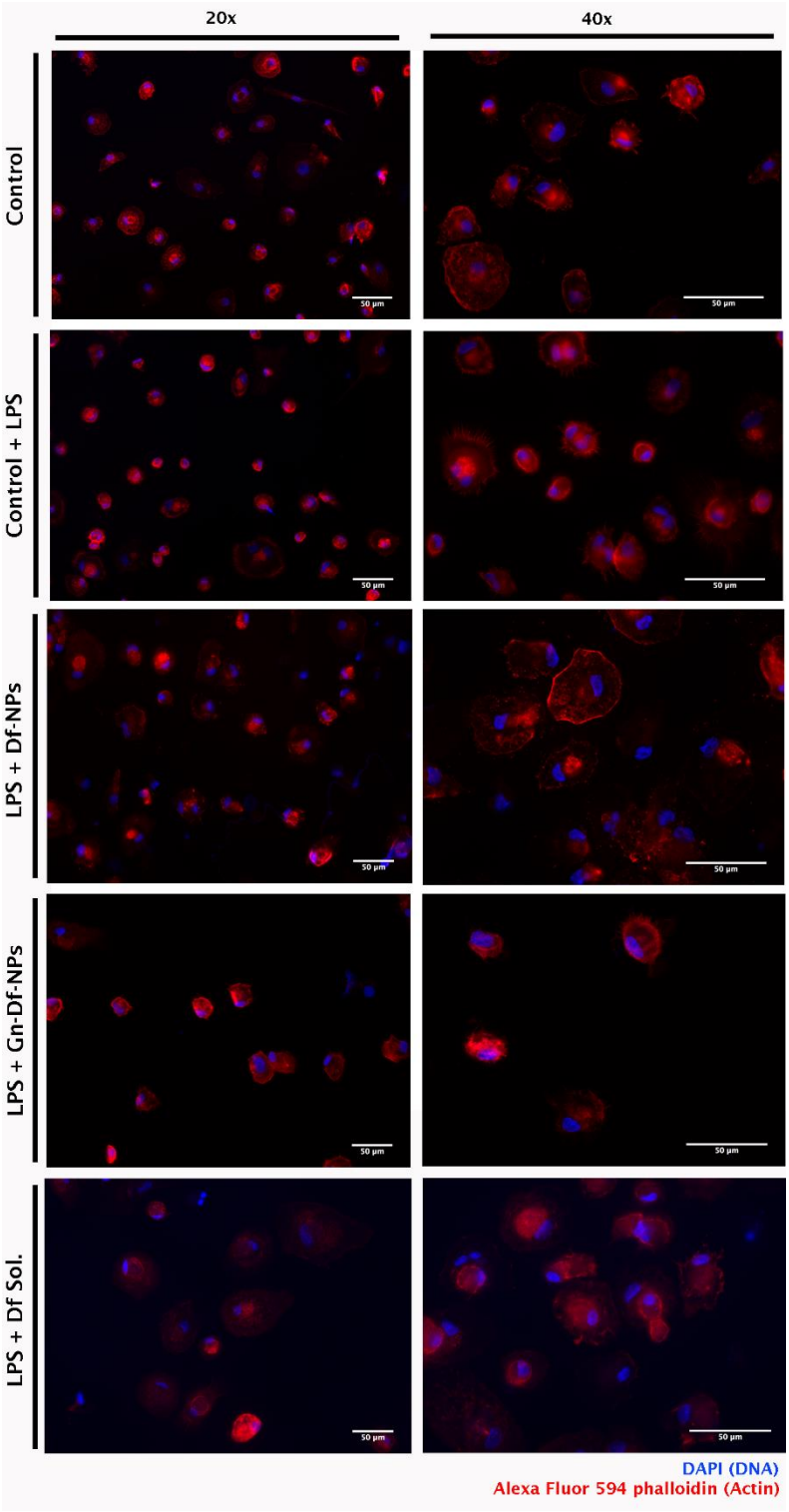

Figure 32. Macrophage without stimulus (control) and LPS-stimulated macrophages morphology in the presence of Df-NPs and Gn-Df-NPs at a concentration of 10% (v/v). Two different images are presented for each condition at different magnifications: 20x and 40x.

CONCLUSIONS AND FUTURE PERSPECTIVES

The development of new nanobiomaterials with improved immunomodulatory potential was the main goal of the present work. The need of control the inflammatory response within the IVD degenerative microenvironment in order to solve degeneration associated inflammation lead us to design new strategies to improve previously developed nanomaterials (Goncalves *et al.*, 2015; Pereira *et al.*, 2012), and play with their immunomodulatory potential.

Based on the previously developed Ch/γ-PGA NPs, we engineered these nanostructures using two distinct methodologies: 1) modifying it chemically, with a chemical cross-linking, to achieve new Df release rates and potentially, new immunomodulatory roles and 2) increase the amounts of loaded Df by electrostatic interaction through an LbL system on Ch/γ-PGA NPs and on Si-NPs as a core.

First, chemical modification of these NPs was successfully achieved through the cross-linking of Ch/γ-PGA NPs and Df-NPs with two different compounds: EDC and Gn. Although both agents performed similarly in what regards to size, PdI and charge, Gn was selected to continue our studies, because it is a natural agent, non-toxic (Sung *et al.*, 1999) and have been combined in several Ch-based biomaterials applications (Fernandes *et al.*, 2013; Jin *et al.*, 2004; Li *et al.*, 2016). Chemical cross-linking with Gn was further optimized to an optimal concentration of 20 mM and 2h of incubation to preserve NPs size and PdI.

In an attempt to increase Df delivery, LbL using Ch and γ-PGA was performed using as templates both Ch/γ-PGA NPs and a Si-core. Although promising, this strategy did non-resulted in a reliable platform to test Df incorporation and release, particularly due to particles aggregation, that hindered a homogenous LbL deposition, and consequently, the NCs formation. Further studies need to be performed to solve the aggregation issues, such as the modification of Si surface and/or the use of alternative solvents. LbL was performed in Ch/γ-PGA NPs successfully as it was possible to confirm by charge alterations. Although NPs size did not seem to increase, with the increased layers number, huge variations in the particles PdI hindered the utilization of these nanostructures in further experiments.

We conducted stability tests on the developed nanostructures. The results demonstrated that at pH 5.0 (optimal interaction pH), these nanostructures were stable up to 3 weeks, but this was not true at the physiological pH. The stability was higher as close was the pH, to pH 5.0. This is a good indication that Df release might occur, upon particles disintegration at the physiological pH, but can impair local approaches to severe degenerated intervertebral discs due to the low pH. To address that, in this study, the release of Df was performed at 3 different

pHs, in order to mimic the different physiological conditions of IVD from degenerated to healthy state: pH 6.2, pH 6.8 and pH 7.4 (Li *et al.*, 2012; Razaq *et al.*, 2003). Few differences were found among the different pHs studied. For the lower pHs (pH 6.2 and pH 6.8), a lower Df release was observed, that can be explained by the closer pH value to the ideal for the electrostatically interaction between Ch and γ-PGA. Moreover, this might be due to the Ch and γ-PGA properties, such as DA and Mw, respectively. A higher Ch DA was obtained here (14.2 %), comparing to the previous one obtained by our team (10.4 %) (Goncalves *et al.*, 2015), which represents less free positive groups to attract Df electrostatic interaction, thus explaining the lower entrapment efficiency observed in this work and consequently, lower release rates. Future studies should explore new strategies to improve Df release at lower pHs, namely for IVD applications. On the other hand, Gn-NPs proved to provide a slower release rate, and therefore can be useful in contexts of chronic inflammation, thus avoiding repeatedly injections of NPs to control inflammation, i.e. in cancer immunotherapies, as has been suggested in previous studies from our group (Cardoso *et al.*, 2015a; Castro *et al.*, 2017).

Gn cross-linking could have tuned the immunomodulatory properties of Ch/γ-PGA NPs to a less pro-inflammatory profile, which may be useful in several applications in tissue regeneration. Future studies will address the real potential of Gn-NPs in reducing the immune response. This effect could beneficial to IVD degeneration applications, where control of inflammation is key to the control of low back pain. Furthermore, it might play a synergic effect when combined with Df. Although we could not verify this in the course of this work, future studies to explore this combination should be performed using longer time points, thus allowing a higher release of Df. *In vitro*, more conditions should be tested, namely, different concentrations of LPS and inhibition/reversion studies, to address the real potential of these nanostructures in the immunomodulation of inflammation.

Overall, Gn-NPs developed might be a potential candidate to modulate macrophages pro-inflammatory profile and to treat IVD degeneration associated inflammation.

REFERENCES

Acosta, F. L., Metz, L., Adkisson, H. D., Liu, J., Carruthers-Liebenberg, E., Milliman, C., Maloney, M. & Lotz, J. C. (2011). Porcine intervertebral disc repair using allogeneic juvenile articular chondrocytes or mesenchymal stem cells. *Tissue Eng Part A, 17*(23-24), 3045-3055. doi:10.1089/ten.tea.2011.0229

Adriani, G., de Tullio, M. D., Ferrari, M., Hussain, F., Pascazio, G., Liu, X. & Decuzzi, P. (2012). The preferential targeting of the diseased microvasculature by disk-like particles. *Biomaterials, 33*, 5504-5513.

Alessandrini, F., Vennemann, A., Gschwendtner, S., Neumann, A. U., Rothballer, M., Seher, T., Wimmer, M., Kublik, S., Traidl-Hoffmann, C., Schloter, M., Wiemann, M. & Schmidt-Weber, C. B. (2017). Pro-Inflammatory versus Immunomodulatory Effects of Silver Nanoparticles in the Lung: The Critical Role of Dose, Size and Surface Modification. *Nanomaterials (Basel), 7*(10). doi:10.3390/nano7100300

Amaral, I. F., Cordeiro, A. L., Sampaio, P. & Barbosa, M. A. (2007). Attachment, spreading and short-term proliferation of human osteoblastic cells cultured on chitosan films with different degrees of acetylation. *J Biomater Sci Polym Ed, 18*(4), 469-485. doi:10.1163/156856207780425068

Anderson, J. M. (2001). Biological responses to materials. *Annu Rev Mater Res, 31*(81).

Anderson, J. M. & McNally, A. K. (2011). Biocompatibility of implants: lymphocyte/macrophage interactions. *Seminars in Immunopathology, 33*(3), 221-233.

Anderson, J. M., Rodriguez, A. & Chang, D. T. (2008). Foreign Body Reaction to Biomaterials. *Semin Immunol., 20*(2), 86-100.

Anderson, P. M., Hanson, D. C., Hasz, D. E., Halet, M. R., Blazar, B. R. & Ochoa, A. C. (1994). Cytokines in liposomes: preliminary studies with IL-1, IL-2, IL-6, GM-CSF and interferon-gamma. *Cytokine, 6*, 92-101.

Andorko, J. I. & Jewell, C. M. (2017). Designing biomaterials with immunomodulatory properties for tissue engineering and regenerative medicine. *Bioeng Transl Med, 2*(2), 139-155. doi:10.1002/btm2.10063

Anselme, K. (2000). Osteoblast adhesion on biomaterials. *Biomaterials, 21*(7), 667-681.

Antunes, J. C., Goncalves, R. M. & Barbosa, M. A. (2016). Chitosan/Poly(γ-glutamic acid) Polyelectrolyte Complexes: From Self- Assembly to Application in Biomolecules Delivery and Regenerative Medicine. *Research & Reviews: Journal of Material Sciences, 04*(04). doi:10.4172/2321-6212.1000153

Antunes, J. C., Pereira, C. L., Molinos, M., Ferreira-da-Silva, F., Dessi, M., Gloria, A., Ambrosio, L., Goncalves, R. M. & Barbosa, M. A. (2011). Layer-by-layer self-assembly of chitosan and poly(gamma-glutamic acid) into polyelectrolyte complexes. *Biomacromolecules, 12*(12), 4183-4195. doi:10.1021/bm2008235

Ashiuchi, M. & Misono, H. (2002). Biochemistry and molecular genetics of poly-gamma-glutamate synthesis. *Appl Microbiol Biotechnol, 59*(1), 9-14. doi:10.1007/s00253-002-0984-x

Ashiuchi, M., Soda, K. & Misono, H. (1999). A poly-gamma-glutamate synthetic system of Bacillus subtilis IFO 3336: gene cloning and biochemical analysis of poly-gamma-glutamate produced by Escherichia coli clone cells. *Biochem Biophys Res Commun, 263*(1), 6-12. doi:10.1006/bbrc.1999.1298

Balakrishnan, B., Kumar, D. S., Yoshida, Y. & Jayakrishnan, A. (2005). Chemical modification of poly(vinyl chloride) resin using poly(ethylene glycol) to improve blood compatibility. *Biomaterials, 26*(17), 3495-3502. doi:10.1016/j.biomaterials.2004.09.032

Ban, M., Langonne, I., Huguet, N., Guichard, Y. & Goutet, M. (2013). Iron oxide particles modulate the ovalbumin-induced Th2 immune response in mice. *Toxicology Letters, 216*(1), 31-39.

Barbosa, J. N., Amaral, I. F., Aguas, A. P. & Barbosa, M. A. (2010). Evaluation of the effect of the degree of acetylation on the inflammatory response to 3D porous chitosan scaffolds. *J Biomed Mater Res A, 93*(1), 20-28. doi:10.1002/jbm.a.32499

Battie, M. C., Videman, T. & Parent, E. (2004). Lumbar disc degeneration: epidemiology and genetic influences. *Spine, 29*(23), 2679-2690.

Baxter, A., Dillon, M., Taylor, K. D. & Roberts, G. A. (1992). Improved method for i.r. determination of the degree of N-acetylation of chitosan. *Int J Biol Macromol, 14*(3), 166-169.

Bikiaris, D., Koutris, E. & Karavas, E. (2007). New aspects in sustained drug release formulations. *Recent Pat Drug Deliv Formul, 1*(3), 201-213.

Birrer, G. A., Cromwick, A. M. & Gross, R. A. (1994). Gamma-poly(glutamic acid) formation by Bacillus licheniformis 9945a: physiological and biochemical studies. *Int J Biol Macromol, 16*(5), 265-275.

Brown, B. N., Ratner, B. D., Goodman, S. B., Amar, S. & Badylak, S. F. (2012). Macrophage polarization: an opportunity for improved outcomes in biomaterials and regenerative medicine. *Biomaterials, 33*(15), 3792-3802. doi:10.1016/j.biomaterials.2012.02.034

Brugnerotto, J., Lizardib, J., Goycooleab, F. M., ArguÈelles-Monalc, W., DesbrieÁresa, J. & Rinaudoa, M. (2001). An infrared investigation in relation with chitin and chitosan characterization. *Polymer, 42*, 3569-3580.

Calvo, P., Vila-Jato, J. L. & Alonso, M. J. (1997). Evaluation of cationic polymer-coated nanocapsules as ocular drug carriers. *Int. J. of Pharmaceuticals, 153*, 41-50.

Cardoso, A. P., Goncalves, R. M., Antunes, J. C., Pinto, M. L., Pinto, A. T., Castro, F., Monteiro, C., Barbosa, M. A. & Oliveira, M. J. (2015a). An interferon-gamma-delivery system based on chitosan/poly(gamma-glutamic acid) polyelectrolyte complexes modulates macrophage-derived stimulation of cancer cell invasion in vitro. *Acta Biomater, 23*, 157-171. doi:10.1016/j.actbio.2015.05.022

Cardoso, A. P., Pinto, M. L., Pinto, A. T., Oliveira, M. I., Pinto, M. T., Goncalves, R., Relvas, J. B., Figueiredo, C., Seruca, R., Mantovani, A., Mareel, M., Barbosa, M. A. & Oliveira, M. J. (2014). Macrophages stimulate gastric and colorectal cancer invasion through EGFR Y(1086), c-Src, Erk1/2 and Akt phosphorylation and smallGTPase activity. *Oncogene, 33*(16), 2123-2133. doi:10.1038/onc.2013.154

Cardoso, A. P., Pinto, M. L., Pinto, A. T., Pinto, M. T., Monteiro, C., Oliveira, M. I., Santos, S. G., Relvas, J. B., Seruca, R., Mantovani, A., Mareel, M., Barbosa, M. A. & Oliveira, M. J. (2015b). Matrix metalloproteases as maestros for the dual role of LPS- and IL-10-stimulated macrophages in cancer cell behaviour. *BMC Cancer, 15*, 456. doi:10.1186/s12885-015-1466-8

Caruso, F., Best, J. P. & Yan, Y. (2012). The role of particle geometry and mechanics in the biological domain. *Adv Healthc Mater, 1*, 35-47.

Castro, F., Pinto, M. L., Silva, A. M., Pereira, C. L., Teixeira, G. Q., Gomez-Lazaro, M., Santos, S. G., Barbosa, M. A., Goncalves, R. M. & Oliveira, M. J. (2017). Pro-inflammatory chitosan/poly(gamma-glutamic acid) nanoparticles modulate human antigen-presenting cells phenotype and revert their pro-invasive capacity. *Acta Biomater, 63*, 96-109. doi:10.1016/j.actbio.2017.09.016

Chatelet, C., Damour, O. & Domard, A. (2001). Influence of the degree of acetylation on some biological properties of chitosan films. *Biomaterials, 22*(3), 261-268.

Chen, Q., Xue, Y. & Sun, J. (2013). Kupffer cell-mediated hepatic injury induced by silica nanoparticles in vitro and in vivo. *Int J Nanomedicine, 8*, 1129-1140. doi:10.2147/IJN.S42242

Cheung, K. M., Karppinen, J., Chan, D., Ho, D. W., Song, Y. Q., Sham, P., Cheah, K. S., Leong, J. C. & Luk, K. D. (2009). Prevalence and pattern of lumbar magnetic resonance imaging

changes in a population study of one thousand forty-three individuals. *Spine, 34*(9), 934-940.

Chithrani, B. D. & Chan, C. W. (2007). Elucidating the Mechanism of Cellular Uptake and Removal of Protein-Coated Gold Nanoparticles of Different Sizes and Shapes. *Nano Lett, 7*(6), 1542-1550.

Chithrani, B. D., Ghazani, A. A. & Chan, C. W. (2006). Determining the Size and Shape Dependence of Gold Nanoparticle Uptake into Mammalian Cells. *Nano Lett, 6*(4), 662-668.

Cho, E. C., Xie, J., Wurm, P. A. & Xia, Y. (2009a). Understanding the role of surface charges in cellular adsorption versus internalization by selectively removing gold nanoparticles on the cell surface with a I2/KI etchant. *Nano Lett, 9*(3), 1080-1084. doi:10.1021/nl803487r

Cho, W. S., Cho, M., Jeong, J., Choi, M., Cho, H. Y., Han, B. S., Kim, S. H., Kim, H. O., Lim, Y. T., Chung, B. H. & Jeong, J. (2009b). Acute toxicity and pharmacokinetics of 13 nm-sized PEG-coated gold nanoparticles. *Toxicol Appl Pharmacol, 236*(1), 16-24. doi:10.1016/j.taap.2008.12.023

Chong, C. S., Cao, M., Wong, W. W., Fischer, K. P., Addison, W. R., Kwon, G. S., Tyrrell, D. L. & Samuel, J. (2005). Enhancement of T helper type 1 immune responses against hepatitis B virus core antigen by PLGA nanoparticle vaccine delivery. *J Control Release, 102*(1), 85-99. doi:10.1016/j.jconrel.2004.09.014

Clogston, J. D. & Patri, A. K. (2010). *Zeta Potential Measurement* (Vol. 697): Springer.

Cozens-Roberts, C., Quinn, J. A. & Lauffenberger, D. A. (1990). Receptor-mediated adhesion phenomena. Model studies with the Radical-Flow Detachment Assay. *Biophys. J., 58*, 107-125.

Crompton, K. E., Goud, J. D., Bellamkonda, R. V., Gengenbach, T. R., Finkelstein, D. I., Horne, M. K. & Forsythe, J. S. (2007). Polylysine-functionalised thermoresponsive chitosan hydrogel for neural tissue engineering. *Biomaterials, 28*(3), 441-449. doi:10.1016/j.biomaterials.2006.08.044

Cui, Z., Han, S., Vangasseri, D. P. & Huang, L. (2005). Immunostimulation mechanism of LPD nanoparticle as a vaccine carrier. *Mol. Pharm., 2*(1), 22-28.

De Clercq, K., Schelfhout, C., Bracke, M., De Wever, O., Van Bockstal, M., Ceelen, W., Remon, J. P. & Vervaet, C. (2016). Genipin-crosslinked gelatin microspheres as a strategy to prevent postsurgical peritoneal adhesions: In vitro and in vivo characterization. *Biomaterials, 96*, 33-46. doi:10.1016/j.biomaterials.2016.04.012

Dileo, J., Banerjee, R., Whitmore, M., Nayak, J. V., Falo, L. D., Jr. & Huang, L. (2003). Lipid-protamine-DNA-mediated antigen delivery to antigen-presenting cells results in enhanced anti-tumor immune responses. *Mol Ther, 7*(5 Pt 1), 640-648.

Diwan, M., Elamanchili, P., Cao, M. & Samuel, J. (2004). Dose sparing of CpG oligodeoxynucleotide vaccine adjuvants by nanoparticle delivery. *Curr Drug Deliv, 1*(4), 405-412.

Dobrovolskaia, M. A. & McNeil, S. E. (2007). Immunological properties of engineered nanomaterials. *Nat Nanotechnol, 2*(8), 469-478. doi:10.1038/nnano.2007.223

Dube, A., Reynolds, J. L., Law, W. C., Maponga, C. C., Prasad, P. N. & Morse, G. D. (2014). Multimodal nanoparticles that provide immunomodulation and intracellular drug delivery for infectious diseases. *Nanomedicine, 10*(4), 831-838. doi:10.1016/j.nano.2013.11.012

Edwards, J. P., Zhang, X., Frauwirth, K. A. & Mosser, D. M. (2006). Biochemical and functional characterization of three activated macrophage populations. *J Leukoc Biol, 80*(6), 1298-1307. doi:10.1189/jlb.0406249

Esche, C., Stellato, C. & Beck, L. A. (2005). Chemokines: key players in innate and adaptative immunity. *J. Invest. Dermatol., 125*, 615-628.

Fahy, N., de Vries-van Melle, M. L., Lehmann, J., Wei, W., Grotenhuis, N., Farrell, E., van der Kraan, P. M., Murphy, J. M., Bastiaansen-Jenniskens, Y. M. & van Osch, G. J. (2014). Human osteoarthritic synovium impacts chondrogenic differentiation of mesenchymal stem cells via macrophage polarisation state. *Osteoarthritis Cartilage, 22*(8), 1167-1175. doi:10.1016/j.joca.2014.05.021

Fang, J., Nakamura, H. & Maeda, H. (2011). The EPR effect: Unique features of tumor blood vessels for drug delivery, factors involved, and limitations and augmentation of the effect. *Adv Drug Deliv Rev, 63*(3), 136-151. doi:10.1016/j.addr.2010.04.009

Feng, W., Nie, W., He, C., Zhou, X., Chen, L., Qiu, K., Wang, W. & Yin, Z. (2014). Effect of pH-responsive alginate/chitosan multilayers coating on delivery efficiency, cellular uptake and biodistribution of mesoporous silica nanoparticles based nanocarriers. *ACS Appl Mater Interfaces, 6*(11), 8447-8460. doi:10.1021/am501337s

Fernandes, M., Goncalves, I. C., Nardecchia, S., Amaral, I. F., Barbosa, M. A. & Martins, M. C. (2013). Modulation of stability and mucoadhesive properties of chitosan microspheres for therapeutic gastric application. *Int J Pharm, 454*(1), 116-124. doi:10.1016/j.ijpharm.2013.06.068

Fessi, H., Puisieux, F. & Devissaguet, J. P. (1988). Procédé de préparation de systèmes colloïdaux dispersibles d'une substance sous forme de nanocapsules.

Garti, N. (1997). Double emulsions - scope, limitations and new achievements. *Colloids and Surfaces*, 233-246.

Gessner, A., Lieske, A., Paulke, B. & Muller, R. (2002). Influence of surface charge density on protein adsorption on polymeric nanoparticles: analysis by two-dimensional electrophoresis. *Eur J Pharm Biopharm, 54*(2), 165-170.

Goncalves, R. M., Pereira, A. C., Pereira, I. O., Oliveira, M. J. & Barbosa, M. A. (2015). Macrophage response to chitosan/poly-(gamma-glutamic acid) nanoparticles carrying an anti-inflammatory drug. *J Mater Sci Mater Med, 26*(4), 167. doi:10.1007/s10856-015-5496-1

Gorth, D. J., Martin, J. T., Mauck, R. L., Malhotra, N. R., Dodge, G. R., Elliott, D. M. & Smith, L. J. (2014). In vivo retention and bioactivity of IL-1ra microspheres in the rat intervertebral disc a preliminary investigation. *Journal of Experimental Orthopaedics, 1*(15).

Gorth, D. J., Mauck, R. L., Chiaro, J. A., Mohanraj, B., Hebela, N. M., Dodge, G. R., Elliott, D. M. & Smith, L. J. (2012). IL-1ra delivered from poly(lactic-co-glycolic acid) microspheres attenuates IL-1beta-mediated degradation of nucleus pulposus in vitro. *Arthritis Res Ther, 14*(4), R179. doi:10.1186/ar3932

Goto, A. & Kunioka, M. (1992). Biosynthesis and Hydrolysis of Poly(gamma-glutamic acid) from Bacillus subtilis IF03335. *Biosci Biotechnol Biochem, 56*(7), 1031-1035. doi:10.1271/bbb.56.1031

Hajdu, I., Bodnár, M., Filipcsei, G., Hartmann, J. F., Daróczi, L., Zrínyi, M. & Borbély, J. (2007). Nanoparticles prepared by self-assembly of Chitosan and poly-γ-glutamic acid. *Colloid and Polymer Science, 286*(3), 343-350. doi:10.1007/s00396-007-1785-7

Hardy, C. L., LeMasurier, J. S., Belz, G. T., Scalzo-Inguanti, K., Yao, J., Xiang, S. D., Kanellakis, P., Bobik, A., Strickland, D. H., Rolland, J. M., O'Hehir, R. E. & Plebasnki, M. (2012). Inert 50-nm polystyrene nanoparticles that modify pulmonary dendritic cell function and inhibit allergic airway inflammation. *Journal of Immunology, 188*(3), 1431-1441.

He, C., Hu, Y., Yin, L., Tang, C. & Yin, C. (2010). Effects of particle size and surface charge on cellular uptake and biodistribution of polymeric nanoparticles. *Biomaterials, 31*(13), 3657-3666. doi:10.1016/j.biomaterials.2010.01.065

Henry, N., Clouet, J., Fragale, A., Griveau, L., Chedeville, C., Veziers, J., Weiss, P., Le Bideau, J., Guicheux, J. & Le Visage, C. (2017). Pullulan microbeads/Si-HPMC hydrogel injectable system for the sustained delivery of GDF-5 and TGF-beta1: new insight into

intervertebral disc regenerative medicine. *Drug Deliv, 24*(1), 999-1010. doi:10.1080/10717544.2017.1340362

Hu, L., Sun, H., Zhao, Q., Han, N., Bai, L., Wang, Y., Jiang, T. & Wang, S. (2015). Multilayer encapsulated mesoporous silica nanospheres as an oral sustained drug delivery system for the poorly water-soluble drug felodipine. *Mater Sci Eng C Mater Biol Appl, 47*, 313-324. doi:10.1016/j.msec.2014.10.067

Huang, C., Zhang, Y., Yuan, H., Gao, H. & Zhang, S. (2013). Role of nanoparticle geometry in endocytosis: laying down to stand up. *Nano Lett, 13*, 4546-4550.

Hubner, C., Fettkenhauer, C., Voges, K. & Lupascu, D. C. (2018). Agglomeration-Free Preparation of Modified Silica Nanoparticles for Emulsion Polymerization-A Well Scalable Process. *Langmuir, 34*(1), 376-383. doi:10.1021/acs.langmuir.7b03753

Hussain, S., Vanoirbeek, J. A. & Hoet, P. H. (2012). Interactions of nanomaterials with the immune system. *Wiley Interdiscip Rev Nanomed Nanobiotechnol, 4*(2), 169-183. doi:10.1002/wnan.166

Imoto, T., Kida, T., Matsusaki, M. & Akashi, M. (2010). Preparation and unique pH-responsive properties of novel biodegradable nanocapsules composed of poly(gamma-glutamic acid) and chitosan as weak polyelectrolytes. *Macromol Biosci, 10*(3), 271-277. doi:10.1002/mabi.200900272

Inoue, K. I., Takano, H., Ohnuki, M., Yanagisawa, R., Sakurai, M., Shimada, A., Mizushima, K. & Yoshikawa, T. (2008). Size effects of nanomaterials on lung inflammation and coagulatory disturbance. *Int. J. Pathology and Pharmacology, 21*(1), 197-206.

Janeway, C., Travers, P., Walport, M. & Sholmchik, M. J. (1996). Immunobiology: The Immune System in Health and Disease. *Current Biology, 7*.

Jeon, W. K., Hong, H. Y. & Kim, B. C. (2011). Genipin up-regulates heme oxygenase-1 via PI3-kinase-JNK1/2-Nrf2 signaling pathway to enhance the anti-inflammatory capacity in RAW264.7 macrophages. *Arch Biochem Biophys, 512*(2), 119-125. doi:10.1016/j.abb.2011.05.016

Jiang, Y., Zhang, H., Wang, Y., Chen, M., Ye, S., Hou, Z. & Ren, L. (2013). Modulation of apoptotic pathways of macrophages by surface-functionalized multi-walled carbon nanotubes. *PLoS ONE, 8*(6), e65756. doi:10.1371/journal.pone.0065756

Jiao, Q., Li, L., Mu, Q. & Zhang, Q. (2014). Immunomodulation of nanoparticles in nanomedicine applications. *Biomed Res Int, 2014*, 426028. doi:10.1155/2014/426028

Jin, J., Song, M. & Hourston, D. J. (2004). Novel chitosan-based films cross-linked by genipin with improved physical properties. *Biomacromolecules, 5*(1), 162-168. doi:10.1021/bm034286m

Jintapattanakit, A., Junyaprasert, V. B., Mao, S., Sitterberg, J., Bakowsky, U. & Kissel, T. (2007). Peroral delivery of insulin using chitosan derivatives: a comparative study of polyelectrolyte nanocomplexes and nanoparticles. *Int J Pharm, 342*(1-2), 240-249. doi:10.1016/j.ijpharm.2007.05.015

Jones, P., Gardner, L., Menage, J., Williams, G. T. & Roberts, S. (2008). Intervertebral disc cells as competent phagocytes in vitro: implications for cell death in disc degeneration. *Arthritis Res Ther, 10*(4), R86. doi:10.1186/ar2466

Joshi, M. D. & Muller, R. H. (2009). Lipid nanoparticles for parenteral delivery of actives. *Eur J Pharm Biopharm, 71*(2), 161-172. doi:10.1016/j.ejpb.2008.09.003

Kapellos, T. S., Taylor, L., Lee, H., Cowley, S. A., James, W. S., Iqbal, A. J. & Greaves, D. R. (2016). A novel real time imaging platform to quantify macrophage phagocytosis. *Biochem Pharmacol, 116*, 107-119. doi:10.1016/j.bcp.2016.07.011

Kato, M., Nishida, S., Kitasato, H., Sakata, N. & Kawai, S. (2001). Cyclooxygenase-1 and cyclooxygenase-2 selectivity of non-steroidal anti-inflammatory drugs: investigation using human peripheral monocytes. *J Pharm Pharmacol, 53*(12), 1679-1685.

Khan, H., Shukla, R. N. & Bajpai, A. K. (2016). Genipin-modified gelatin nanocarriers as swelling controlled drug delivery system for in vitro release of cytarabine. *Mater Sci Eng C Mater Biol Appl, 61*, 457-465. doi:10.1016/j.msec.2015.12.085

Kim, Y. K., Chen, E. Y. & Liu, W. F. (2016). Biomolecular strategies to modulate the macrophage response to implanted materials. *Journal of Materials Chemistry B, 4*(9), 1600-1609. doi:10.1039/c5tb01605c

Koziara, J. M., Oh, J. J., Akers, W. S., Ferraris, S. P. & Mumper, R. J. (2005). Blood compatibility of cetyl alcohol/polysorbate-based nanoparticles. *Pharm Res, 22*(11), 1821-1828. doi:10.1007/s11095-005-7547-7

Kruger, P., Saffarzadeh, M., Weber, A. R. W., Rieber, N., Radsak, M., von Bernuth, H., Benarafa, C., Roos, D., Skokowa, J. & Hartl, D. (2015). Neutrophils: between host defence, immune modulation, and tissue injuty. *PLoS Pathog., 11*.

Lee, H. S., Stachelek, S. J., Tomczyk, N., Finley, M. J., Composto, R. J. & Eckmann, D. M. (2013). Correlating macrophage morphology and cytokine production resulting from biomaterial contact. *J Biomed Mater Res A, 101*(1), 203-212. doi:10.1002/jbm.a.34309

Lee, H. Y., Choi, Y. J., Jung, E. J., Yin, H. Q., Kwon, J. T., Kim, J. E., Im, H. T., Cho, M. H., Kim, J. H., Kim, H. Y. & Lee, B. H. (2010). Genomics-based screening of differentially expressed genes in the brains of mice exposed to silver nanoparticles via inhalation. *Journal of Nanoparticle Research, 12*(5), 1567-1578. doi:10.1007/s11051-009-9666-2

Lee, P. W., Peng, S. F., Su, C. J., Mi, F. L., Chen, H. L., Wei, M. C., Lin, H. J. & Sung, H. W. (2008). The use of biodegradable polymeric nanoparticles in combination with a low-pressure gene gun for transdermal DNA delivery. *Biomaterials, 29*(6), 742-751. doi:10.1016/j.biomaterials.2007.10.034

Li, H., Liang, C., Tao, Y., Zhou, X., Li, F., Chen, G. & Chen, Q. X. (2012). Acidic pH conditions mimicking degenerative intervertebral discs impair the survival and biological behavior of human adipose-derived mesenchymal stem cells. *Exp Biol Med (Maywood), 237*(7), 845-852. doi:10.1258/ebm.2012.012009

Li, Y. & Jiang, L. (2016). Preparation of graphene oxide–chitosan nanocapsules and their applications as carriers for drug delivery. *RSC Advances, 6*(106), 104522-104528. doi:10.1039/c6ra24401g

Lin, X., Zuo, Y. Y. & Gu, N. (2015). Shape affects the interactions of nanoparticles with pulmonary surfactant. *Sci China Mater, 58*, 28-37. doi:10.1007/s40843-014-0018-5

Lin, Y. H., Chung, C. K., Chen, C. T., Liang, H. F., Chen, S. C. & Sung, H. W. (2005). Preparation of nanoparticles composed of chitosan/poly-gamma-glutamic acid and evaluation of their permeability through Caco-2 cells. *Biomacromolecules, 6*(2), 1104-1112. doi:10.1021/bm049312a

Liu, H., Yang, D., Yang, H., Zhang, H., Zhang, W., Fang, Y., Lin, Z., Tian, L., Lin, B., Yan, J. & Xi, Z. (2013a). Comparative study of respiratory tract immune toxicity induced by three sterilisation nanoparticles: silver, zinc oxide and titanium dioxide. *J Hazard Mater, 248-249*, 478-486. doi:10.1016/j.jhazmat.2013.01.046

Liu, Q., Jin, L., Mahon, B. H., Chordia, M. D., Shen, F. H. & Li, X. (2013b). A Novel Treatment of Neuroinflammation against Low Back Pain by soluble fullerol nanoparticles. *Spine, 38*(17), 1443–1451. doi:10.1097/BRS.0b013e31828fc6b7

Liu, Q., Jin, L., Shen, F. H., Balian, G. & Li, X. J. (2013c). Fullerol nanoparticles suppress inflammatory response and adipogenesis of vertebral bone marrow stromal cells - A potential novel treatment for intervertebral disc degeneration. *Spine, 13*(11). doi:10.1016/j.spinee.2013.04.004

Liu, Y., Tan, J., Thomas, A., Ou-Yang, H. D. & Muzykantov, V. R. (2012). The shape of things to come: importance of design in nanotechnology for drug delivery. . *Ther Deliv., 3*, 181-194.

Lucarelli, M., Gatti, A. M., Savarino, G., Quattroni, P., Martinelli, L., Monari, E. & Boraschi, D. (2004). Innate defence functions of macrophages can be biased by nano-sized ceramic and metallic particles. *Eur Cytokine Netw, 15*(4), 339-346.

Luck, M., Paulke, B. R., Schroder, W., Blunk, T. & Muller, R. H. (1998). Analysis of plasma protein adsorption on polymeric nanoparticles with different surface characteristics. *J Biomed Mater Res, 39*(3), 478-485.

Lundqvist, M., Stigler, J., Elia, G., Lynch, I., Cedervall, T. & Dawson, K. A. (2008). Nanoparticle size and surface properties determine the protein corona. *PNAS, 105*(38), 14265–14270.

Luo, Y. H., Chang, L. W. & Lin, P. (2015). Metal-Based Nanoparticles and the Immune System: Activation, Inflammation, and Potential Applications. *Biomed Res Int, 2015*, 143720. doi:10.1155/2015/143720

Makidon, P. E., Bielinska, A. U., Nigavekar, S. S., Janczak, K. W., Knowlton, J., Scott, A. J., Mank, N., Cao, Z., Rathinavelu, S., Beer, M. R., Wilkinson, J. E., Blanco, L. P., Landers, J. J. & Baker, J. R., Jr. (2008). Pre-clinical evaluation of a novel nanoemulsion-based hepatitis B mucosal vaccine. *PLoS ONE, 3*(8), e2954. doi:10.1371/journal.pone.0002954

Martinez, F. O. & Gordon, S. (2014). The M1 and M2 paradigm of macrophage activation. *F1000 Prime Reports*. doi:10.12703/P6-13)

McWhorter, F. Y., Wang, T., Nguyen, P., Chung, T. & Liu, W. F. (2013). Modulation of macrophage phenotype by cell shape. *Proc Natl Acad Sci U S A, 110*(43), 17253-17258. doi:10.1073/pnas.1308887110

Mitchell, L. A., Lauer, F. T., Burchiel, S. W. & McDonald, J. D. (2009). Mechanisms for how inhaled multiwalled carbon nanotubes suppress systemic immune function in mice. *Nature Nanotechnology, 4*(7), 451-456.

Mohanraj, V. & Chen, Y. (2006). Nanoparticles – A Review. *Tropical Journal of Pharmaceutical Research, 5*(1), 561-573.

Molinos, M., Almeida, C. R., Caldeira, J., Cunha, C., Goncalves, R. M. & Barbosa, M. A. (2015). Inflammation in intervertebral disc degeneration and regeneration. *J R Soc Interface, 12*(104), 20141191. doi:10.1098/rsif.2014.1191

Moon, S. H., Nishida, K., Gilbertson, L. G., Lee, H. M., Kim, H., Hall, R. A., Robbins, P. D. & Kang, J. D. (2008). Biologic response of human intervertebral disc cells to gene therapy

cocktail. *Spine (Phila Pa 1976), 33*(17), 1850-1855. doi:10.1097/BRS.0b013e31817e1cd7

Morishige, T., Yoshioka, Y., Inakura, H., Tanabe, A., Narimatsu, S., Yao, X., Monobe, Y., Imazawa, T., Tsunoda, S., Tsutsumi, Y., Mukai, Y., Okada, N. & Nakagawa, S. (2012). Suppression of nanosilica particle-induced inflammation by surface modification of the particles. *Arch Toxicol, 86*(8), 1297-1307. doi:10.1007/s00204-012-0823-5

Mosser, D. M. & Edwards, J. P. (2008). Exploring the full spectrum of macrophage activation. *Nat Rev Immunol, 8*(12), 958-969. doi:10.1038/nri2448

Mundargi, R. C., Babu, V. R., Rangaswamy, V., Patel, P. & Aminabhavi, T. M. (2008). Nano/micro technologies for delivering macromolecular therapeutics using poly(D,L-lactide-co-glycolide) and its derivatives. *J Control Release, 125*(3), 193-209. doi:10.1016/j.jconrel.2007.09.013

Murray, P. J., Allen, J. E., Biswas, S. K., Fisher, E. A., Gilroy, D. W., Goerdt, S., Gordon, S., Hamilton, J. A., Ivashkiv, L. B., Lawrence, T., Locati, M., Mantovani, A., Martinez, F. O., Mege, J. L., Mosser, D. M., Natoli, G., Saeij, J. P., Schultze, J. L., Shirey, K. A., Sica, A., Suttles, J., Udalova, I., van Ginderachter, J. A., Vogel, S. N. & Wynn, T. A. (2014). Macrophage activation and polarization: nomenclature and experimental guidelines. *Immunity, 41*(1), 14-20. doi:10.1016/j.immuni.2014.06.008

Nakagawa, T., Kawamura, T., Matsumura, Y., Yoshikawa, Y., Takada, K., Ike, O., Wada, H. & Hitomi, S. (1998). [Design and application of oral sustained-release anticancer drug--a new oral dosage form of cisplatin]. *Nihon Rinsho, 56*(3), 680-685.

Nakanishi, T., Kunisawa, J., Hayashi, A., Tsutsumi, Y., Kubo, K., Nakagawa, S., Nakanishi, M., Tanaka, K. & Mayumi, T. (1999). Positively charged liposome functions as an efficient immunoadjuvant in inducing cell mediated immune response to soluble proteins. *Journal of Controlled Release, 61*, 233-240.

Nakazawa, K. R., Walter, B. A., Laudier, D. M., Krishnamoorthy, D., Mosley, G. E., Spiller, K. L. & Iatridis, J. C. (2017). Accumulation and localization of macrophage phenotypes with human intervertebral disc degeneration. *Spine J*. doi:10.1016/j.spinee.2017.09.018

Nerlich, A. G., Weiler, C., Zipperer, J., Narozny, M. & Boos, N. (2002). Immunolocalization of phagocytic cells in normal and degenerated intervertebral discs. *Spine (Phila Pa 1976), 27*(22), 2484-2490. doi:10.1097/01.BRS.0000031266.31284.75

Nguyen, T. T. B., Hein, S., Ng, C.-H. & Stevens, W. F. (2008). Molecular stability of chitosan in acid solutions stored at various conditions. *Journal of Applied Polymer Science, 107*(4), 2588-2593. doi:10.1002/app.27376

Oliveira, M. I., Santos, S. G., Oliveira, M. J., Torres, A. L. & Barbosa, M. A. (2012). Chitosan drives anti-inflammatory macrophage polarisation and pro-inflammatory dendritic cell stimulation. *Eur Cell Mater, 24*, 136-152; discussion 152-133.

Owens, D. E. & Peppas, N. A. (2006). Opsonization, biodistribution, and pharmacokinetics of polymeric nanoparticles. *Int J Pharm, 307*(1), 93-102. doi:10.1016/j.ijpharm.2005.10.010

Oyewumi, M. O., Yokel, R. A., Jay, M., Coakley, T. & Mumper, R. J. (2004). Comparison of cell uptake, biodistribution and tumor retention of folate-coated and PEG-coated gadolinium nanoparticles in tumor-bearing mice. *J Control Release, 95*(3), 613-626. doi:10.1016/j.jconrel.2004.01.002

Pan, X., Chen, L., Liu, S., Yang, X., Gao, J. X. & Lee, R. J. (2009). Antitumor activity of G3139 lipid nanoparticles (LNPs). *Mol Pharm, 6*, 211-220.

Park, J., Wrzesinski, S. H., Stern, E., Look, M., Criscione, J., Ragheb, R., Jay, S. M., Demento, S. L., Agawu, A., Licona Limon, P., Ferrandino, A. F., Gonzalez, D., Habermann, A., Flavell, R. A. & Fahmy, T. M. (2012). Combination delivery of TGF-beta inhibitor and IL-2 by nanoscale liposomal polymeric gels enhances tumour immunotherapy. *Nat Mater, 11*(10), 895-905. doi:10.1038/nmat3355

Pattappa, G., Li, Z., Peroglio, M., Wismer, N., Alini, M. & Grad, S. (2012). Diversity of intervertebral disc cells: phenotype and function. *J Anat, 221*(6), 480-496. doi:10.1111/j.1469-7580.2012.01521.x

Peng, S. F., Yang, M. J., Su, C. J., Chen, H. L., Lee, P. W., Wei, M. C. & Sung, H. W. (2009). Effects of incorporation of poly(gamma-glutamic acid) in chitosan/DNA complex nanoparticles on cellular uptake and transfection efficiency. *Biomaterials, 30*(9), 1797-1808. doi:10.1016/j.biomaterials.2008.12.019

Peracchia, M. T., Harnisch, S., Pinto-Alphandary, H., Gulik, A., Dedieu, J. C., Desmaele, D., d'Angelo, J., Muller, R. H. & Couvreur, P. (1999). Visualization of in vitro protein-rejecting properties of PEGylated stealth polycyanoacrylate nanoparticles. *Biomaterials, 20*(14), 1269-1275.

Pereira, C. L., Antunes, J. C., Gonçalves, R. M., Ferreira-da-Silva, F. & Barbosa, M. A. (2012). Biosynthesis of highly pure poly-gamma-glutamic acid for biomedical applications. *J Mater Sci: Mater Med*.

Porporatto, C., Bianco, I. D., Riera, C. M. & Correa, S. G. (2003). Chitosan induces different l-arginine metabolic pathways in resting and inflammatory macrophages. *Biochemical and Biophysical Research Communications, 304*(2), 266-272. doi:10.1016/s0006-291x(03)00579-5

Pourjavadi, A., Zeidabadi, F. & Barzegar, S. (2010). Alginate-based biodegradable superabsorbents as candidates for diclofenac sodium delivery systems. *Journal of Applied Polymer Science*, n/a-n/a. doi:10.1002/app.32205

Qiu, H., Min, Y., Rodgers, Z., Zhang, L. & Wang, A. Z. (2017). Nanomedicine approaches to improve cancer immunotherapy. *Wiley Interdiscip Rev Nanomed Nanobiotechnol, 9*(5). doi:10.1002/wnan.1456

Raes, G., De Baetselier, P., Noel, W., Beschin, A., Brombacher, F. & Hassanzadeh, G. (2002). Differential expression of FIZZ1 and Ym1 in alternatively versus classically activated macrophages. *J. Leukoc. Biol., 71*, 597-602.

Raj, P. P. (2008). Intervertebral Disc: Anatomy-Physiology-Pathophysiology-Treatment. *Pain Practice, 8*(1), 18-44.

Razaq, S., Wilkins, R. J. & Urban, J. P. (2003). The effect of extracellular pH on matrix turnover by cells of the bovine nucleus pulposus. *Eur Spine J, 12*(4), 341-349. doi:10.1007/s00586-003-0582-3

Roelofs, P. D., Deyo, R. A., Koes, B. W., Scholten, R. J. & van Tulder, M. W. (2008). Nonsteroidal anti-inflammatory drugs for low back pain: an updated Cochrane review. *Spine (Phila Pa 1976), 33*(16), 1766-1774. doi:10.1097/BRS.0b013e31817e69d3

Rostam, H. M., Reynolds, P. M., Alexander, M. R., Gadegaard, N. & Ghaemmaghami, A. M. (2017). Image based Machine Learning for identification of macrophage subsets. *Sci Rep, 7*(1), 3521. doi:10.1038/s41598-017-03780-z

Roy, S., Dixit, C. K., Woolley, R., MacCraith, B. D., O'Kennedy, R. & McDonagh, C. (2010). Novel multiparametric approach to elucidate the surface amine-silanization reaction profile on fluorescent silica nanoparticles. *Langmuir, 26*(23), 18125-18134. doi:10.1021/la103212d

Sakai, D. (2008). Future perspectives of cell-based therapy for intervertebral disc disease. *Eur Spine J, 17 Suppl 4*, 452-458. doi:10.1007/s00586-008-0743-5

Santos, S. G., Lamghari, M., Almeida, C. R., Oliveria, M. I., Neves, N., Ribeiro, A. C., Barbosa, J. N., Barros, R., Maciel, J., Martins, M. C., Gonçalves, R. M. & Barbosa, M. A. (2013). Adsorbed fibrinogen leads to improved bone regeneration and correlates with differences in the systemic immune response. *Acta Biomater, 9*(7), 7209-7217. doi:10.1016/j.actbio.2013.04.008

Schlenoff, J. B., Ly, H. & Li, M. (1998). Charge and Mass Balance in Polyelectrolyte Multilayers. *J. Am. Chem. Soc., 120*, 7626-7634.

Shimamura, Y., Holding, C., Haynes, D. R., Vernon-Roberts, B., Blumbergs, P. C., Fraser, R. D. & Moore, R. J. (2008). The biologic response to particles from a potential disc prosthesis material. *Spine (Phila Pa 1976), 33*(4), 351-355. doi:10.1097/BRS.0b013e318163f323

Simms, H., D'Amico, R. & Bland, K. I. (1997). Integrin stimulation regulates polymorphonuclear leukocytes inflammatory cytokine expression. *Ann. Surg., 225*, 757-763.

Smith, L. J., Nerurkar, N. L., Choi, K. S., Harfe, B. D. & Elliott, D. M. (2011). Degeneration and regeneration of the intervertebral disc: lessons from development. *Dis Model Mech, 4*(1), 31-41. doi:10.1242/dmm.006403

Stout, R. D., Jiang, C., Matta, B., Tietzel, I., Watkins, S. K. & Suttles, J. (2005). Macrophages Sequentially Change Their Functional Phenotype in Response to Changes in Microenvironmental Influences. *The Journal of Immunology, 175*(1), 342-349. doi:10.4049/jimmunol.175.1.342

Sukhorukov, G. B., Donath, E., Lichtenfeld, H., Knippel, E., Knippel, M., Budde, A. & Mohwald, H. (1998). Layer-by-layer self assembly of polyelectrolytes on colloidal particles. *Colloids and Surfaces, 137*, 253-266.

Sumbayev, V. V., Yasinska, I. M., Garcia, C. P., Gilliland, D., Lall, G. S., Gibbs, B. F., Bonsall, D. R., Varani, L., Rossi, F. & Calzolai, L. (2013). Gold nanoparticles downregulate interleukin-1beta-induced pro-inflammatory responses. *Small, 9*(3), 472-477. doi:10.1002/smll.201201528

Sung, H.-W., Huang, R.-N., Huang, L. L. H. & Tsai, C.-C. (1999). In vitro evaluation of cytotoxicity of a naturally occurring cross-linking reagent for biological tissue fixation. *Journal of Biomaterials Science, Polymer Edition, 10*(1), 63-78. doi:10.1163/156856299x00289

Sutherland, M. D., Thorkildson, P., Parks, S. D. & Kozel, T. R. (2008). In vivo fate and distribution of poly-gamma-D-glutamic acid, the capsular antigen from Bacillus anthracis. *Infect Immun, 76*(3), 899-906. doi:10.1128/IAI.01176-07

Tadano, T., Zhu, R., Muroga, Y., Hoshi, T., Sasaki, D., Yano, S. & Sawaguchi, T. (2014). A new mechanism for the silica nanoparticle dispersion–agglomeration transition in a poly(methyl methacrylate)/silica hybrid suspension. *Polymer Journal, 46*(6), 342-348. doi:10.1038/pj.2014.6

Tan, J., Shah, S., Thomas, A., Ou-Yang, H. D. & Liu, Y. (2013). The influence of size, shape and vessel geometry on nanoparticle distribution. *Microfluid Nanofluidics, 14*(1-2), 77-87. doi:10.1007/s10404-012-1024-5

Teixeira, G. Q., Leite Pereira, C., Castro, F., Ferreira, J. R., Gomez-Lazaro, M., Aguiar, P., Barbosa, M. A., Neidlinger-Wilke, C. & Goncalves, R. M. (2016). Anti-inflammatory Chitosan/Poly-gamma-glutamic acid nanoparticles control inflammation while remodeling extracellular matrix in degenerated intervertebral disc. *Acta Biomater, 42*, 168-179. doi:10.1016/j.actbio.2016.06.013

ten Hagen, T. L., Seynhaeve, A. L., van Tiel, S. T., Ruiter, D. J. & Eggermont, A. M. (2002). Pegylated liposomal tumor necrosis factor results in reduced toxicity and synergestic anyitumor activity after systemic administration in combination with liposomal doxorubicin in soft tissue sarcoma-bearing rats. *Int. J. Cancer*, 115-120.

Tomihata, K. & Ikada, Y. (1997). In vitro and in vivo degradation of films of chitin and its deacetylated derivatives. *Biomaterials, 18*(7), 567-575.

Treuel, L., Malissek, M., Gebauer, J. S. & Zellner, R. (2010). The influence of surface composition of nanoparticles on their interactions with serum albumin. *Chemphyschem, 11*(14), 3093-3099. doi:10.1002/cphc.201000174

Tufail, S., Sherwani, M. A., Shoaib, S., Azmi, S., Owais, M. & Islam, N. (2018). Ovalbumin self-assembles into amyloid nanosheets that elicit immune responses and facilitate sustained drug release. *J Biol Chem*. doi:10.1074/jbc.RA118.002550

Urban, J. P., Smith, S. & Fairbank, J. C. (2004). Nutrition of the intervertebral disc. *Spine (Phila Pa 1976), 29*(23), 2700-2709.

Vadala, G. & al., e. (2016). Stem cells sources for intervertebral disc regeneration. *World J Stem Cells, 8*(5), 185-201. doi:10.4252/wjsc.v8.i5.185

Vadala, G., Sowa, G. A. & Kang, J. D. (2007). Gene therapy for disc degeneration. *Expert Opin Biol Ther, 7*(2), 185-196. doi:10.1517/14712598.7.2.185

Vasconcelos, D. M., Goncalves, R. M., Almeida, C. R., Pereira, I. O., Oliveira, M. I., Neves, N., Silva, A. M., Ribeiro, A. C., Cunha, C., Almeida, A. R., Ribeiro, C. C., Gil, A. M., Seebach, E., Kynast, K. L., Richter, W., Lamghari, M., Santos, S. G. & Barbosa, M. A. (2016). Fibrinogen scaffolds with immunomodulatory properties promote in vivo bone regeneration. *Biomaterials, 111*, 163-178. doi:10.1016/j.biomaterials.2016.10.004

Vasconcelos, D. P., Fonseca, A. C., Costa, M., Amaral, I. F., Barbosa, M. A., Aguas, A. P. & Barbosa, J. N. (2013). Macrophage polarization following chitosan implantation. *Biomaterials, 34*(38), 9952-9959. doi:10.1016/j.biomaterials.2013.09.012

Verma, A. & Stellacci, F. (2010). Effect of surface properties on nanoparticle-cell interactions. *Small, 6*(1), 12-21. doi:10.1002/smll.200901158

Vishwakarma, A., Bhise, N. S., Evangelista, M. B., Rouwkema, J., Dokmeci, M. R., Ghaemmaghami, A. M., Vrana, N. E. & Khademhosseini, A. (2016). Engineering Immunomodulatory Biomaterials To Tune the Inflammatory Response. *Trends Biotechnol, 34*(6), 470-482. doi:10.1016/j.tibtech.2016.03.009

Wang, C., Xu, L., Liang, C., Xiang, J., Peng, R. & Liu, Z. (2014). Immunological responses triggered by photothermal therapy with carbon nanotubes in combination with anti-CTLA-4 therapy to inhibit cancer metastasis. *Adv Mater, 26*(48), 8154-8162. doi:10.1002/adma.201402996

Wang, X., Podila, R., Shannahan, J. H., Rao, A. M. & Brown, J. M. (2013). Intravenously delivered graphene nanosheets and multiwalled carbon nanotubes induce site-specific Th2 inflammatory responses via the IL-33/ST2 axis. *Int J Nanomedicine, 8*, 1733-1748. doi:10.2147/IJN.S44211

Xu, B., Xu, H., Wu, Y., Li, X., Zhang, Y., Ma, X. & Yang, Q. (2015). Intervertebral Disc Tissue Engineering with Natural Extracellular Matrix-Derived Biphasic Composite Scaffolds. *PLoS ONE, 10*(4), e0124774. doi:10.1371/journal.pone.0124774

Xu, Z., Wang, Y., Zhang, L. & Huang, L. (2014). Nanoparticle-Delivered Transforming Growth Factor-β siRNA Enhances Vaccination against Advanced Melanoma by Modifying Tumor Microenvironment. *American Chemical Society, 8*(4), 3636-3645.

Yang, C., Cao, P., Gao, Y., Wu, M., Lin, Y., Tian, Y. & Yuan, W. (2016a). Differential expression of p38 MAPK alpha, beta, gamma, delta isoforms in nucleus pulposus modulates macrophage polarization in intervertebral disc degeneration. *Sci Rep, 6*, 22182. doi:10.1038/srep22182

Yang, E. J. & Choi, I. H. (2013). Immunostimulatory effects of silica nanoparticles in human monocytes. *Immune Netw, 13*(3), 94-101. doi:10.4110/in.2013.13.3.94

Yang, J., Shim, S. M., Nguyen, T. Q., Kim, E. H., Kim, K., Lim, Y. T., Sung, M. H., Webby, R. & Poo, H. (2017). Poly-gamma-glutamic acid/chitosan nanogel greatly enhances the efficacy and heterosubtypic cross-reactivity of H1N1 pandemic influenza vaccine. *Sci Rep, 7*, 44839. doi:10.1038/srep44839

Yang, X., Jin, L., Yao, L., Shen, F. H., Shimer, A. L. & Li, X. (2014). Antioxidative nanofullerol prevents intervertebral disk degeneration. *Int J Nanomedicine, 9*, 2419-2430. doi:10.2147/IJN.S60853

Yang, Y. W. & Luo, W. H. (2016b). Cellular biodistribution of polymeric nanoparticles in the immune system. *J Control Release, 227*, 82-93. doi:10.1016/j.jconrel.2016.02.011

Yen, H. J., Hsu, S. H. & Tsai, C. L. (2009). Cytotoxicity and immunological response of gold and silver nanoparticles of different sizes. *Small, 5*(13), 1553-1561. doi:10.1002/smll.200900126

Yilmaz, M. D. (2016). Layer-by-layer hyaluronic acid/chitosan polyelectrolyte coated mesoporous silica nanoparticles as pH-responsive nanocontainers for optical bleaching of cellulose fabrics. *Carbohydr Polym, 146*, 174-180. doi:10.1016/j.carbpol.2016.03.037

Zhang, B., Sai Lung, P., Zhao, S., Chu, Z., Chrzanowski, W. & Li, Q. (2017). Shape dependent cytotoxicity of PLGA-PEG nanoparticles on human cells. *Sci Rep, 7*(1), 7315. doi:10.1038/s41598-017-07588-9

Zhang, Y., Hsu, B. Y., Ren, C., Li, X. & Wang, J. (2015). Silica-based nanocapsules: synthesis, structure control and biomedical applications. *Chem Soc Rev, 44*(1), 315-335. doi:10.1039/c4cs00199k

Zhao, Y., Chen, Z., Zhu, X. & Möller, M. (2015). Silica nanoparticles catalyse the formation of silica nanocapsules in a surfactant-free emulsion system. *Journal of Materials Chemistry A, 3*(48), 24428-24436. doi:10.1039/c5ta06947e

Zolnik, B. S. & Sadrieh, N. (2009). Regulatory perspective on the importance of ADME assessment of nanoscale material containing drugs. *Adv Drug Deliv Rev, 61*(6), 422-427. doi:10.1016/j.addr.2009.03.006